Fall 12-16-2016

The Functions of the CID and lRG Operons in S. Aureus Programmed Cell Death

Xinyan Zhang
University of Nebraska Medical Center

Recommended Citation

The functions of the cid and lrg operons in S. aureus programmed cell death

by

Xinyan Zhang

A DISSERTATION

Presented to the Faculty of

the University of Nebraska Graduate College

in Partial Fulfillment of the Requirements

for the Degree of Doctor of Philosophy

Department of Pharmaceutical Sciences

Under the Supervision of Professor Sorin Luca

University of Nebraska Medical Center

Omaha, Nebraska

April, 2016

Supervisory Committee:

Kenneth W. Bayles, Ph.D.   Luis A. Marky, Ph.D.

Jonathan L. Vennerstrom, Ph.D.

Acknowledgments

Foremost, I would like to express my sincere gratitude to my advisor Dr. Sorin Luca for the continuous support of my Ph.D study and research, for his patience, motivation, enthusiasm, and immense knowledge. His guidance helped me in all the time of research, writing of this thesis and even landing the ideal jobs. I could not have imagined having a better advisor and mentor for my Ph.D study.

Besides my advisor, I would like to thank the rest of my thesis committee: Prof. Luis Marky, Prof. Kenneth Bayles, and Prof. Jonathan Vennerstrom, for their encouragement, insightful comments, and inspiring questions. I am also grateful to them because most of my research is based on their previous work.

I would like to thank Katina Winters, Michelle Parks, Jaclyn Ostronic, Elaine Payne, Ashley Calhoon for helping me with lots of student paperworks and purchasing lab products during my entire PhD career.

I thank my fellow labmates: Yanli Zhang, Shuqi Wang and Maria Podariu for the stimulating discussions and for the help on my experiments. I want to thank my friends in UNMC: Xin Wei, Gang Zhao, Huocong Huang, Yinbo Zhang, Han Liu, Wenfeng Hu, Dongze Zhang, Zhengfeng Wang and Zhengjian Lv. Also I thank my friends in Jilin University: Qiu Xia and Long Cao.

My sincere thanks also go to Dr. Rajni Singh, Dr. Kathy Taylor and Dr. Sujit Basu, for offering me the summer internship opportunities in their group at Shire Pharmaceuticals and leading me working on diverse exciting industrial projects.

Abstract

Xinyan Zhang, PhD

University of Nebraska Medical Center, 2016

Advisor: Sorin Luca, PhD.

Staphylococcus aureus cid/lrg operons regulate the formation of *S.aureus* biofilm formation and programmed cell death based on previous in vivo work done in Dr. Bayles's lab. *cid* operon, which encodes CidA/CidB/CidC proteins, has been shown to be an effector in leading to the lysis and death of the *S.aureus*; While *lrg* operon, encoding LrgA and LrgB proteins, is an inhibitor of the lysis and death. Recent studies suggest that CidA behaves like holin proteins from bacterial phage, by increasing the murein hydrolysis activity under aerobic culturing conditions. LrgA, together with LrgB, appears to inhibit this function. Another important studies on *S.aureus* under carbon-overflow condition indicates that CidC plays a critical function in the autolysis of the bacteria by producing acetic acid, and finally lead to the death of the bacteria.

Based on these findings, we further characterize these proteins in this project with in vitro high concentration of purified proteins. Our result indicates that CidA/LrgA causes the leakage of smaller fluorescent dyes, but not large proteins, from the artificial membrane. And CidA showed a more rapid leakage compare to LrgA at the same concentration. This result may indicate that the function of CidA is penetrating the bacterial membrane and may induce the formation of nanometer level pores.

CidC is also overexpressed and purified. The assay has conclusively proved that CidC is a pyruvate oxidoreductase and binds to the biological membrane, It passes the electron to

menaquinone in vivo and produces acetate instead of hydrogen peroxide. The activity of CidC is strongly pH dependent and replies on the cofactor thiamine pyrophsophate and Mg^{2+} ion.

In my last project, the effect of GC-rich sequence on the stability of thrombin-binding aptamer G-quadruplex was investigated. Two complementary GC-rich single strands are attached to the aptamer separately or both at the same time. The results showed that one single strand has a deleterious effect on the formation of the G-quadruplex but the other single strand has little effect on it, when both attached, they form a duplex on top of the G-quadruplex. The study has great indication on the mechanism of how the flanking sequence affects the stability of the thrombin-binding aptamer as well as the in vivo telomeric G-quadruplex.

Table of Contents

Abbreviation

AC	*Affinity chromatography*
Bcl-2	*B cell lymphoma 2*
Caspases	Cysteine aspartic proteases
DISC	*death-inducing signaling complex*
E.coli	*Escherichia coli*
eDNA	*extracellular*DNA
ETC	Electron transport chain
FAD	Flavin adenine dinucleotide
FMN	Flavin Mononucleotide
GFC	Gel filtration chromatography
GST	glutathione s-transferase
ITC	Isothermal Titration Calorimetry
MM	Michaelis-Menten
MOM	mitochondria outer membrane
MRSA	Methicillin-resistant *Staphylococcus aureus*

NAD	Nicotinamide adenine dinucleotide
NADP	Nicotinamide adenine dinucleotide phosphate
ODN	oligonucleotides
PCD	programmed cell death
POX	pyruvate oxidase
PQO	pyruvate quinone oxidase
ROS	Reactive oxygen species
SAR	signal-arrest-release
S.aureus	*Staphylococcus aureus*
SELEX	systematic evolution of ligands by exponential enrichment
SMACs	second mitochondria-derived activator of caspases
TA	*Toxin–antitoxin*
TPP	Thiamine pyrophosphate
TNF	tumor necrosis factor
VDAC	voltage-dependent anion channel

Figures and tables

Chapter 1

Introduction

Methicillin-resistant Staphylococcus aureus (MRSA) refers to strains of *Staphylococcus aureus* (*S. aureus*) that are resistant to the antibiotic methicillin (including other beta-lactam antibiotics) and a host of other drugs used to treat infection. MRSA has been recently responsible for 11,000 deaths and 80,000 invasive infections per year in the U.S.[1] The MRSA virulence has been associated with the capacity of *S. aureus* to form biofilm, which is a bacterial conglomeration embedded in a self-produced and protective matrix. [2,3]

Apoptosis is usually associated with complex eukaryotes, where the genetically well-controlled elimination of a damaged (in diseased tissues) or unnecessary (during development) subpopulation of cells benefits the organism as a whole. Interestingly, bacterial biofilm also consists of complex and well organized cellular subpopulations structures, which is similar to multicellular organisms and significantly distinct from the planktonic bacteria that live in isolation. Because of the multicellular nature of biofilm, selective pressure exists to eliminate damaged and/or malfunctional individual cells, thus enhancing the survival of the remaining healthy population. The death of the subpopulation may not only increase the availability of external nutrients to the entire community, but also release cellular DNA which is an essential structural component of the biofilm matrix[4–6]. Dr. Bayles proposed that there could even be a subtle and genetically well-programmed mechanism behind the above hypothesis. More specifically, the Cid/Lrg system has been proposed to relate to the control of cell death and lysis in the context of a developing biofilm within *S. aureus*[7–10]

1.1 Eukaryotic programmed cell death

Regulated cell proliferation and death are common phenomena observed in multicellular organisms, keeping a balanced life-and-death cycle has a vital rule in the survival of individuals[11]. The programmed cell death (PCD or apoptosis) of the cell is accompanied by a series morphological changes and biochemical events, including blebbing, cell shrinkage, nuclear fragmentation, chromatin condensation, chromosomal DNA fragmentation, and global mRNA decay. Between 50 and 70 billion cells die each day due to apoptosis in an average human adult. For an average child between the ages of 8 and 14, approximately 20 billion to 30 billion cells die a day. Excessive apoptosis causes atrophy, whereas insufficient amount of apoptosis results in uncontrolled cell proliferation, such as cancer.

Unlike necrosis, which is a form of traumatic cell death as a result of acute cell injury, apotosis is a highly gene regulated and controlled process which confers advantage to an organism. A well-known example of apoptosis is the separation of fingers and toes in a developing human embryo, because cells between the digits undergo apoptosis.

The mechanism of apoptosis in mammalian cells has been well studied since early 1990s. Apoptosis can be initiated through one of two pathways. In the intrinsic pathway the cell kills itself because it senses cell stress, whereas in the extrinsic pathway the cell kills itself because of signals from other cells. Both pathways induce cell death by activating cysteine-aspartic proteases (caspases). The two pathways both activate initiator caspases, which then activate executioner caspases, which then kill the cell by degrading proteins indiscriminately. Once apoptosis has begun, there is no going back for the cells.

1.1.1 Intrinsic pathway

The intrinsic pathway, also as known as mitochondria pathway, of apoptosis is activated by intracellular signals generated when cells are stressed and it's dependent on the release of proteins from the intermembrane space of mitochondria[12]. Many apoptotic proteins initiate and mediate the intrinsic pathway by targeting mitochondria, they may cause swelling of the mitochondria though formation of pores and lead to the ceasing of aerobic respiration, or they may increase the permeability and cause the leakage of apoptotic effector proteins such as SMACs (second mitochondria-derived activator of caspases) and cytochrome c (see **Figure 1.1**). Once released, SMAC and cytochrome c triggers the caspase cascade and the down stream morphological changes that are associated with cellular disassembly[13,14].

At the heart of apoptosis is B cell lymphoma 2 (Bcl-2) family of proteins, which includes pro-apoptotic proteins Bax, Bak and Bok; BH-3 domain only protein, BID, BIM, BAD, etc. and anti-apoptotic proteins such as Bcl-2, Bcl-X, Bcl-W, etc[15]. Studies has shown that the apoptotic process in mitochondria is initiated by the oligomerization of Bax/Bak proteins in the mitochondria outer membrane (MOM)[15], these proteins interact with, and increase the opening of mitochondria voltage-dependent anion channel (VDAC) and lead to the loss of membrane potential and the release of cytochrome c, more recent findings suggest that Bax and Bak directly involve in the release of cytochrome c by inducing pore formation on MOM[16]. On the other hand, the anti-apoptotic proteins act as inhibitors of the above process by interacting with Bax and Bak (**Figure 1.1**). The entire intrinsic pathway is under tight control by eukaryotic genome, for example, the expression of Bax protein is regulated by p53 gene, which is one of the most important tumor suppressor genes[17].

1.1.2 Extrinsic pathway

The extrinsic pathway of apoptosis is activated by extracellular ligands binding to

cell-surface death receptors, which are members of tumor necrosis factor (TNF) receptor gene superfamily[18]. Members of the TNF receptor family share similar cyteine-rich extracellular domains and have a cytoplasmic domain of about 80 amino acids called the "death domain" [19]. This death domain plays a critical role in death signal transduction. To date, the best-characterized ligands and corresponding death receptors are FasL/FasR and TNF-α/TNFR1 (see **Figure 1.1**).

In the FasL/FasR and TNF-α/TNFR1 models, there is clustering of receptors and binding with the homologous trimeric ligand. Upon ligand binding, cytoplasmic adapter proteins are recruited and exhibit corresponding death domains that bind with the receptors. The binding of Fas ligand to Fas receptor results in the binding of the adapter protein FADD and the binding of TNF ligand to TNF receptor results in the binding of the adapter protein TRADD with recruitment of FADD and RIP[20–22]. FADD then associates with procaspase-8 via dimerization of the death effector domain. At this point, a death-inducing signaling complex (DISC) is formed, resulting in the auto-catalytic activation of procaspase-8[23].

Once caspase-8 is activated, the execution phase of apoptosis is triggered. Death receptor mediated apoptosis can be inhibited by a protein called c-FLIP which will bind to FADD and caspase-8, rendering them ineffective[24,25]. Another point of potential apoptosis regulation involves a protein called Toso, which has been shown to block Fas-induced apoptosis in T cells via inhibition of caspase-8 processing[26].
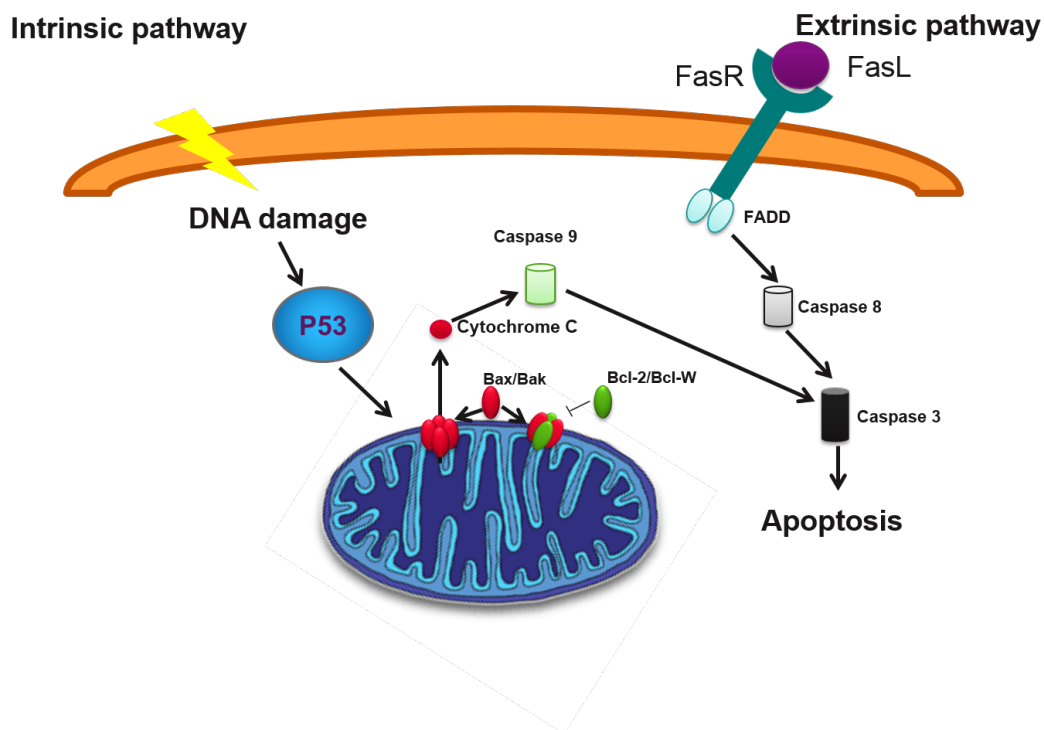
Figure 1.1. Simplified Apoptosis Intrinsic and Extrinsic pathway. Intrinsic pathway is initiated by intracellular signal like DNA damage, Extrinsic pathway is induced by extracellular ligands (e.g. FasL). Bcl-2 family proteins play a critical role in regulating apoptosis by targeting mitochondria.

1.2 Biofilm, bacterial programmed cell death and *cid/lrg* operon

The tolerance of bacteria to common antibiotics has been causing serious health problems in hospitals, prisons, and nursing homes, where patients with open wounds, invasive devices, and weak immune systems are at greater risk of nosocomial infections. Methicillin-resistant *S. aureus* (MRSA) is particularly responsible in the U.S. for at least 11,000 deaths and 80,000 invasive infections per year[27] with associated costs of \$3.2 to 4.2 billions[28]. The virulence of MRSA has been shown to depend on the formation of biofilm, which is a bacterial colony embedded in a self-produced and protective matrix[2,3].

Biofilm can be formed by both gram-positive and gram negative bacteria when they stick to a non-biological or biological surface[29]. Biofilm is composed of proteins, polysaccharides and extracellular DNA, which are released by a subpopulation of bacteria as a result of their autolysis. Recent findings have suggested that bacterial autolysis within the biofilm is a strictly gene-regulated process. Many systems have been reported to control the autolysis in different bacteria[6,10,30–32].

There are evidences suggesting that bacteria autolysis in many ways resembles the eukaryotic apoptosis process. Since the autolysis in many bacteria possesses hallmarks of apoptosis, like DNA fragmentation, elevated caspase-like protein activity, increasing ROS production and respiratory dysfunction, etc[9,33]. In *S.aureus* and many other biofilm-forming bacteria, *cid/lrg operon* has been shown to regulate the bacterial PCD by sensing the membrane potential and abnormality of carbon metabolism under carbon-overflow conditions, thus greatly affecting the formation of biofilm[34,35].

This part of the introduction will review the known facts of biofilm and bacterial programmed cell death with emphasis on *cid/lrg operon*, it will help to better understand the mechanism of *S.aureus* biofilm formation and the role played by *cid/lrg operon* and their gene

products.

1.2.1 Biofilm Development

As mentioned before, biofilm is a sessile community formed by a group of bacteria sticking to a solid surface. The microbial cells growing in a biofilm are physiologically distinct from planktonic cells of the same organism, which, by contrast, are single-cells that may float or swim in a liquid medium. Also, the gene expression pattern of the bacteria growing in the biofilm is much different than the planktonic bacteria. The unique features of bacteria existing in biofilm enabled them to have extraordinary resistance to conventional biocides, antimicrobial treatments and the immune defense responses of the host, thus making biofilm formation the root of many persistent and chronic bacterial infections including the ones that are caused by MRSA[32,36].

Formation of a biofilm begins with the attachment of free-floating microorganisms to a surface (see **Figure 1.2**). The first stage of bacteria attachment to a surface is weak, reversible adhesion via van der Waals forces. For some motile bacteria, if they are not immediately separated from the surface, they can anchor themselves more tightly using cell adhesion structures such as flagella and pili in the case of *Escherichia coli (E.coli)* biofilm[37].

Once irreversible attachment happens, the biofilm start to enter the maturation stage, surface contact triggers gene expression changes and upregulating factors favoring sessility of the biofilm[29,36]. In this stage, bacteria start to secret polysaccharides, protein to form extracellular matrix, in particular a subpopulation of the bacteria even conduct autolysis to release their intracellular contents including their chromosomal DNA (later known as extracellular DNA, eDNA), acting as a stabilizing scaffold of the biofilm[31]. The substances in the extracellular matrix are known as extracellular polymeric substances, which accounts for 90% of the biomass of the biofilm and bring nutrients and structural support to the bacterial

community within the biofilm[29,32].

As the biofilm matures, the bacteria in the biofilm actively communicate and exchange and share products, which play pivotal roles in maintaining the architecture of the biofilm and providing a favorable environment for the bacteria. Following the maturation of biofilm, dispersal of the bacteria may occur. Bacteria have evolved ways to perceive the changes in the environment and gauge whether to remain in the biofilm or resume a plantonic form, biofilm dispersal can be the result of several cues, such as alterations in nutrient availability, oxygen fluctuations and increase of toxic products, or other stress-inducing conditions. Bacteria have systems that can sense those stress and alter their gene expression accordingly, promoting their disposal[29,31].
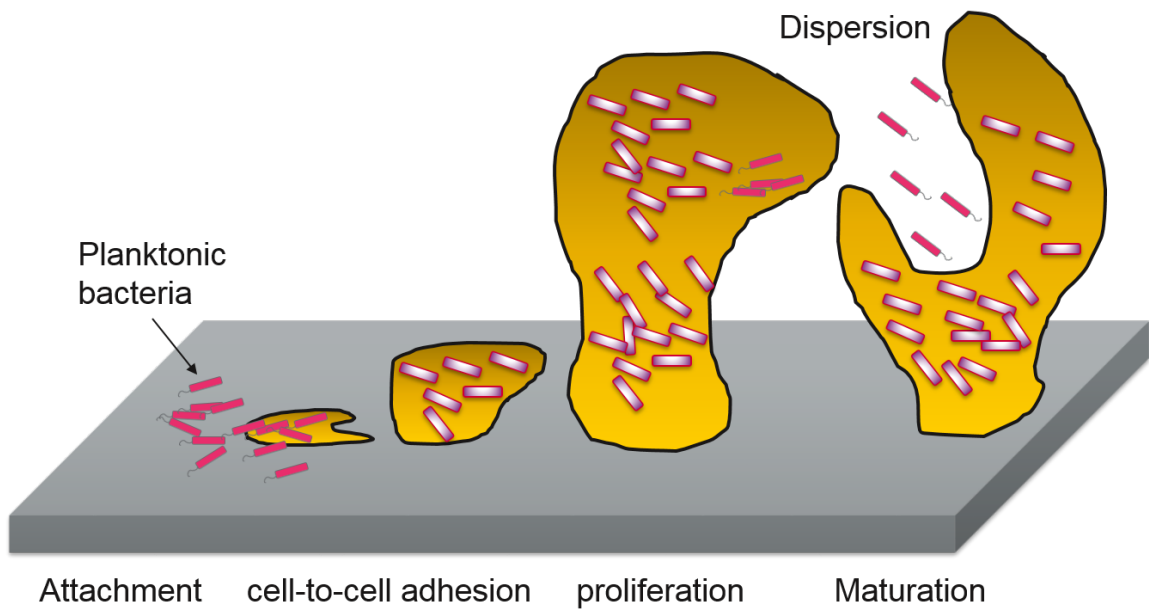
Figure 1.2. Biofilm development. Biofilm forms by planktonic bacteria sticking to a solid biological/non-biological surface. There are four stages in the biofilm development process, (1) Attachment, (2) Cell-to-cell adhesion, (3) Proliferation, (4) Maturation.

1.2.2 Benefits of the biofilm

By adopting this sessile mode of life, biofilm-embedded bacteria benefit from many advantages over their planktonic counterparts. The extracellular matrix is capable of sequestering and concentrating environmental nutrients such as carbon, nitrogen and phosphate[38]. An additional benefit of biofilm is the ability to evade multiple clearance mechanisms produced by host and synthetic sources. Examples of ineffective clearance strategies include antimicrobiotics, physical disruption, host phagocytic and host radical elimination and protease digestion. Resistance to antimicrobial factors is mediated through a dormant phenotype as a result of adaptation to a low oxygen environment and nutrient deprivation, and results in low metabolic and cell division rates. This stressed environment produces many slow growing cells that are tolerant to high levels of antibiotics but also a proportion of persister cells, which shut down the antimicrobial targets or the cellular need for those targets by maintaining a metabolically quiescent state, instead of preventing the antibiotics from hitting its target, as it's the case with many antibiotic resistant bacteria[39,40]. Due to the unique features of persister cells, antibiotics or effectors of host immune system can't clear out these population[41]. Once these treatment regime is halted, these persisters are able to spontaneously shift out of their quiescent state and produce a reactivation of infection[41].

Another hard-to-eliminate benefit for the biofilm-embedded bacteria may be the capability of biofilms to act as a diffusion barrier to slow down the penetration of some antimicrobial agents[42]. A recent study suggested several antibiotics (oxacillin, cefotaxime and vancomycin) had reduced penetration throughout *S. aureus* and *S. epidermidis* biofilms[43].

The final benefit to the biofilm development is the potential for dispersal and

detachment. As mentioned previously, after the mature of biofilm, bacteria has the option of dispersal. Micro-colonies may detach under the direction of fluid shear forces or through a genetically programmed response that mediates the dispersal process[44]. The detached microcolonies migrate from the original biofilm to uninfected regions of the host or other surfaces, attach and promote nascent biofilm formation.

In summary, formation of biofilm becomes the root for many persistent, chronic and recurrent bacterial infections. The bacteria within the biofilm possess quite different features compared to their planktonic counterparts. Due to the physiological and genetic heterogeneity, the biofilm-embedded bacteria has the ability to escape from host or synthetic elimination. The structure of biofilm can protect the bacteria from many antibiotic drugs. And lastly, detachment of the bacteria from mature biofilm enable them to evade environmental stress and form nascent biofilms.

1.2.3 Bacteria programmed cell death

During the past two decades, people start to realize that bacteria are not just some primitive single cellular organisms which can hardly do much more than growing and dividing. Many astonishing facts of bacteria has been discovered, such as quorum sensing, which allows the bacteria to sense the existence of each other based on the secretion of small signal molecules and synchronize their gene expression pattern, thus behave like a multicellular organism and is involved in several bacterial processes such as biofilm, sporulation, production of virulence factors, and competence for DNA uptake[45,46].

Another interesting subject is the controlled autolysis, also known as bacterial PCD, which is one of the fundamental group behaviors conducted by bacteria. The importance of bacterial cell death and lysis was underestimated. It was traditionally thought of as the results of "unbalanced growth" or the passive end stage of the bacterial life cycle that occurs after all

the nutrients have been depleted or all physiological processes have run their course. However, several studies suggested that these processes are highly gene-regulated and are much more complex than previously conceived, processes that might be fundamental to bacterial physiology and essential to our understanding of how bacteria develop within complex communities (e.g., biofilms), just as knowledge of PCD is essential to an understanding of the development of more sophisticated eukaryotic organisms.

There are several systems that were reported to regulate bacterial PCD. Many of them so far are found to be specific for certain bacteria species, however, there are also conserved molecular modules that can regulate most bacterial PCD, such systems include TA system and holin-endolysin system.

1.2.3.1 TA system

A common mechanism to realize PCD in bacteria is through toxin–antitoxin (TA) modules, which exists in almost all bacteria and archaea species that have been sequenced[47]. A TA module typically is composed of genes encoding a stable toxin protein and an unstable antitoxin (a protein or an RNA) that prevents the toxicity of the toxin by either directly interaction or translational inhibition of the toxin. Under certain stressed conditions, antitoxins are quickly degraded thus releasing toxins to exert their poisoning effects. The targets of toxins include DNA replication, translation, cell division, and cell wall synthesis[48]. One of the most studied TA systems is the *mazEF* system, which was first identified on *E. coli* chromosomal DNA and later in other bacterial genome[49]. *mazF* codes for a toxin protein MazF, an endoribonuclease that cleaves mRNAs; mazE codes for an antitoxin MazE, which can be rapidly degraded by the ClpPA serine protease[49]. The mazEF system is activated under various stressful conditions, including DNA damage, antibiotic treatment, amino acid starvation and oxidative stress[50,51]. Once induced, it causes PCD in most of the population by increasing the synthesis of 'death proteins', while allowing survival of a small sub-population

by increasing the synthesis of 'survival proteins'[52]. Moreover, mazEF-regulated death is mediated by a small peptide called extracellular death factor that is secreted by bacteria[53], suggesting fine tuning of PCD through population density and thus a role of quorum sensing.

1.2.3.2 Holin system

Another well-characterized system that regulate the bacterial PCD is the holin-endolysin system that origins from bacteriophage. The system controls the timing of bacterial lysis to make sure that the release of bacteriophage particles from the infected bacteria is at a time that maximize the reproductive potential of the bacteriophage population[54]. The timing of cell lysis is dictated by the holin proteins, which are small membrane proteins. They control the activity of the endolysin (murein hydrolase) and the regulation is achieved by one of two proposed mechanisms. The first mechanism, which is mainly used by holins encoded by lambda- and T4-like bacteriophages, involves the control of murein hydrolase transport across the membrane to the cell wall (see **Figure 1.3**), where it has access to its substrate, peptidoglycan. Although the mechanism by which these holins mediate the transport of murein hydrolases is unclear, it is thought that holins oligomerize in the membrane and eventually lead to the disruption of the membrane, which passively allowing the murein hydrolase to cross into the periplasm[55,56]. The other mechanism, used by bacteriophage P1, involves bacteriophage-encoded murein hydrolases containing "signal-arrest-release" (SAR) domains[57]. Like signal sequences, SAR domains target their cargo to the Sec machinery but anchor the protein in the outer face of the membrane as an inactive form until the holin releases it. Later the production of active murein hydrolases are later achieved by a disulfide isomerization event, upon released by holins[58].

How does the holin achieve the precise releasing timing of murein hydrolase? The answer seems to lie in their structures. The primary sequences of holins are diverse, most contain distinct structural features, including a relatively small size (60 to 145 amino acids),

two or more putative membrane-spanning domains often separated by a predicted beta-turn linker region, a hydrophilic N-terminus, and a highly polar, charged C-terminus[59]. Interestingly, holin genes often contain a "dual-start motif" that produces two different protein products. The shorter form of the protein functions as the holin, while the longer version, which is often different by additional few more amino acids at the N-terminus, functions as the antiholin[60,61]. Despite the minor difference, holin and anti-holin has the completely opposite functions. As the holins accumulate within the membrane, a gradual dissipation of the proton gradient occurs, once it reaches a point when the N terminus of the antiholin flips to the periplasmic face of the membrane, the antiholin functions as a holin, and the complete and rapid de-energization of the bacterial membrane is achieved[61]. Thus, two mechanisms seem to control the "lysis clock": one that is programmed into the structure of the holin protein, probably affecting the rate of proton leakage, and the other that involves changes in the ratio between the holin and antiholin. Once the holin timer has gone off, exactly how it mediates the transport of the endolysin is unclear.
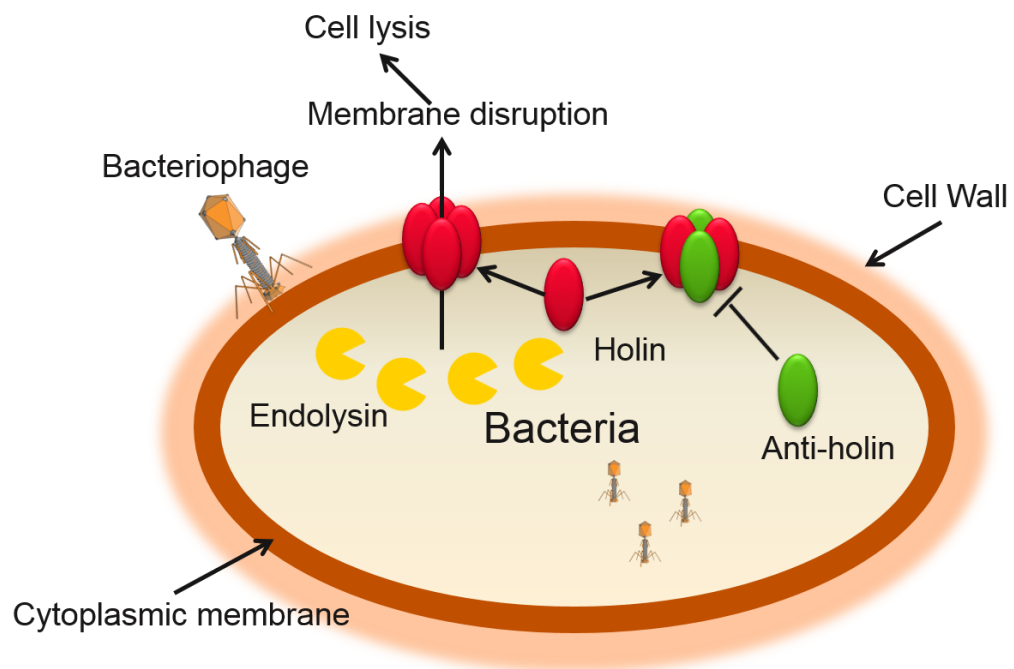
Figure 1.3. Holin-endolysin system. Holins are small membrane proteins and oligomerize in the bacterial inner membrane, they regulate the bacteria lysis by controlling the murein hydrolase activity.

1.2.4 *cid/lrg* regulatory system

Studies have suggested that regulated bacterial cell death is important for biofilm development, especially in the maturation and dispersal stage. Following the cell death, a subpopulation of dead bacteria lyse and release their genomic DNA (later known as eDNA), which increase the intercellular adhesion and biofilm stability[6,30]. During this process, *lytSR* and *cidR* operon has been suggested to play an important role.

The discovery and characterization of the *cid* and *lrg operons* evolved from the initial identification of a novel two-component (two related transcriptional factors) regulatory system from *S. aureus*, termed LytSR, that affected murein hydrolase activity and autolysis[62]. LytSR mutant lead to increased autolysis and altered murein hydrolase activity compared to wild type in the liquid culture of *S.aureus[62]*. LytS protein has a GAF DNA-binding domain and a membrane bound histidine kinase domain which intercepts an environmental cue and through an act of auto-phosphorylation transduces the signal intracellularly, LytS has been reported to sense disruption of membrane potential and lead to the transcription of lytSR downstream gene[63]. LytR is a transcription factor that falls into a novel family of proteins that contain non-helix-turn-helix DNA binding domains, also known as LytTRs. LytR regulates the expression of downstream gene in response to carbohydrate metabolism (e.g. excess of glucose)[63,64].

The downstream genes of *lytSR* are *lrgA* and *lrgB*, *lrgA* encodes a 16.3 kDa membrane protein and *lrgB* encodes a 25.1 kDa membrane protein. The LrgA protein contains four putative membrane-spanning domains, two potential linker regions, and a charged rich amino-terminal domain. It was hypothesized that lrgA is an antiholin-like protein (see **Figure 1.4A**), which was proved by the fact that an *lrgAB* mutation resulted in increased murein

hydrolase activity produced by the bacteria[65]. The function of *lrgB* was also addressed by generating an *lrgB* mutant and examining its phenotypic characteristics. Although no effect of this mutation on growth or autolysis was observed, zymographic analysis of this strain revealed the absence of a 25 to 30kDa murein hydrolase, leading to the speculation that it encodes either a murein hydrolase or a regulator of murein hydrolase activity[62]. Based on these results, it was hypothesized that the *lrgAB operon* encodes an antiholin, although a detailed analysis of the individual genes remains to be conducted. Furthermore, due to the absence of a dual-start motif within the *lrgA* and/or *lrgB* gene, it was predicted that the holin protein component of this system would be encoded by another gene within the *S. aureus* chromosome[10].

Later this prediction was supported by discovery and characterization of *lrgAB* homologues that were designated *cidA* and *cidB*[66]. The *cidA* gene product (CidA) shares 23% amino acid sequence identity with LrgA, whereas the *cidB* product (CidB) shares 31% amino acid sequence identity with LrgB. The putative CidA protein contains 131 amino acids and has a deduced molecular mass of 14.7 kDa, while CidB contains 229 amino acids and has a molecular mass of 25.0 kDa. Like LrgA and LrgB, the CidA and CidB proteins are also membrane proteins containing several predicted membrane-spanning domains. *cidA* mutant produced decreased murein hydrolase activity relative to that of its parental strain, the biofilm produced by the *cidA* mutant is more loosely compacted and is less adherent to the substrate and *cidA* mutant biofilm has much less lysis and eDNA compared to wild-type[5,67], these facts demonstrated that the function of the *cid* operon is an effector of murein hydrolase activity. Furthermore, this mutation was also shown to confer tolerance to various antibiotics including penicillin, rifampin, and vancomycin[67,68]. Overall, these results are consistent with the hypothesis that the *cid operon* encodes a holin and the *lrg operon* encodes an antiholin. Based on the putative functions of the *cidA* and *lrgA* gene products as holins and antiholins, respectively, a model for their roles in murein hydrolase regulation is proposed. The effect of

membrane depolarization would result in the release of murein hydrolase activity. The activation of the CidA proteins via a holin-like mechanism is hypothesized to dissipate the membrane potential, thus triggering murein hydrolase activity and lysis. The presence of LrgA is thought to inhibit the activity of the CidA holin in a way analogous to the inhibitory effect of an antiholin (see **Figure 1.4B**)[8,69].

Another major advance in the study of the *cid* and *lrg* operons was the finding and characterization of a third gene on *cid operon*, *cidC*, encoding a pyruvate oxidoreductase homologue[9,70]. Furthermore, cells containing a *cidC* mutation maintained a much higher level of cell viability in stationary phase than did the parental strain when grown in the presence of excess glucose. CidC was proved to produce acetate from pyruvate under carbon overflow (excess of glucose) condition, thus become a suicidal marker for *S.aureus* by causing acidification. Another two enzymes alsSD, produce acetoin (a neutral molecule), out of pyruvate. Together, CidC and alsSD, apart from CidA/LrgA, are proposed to become another sub-system that regulate the life and death of *S.aureus* and biofilm formation[70].

In fact, transcription of both *cidABC* and *lrgAB* was induced by acetic acid in the presence of excess glucose. This had led to the identification of CidR, a putative regulator of both *cid* and *alsSD operon*[34,71,72]. CidR is a LysR-type transcriptional regulator (LTTR), which is a highly structurally conserved transcriptional factor family in bacteria, LTTRs all have an N-terminal helix-turn-helix DNA binding domain and a C-terminal cofactor binding domain[73]. The function of CidR has been recently described as primarily promoting the cell survival by co-expressing CidA and alsSD to counteract the activities of CidB (proved to promote CidC activity, exact function unknown) and CidC proteins (see **Figure 1.4A**).

A
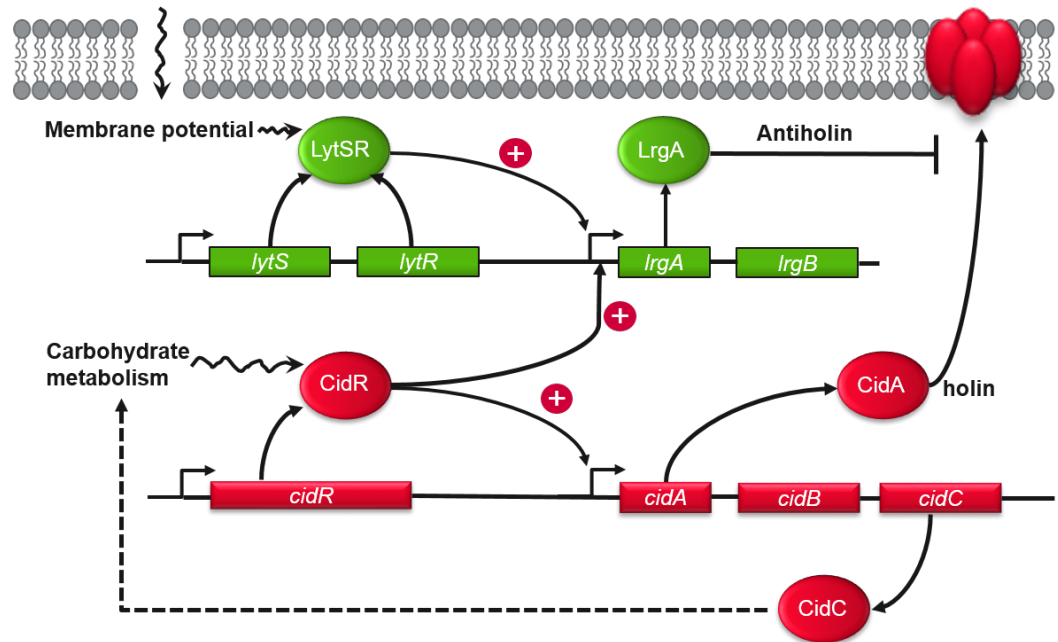
B
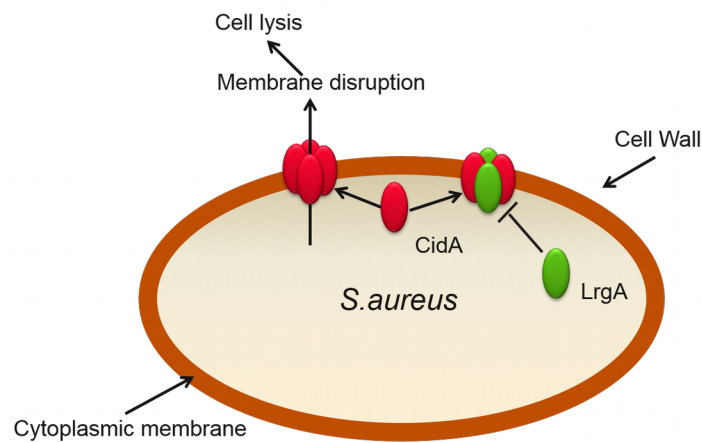
Figure 1.4. Cid/Lrg system. (A) Schematic figure of the regulation network of *cid/lrg*; (B) Proposed mechanism of cell lysis regulated by CidA and LrgA, with CidA being a holin and LrgA being an anti-holin.

1.2.5 Apoptosis in plants and Programmed cell death paradox

Previously we have discussed PCD in mammalians, bacteria and vira system. Not surprisingly, PCD also played an important role in plant development. Although the function of the mitochondria in plant PCD has been demonstrated[74,75], it appears that chloroplasts also have a prominent role as illustrated by the following examples. First, reactive oxygen species (ROS) are involved in various types of PCD, and chloroplasts are the major site of ROS production in plants[76,77]. Many chloroplast expressed genes that are related to plant PCD have been identified.

Interestingly, Bcl-2 family proteins, which are a dominant class of PCD proteins, have not been identified in plant mitochondria. Despite the absence of Bcl-2 paralogs, several studies have demonstrated that the expression of animal Bcl-2 family of proteins in plant cells can both promote and inhibit PCD. For example, overexpression of Bcl-xL and the *Caenorhabditis elegans* homolog Ced-9, suppresses plant cell death[78], whereas overexpression of animal Bax promotes rapid cell death[79]. Moreover, when members of the mitochondria-associated Bcl-2 family of proteins were ectopically expressed in transgenic tobacco (*Nicotiana tabacum*), the Bcl-2 proteins were found to be localized in the chloroplasts as well as the mitochondria, and to regulate PCD induced by chloroplast-targeted herbicides[80]. Thus, although Bcl-2-family proteins have not been identified in plants, these studies suggest that proteins with similar functions to those of the Bcl-2 family exist in plants.

1.2.5.1 AtLrgB and plant programmed cell death

The recent demonstration that a Cid/Lrg ortholog exists in plants suggests that the holin model may apply to these organisms as well. As described above, Bcl-2 family proteins have not been conclusively discovered in plants. However, proteomic studies of Arabidopsis

chloroplast envelope membranes have demonstrated the existence of putative bacterial Cid and Lrg orthologs, suggesting that these novel proteins may have a role in plant PCD[81–83]. In a recent study, the newly discovered protein AtLrgB, was predicted to have a chloroplast transit peptide of 13 amino-acids, and 12 transmembrane helices, five in the N-terminal region and seven in the C-terminal LrgB domain[83]. Sequence analysis suggested that the plant *lrgB* gene may have evolved from a gene fusion of *lrgA* and *lrgB* from bacteria[83]. The subcellular localization of the AtLrgB protein was demonstrated by the fusion of AtLrgB and EGFP. Confirmed by confocal microscopy and protease sensitivity assays, the location of the fusion protein was in the chloroplast inner envelope membrane[83].

AtLrgB mutant generated the phenotype of interveinal chlorotic and premature necrotic leaves, consistent with a role for this gene in plant PCD, as well as changes in carbon partitioning. These leaves also contained large regions of dead cells. Furthermore, overexpression of full-length AtLrgB produced plants exhibiting veinal chlorosis and delayed greening. Also, consistent with the putative membrane-damaging function of the Cid/Lrg protein family as holins/antiholins. (see **Figure 1.5**) AtLrgB could augment nystatin-induced membrane permeability in yeast cells. At this point, however, we cannot exclude the possibility that the effect of the AtLrgB on PCD is indirect, for example, as a result of its potential role in carbohydrate metabolism[83,84].
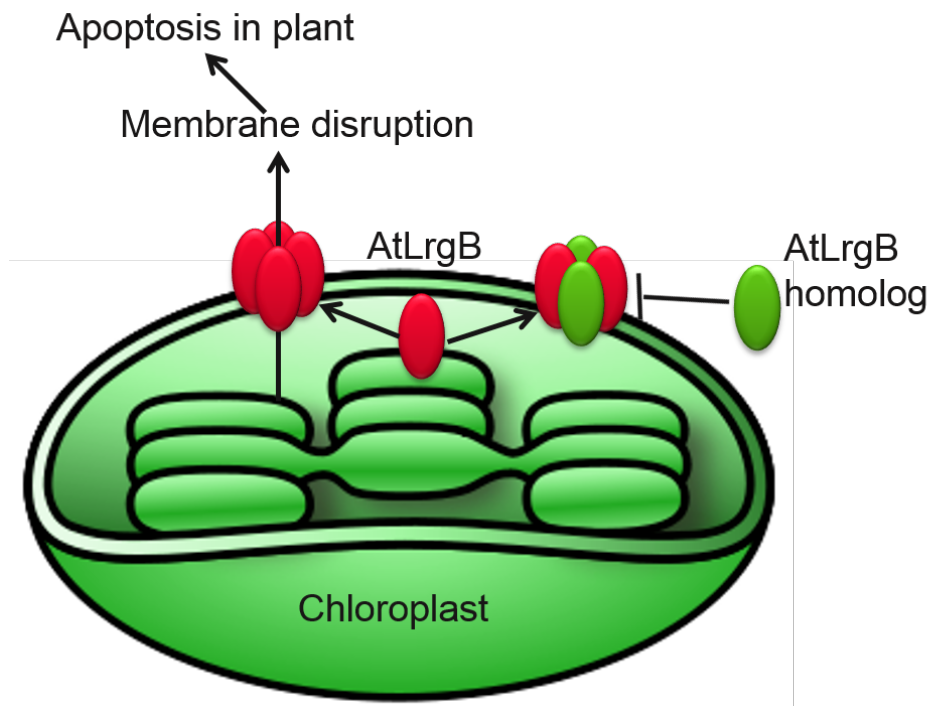
Figure 1.5. Proposed mechanism of apoptosis regulation by AtLrgB in plants.

1.2.5.2 Programmed cell death paradox

It was first proposed in 2003 that the Bcl-2 and holin family of proteins are evolutionarily related functional paralogs[85]. The hypothesis was based on the striking molecular and functional similarities shared by these proteins[4,85]. Both families include small, membrane-associated proteins that oligomerize to form channels or pores that cause permeabilization of biological membrane, and both include structurally similar proteins with opposing functions.

Remarkably, evidence that supports this hypothesis was recently found by demonstrating that the Bcl-2 proteins are able to functionally replace holin system to promote bacterial lysis[86]. These studies not only revealed the oligomerization-dependent lytic activity of Bax/Bak, but also exhibited negative and positive regulation of this activity by Bcl-xL and tBid, respectively, demonstrating that the Bcl-2 family of proteins are functional holins/antiholins and that many molecular components of the apoptotic regulatory machinery might be functionally recapitulated in bacteria.

Also, as discussed previously, Cid/Lrg protein analogs in both bacteria and plant chloroplasts also possess the strikingly similar structural and functional features to Bcl-2 and holins, especially for CidA/LrgA. And they have already been proved to play a critical role in regulating bacterial and plant PCD, respectively. Thus, based on all the evidences, we are are able to expand our hypothesis as bacterial Cid/Lrg, AtLrgB and Bcl-2 together with phage holins belongs to a holin functional superfamily, and their evolutionary origins all come from ancestral bacteria, to function as lysis regulator and release the subsequent signal molecules. *Bcl-2* and *AtLrgB* genes are hypothesized to have been transferred to mitochondria and chloroplast, respectively, during the endosymbiotic process more than a billion years ago.

Apart from membrane-damaging holin-like proteins, PCD, or at least the early events of PCD, have been hypothesized to be caused by abnormality in the carbon metabolism and cellular acidification, the studies on putative pyruvate oxidoreductase CidC in S.aureus have shed light on the molecular mechanism of the PCD induced by acetic acid.

1.3 Enzyme, electron transport chain and flavoproteins

Enzymes are a group of macromolecules that catalyzes chemical reactions, which otherwise will not happen or happen very slowly under physiological conditions. Most enzymes are proteins, although a few are catalytic RNA molecules. Chemically, like any catalyst, enzymes are not consumed during the reaction, nor do they change the equilibrium of the reaction. According to different catalytic mechanisms, enzymes are classified into 6 catergories: Oxidoreductases, Transferases, Hydrolases, Lyases, Isomerases and Ligases. These sections are subdivided by other features such as the substrate, products, and chemical mechanism. Enzymes' specificity comes from their unique three-dimensional structures. They differ from most other catalysts by being much more specific. Enzyme activity can be affected by other molecules: inhibitors are molecules that decrease enzyme activity, and activators are molecules that increase activity. Many drugs and poisons are enzyme inhibitors. Enzymes are evolutionarily designed for certain biological processes, thus each enzyme adapts to its own unique physiological environment, an enzyme's activity decreases markedly outside its optimal temperature and pH.

ETC is a series of peptides and enzymes or enzyme complexes that transfer electrons from electron donors to electron acceptors via redox reactions, and couples this electron transfer with the transfer of protons (H$^+$ ions) across a membrane. Driven by the Gibbs free energy of the reactants and products, each electron donor passes electrons to a more electronegative acceptor, which in turn donates these electrons to another acceptor, a process that continues down the series until electrons are passed to oxygen, the most electronegative

and terminal electron acceptor in the chain. This process creates an electrochemical proton gradient that either drives the synthesis of adenosine triphosphate (ATP) by ATP synthase, which is highly conserved among all domains of lives, or enable mechanical work if the proton flows back through the membrane.

Flavoproteins are proteins that contain a nucleic acid derivative of riboflavin: the flavin adenine dinucleotide (FAD) or flavin mononucleotide (FMN). Flavoproteins are involved in a wide range of biological processes including, but not limited to, bioluminescence, removal of the radicals, DNA repair, energy production (electron transport chain) and apoptosis.

1.3.1 Enzyme and cofactor

Enzymes are usually much larger than their substrates. Thus only a small portion of the enzyme, known as catalytic site, is involved in the catalysis. The catalytic site and substrate-binding site together are called the active site. Other parts of the enzyme help to maintain the precise orientation and dynamics of the active site. Enzyme structures may also contain allosteric sites where the binding of small molecules causes a conformational change that increases or decreases activity. For some enzymes, no amino acids are directly involved in catalysis; instead, the enzyme contains sites to bind and orient catalytic cofactors.

Cofactors or coenzymes are non-protein chemical compounds that acts as helper molecules during biochemical transformations, especially for enzymatic reactions. Cofactors can be subdivided into inorganic ions, such as the metal ions Mg^{2+}, Cu^+, Mn^{2+}, or iron-sulfur clusters, and organic compounds, such as flavin or heme. And in some sources the name "coenzyme" is only for organic compounds. A cofactor that is tightly or even covalently bound to an enzyme is called a "prosthetic group". An inactive enzyme without its cofactor is called "apoenzyme", while the complete enzyme with its cofactor is called "holoenzyme".

Many natural cofactors are soluble vitamin derivatives by phosphorylation. For examples, Nicotinamide adenine dinucleotide (NAD^+) and Nicotinamide adenine dinucleotide phosphate ($NADP^+$) are the phosphorylated products of Vitamin B3, flavin adenine dinuleotide (FAD) and flavin mononucleotide (FMN) are the phosphorylated products of vitamin B2, thiamine pyrophosphate is the phosphorylated product of vitamin B1. The vitamin derived cofactors are actively involved in the chemical reactions that related to biological energy production, they primarily serve as electron shuttles between enzyme complexes in the electron transport chain (ETC).

1.3.2 Electron Transport Chain

Most eukaryotic cells have mitochondria, which produce ATP from products of the citric acid cycle, fatty acid oxidation, and amino acid oxidation. ETC is located at the mitochondria inner membrane, it comprises of multiple enzyme complexes that facilitate the passage of electrons from NADH and succinate to oxygen, which is then reduced to water (**Figure 1.6**). During the process, protons are pumped through complex I, III and IV to the mitochondria intermembrane space, those protons are then transported back to mitochondria matrix by ATP synthase, which uses this proton gradient to make ATP via phosphorylation of ADP.

In prokaryotes, ETCs are more complicated, since there are many different sources of electron donors and acceptors. Individual bacteria often use multiple electron transport chains simultaneously. Bacteria can use a number of different electron donors, a number of different dehydrogenases, a number of different oxidases and reductases, and a number of different electron acceptors. For example, *E. coli* (when growing aerobically using glucose as an energy source) uses two different NADH dehydrogenases and two different quinol oxidases, for a total of four different electron transport chains operating simultaneously.
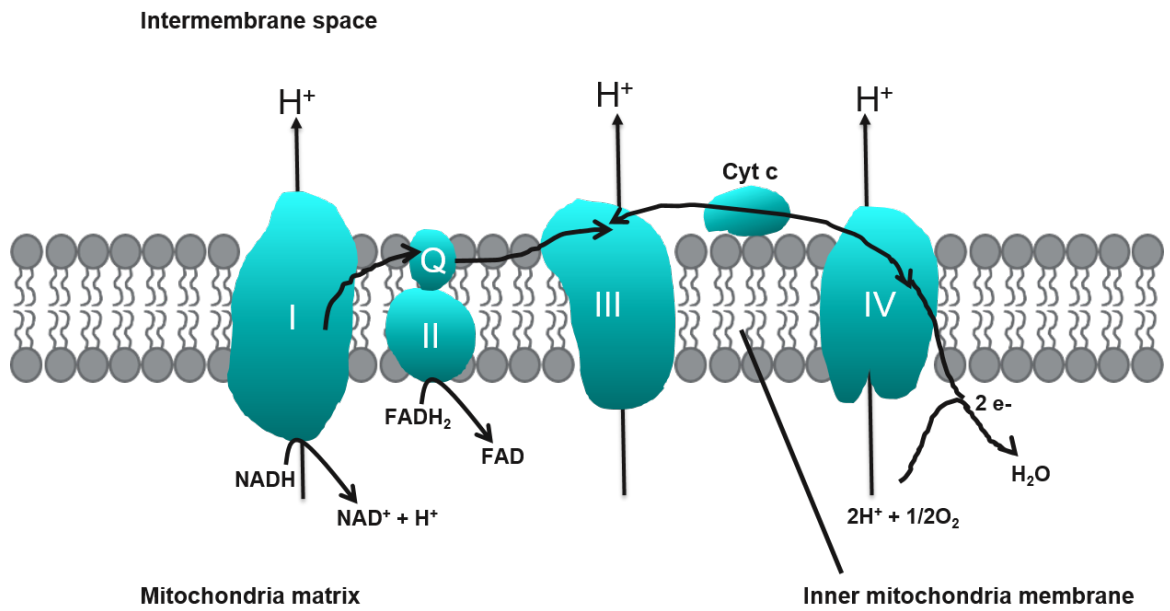
Figure 1.6. The eukaryotes electron transport chain

1.3.3 Flavoprotein and Pyruvate Oxidoreductase

Flavoproteins are proteins that contain a nucleic acid derivative of riboflavin: the flavin adenine dinucleotide (FAD) or flavin mononucleotide (FMN). Flavoproteins are involved in a wide range of biological processes including, but not limited to, bioluminescence, removal of the radicals, DNA repair, energy production and apoptosis. Due to the specific spectrum of flavin cofactors, flavoprotein becomes a natural reporter for changes during chemical reactions, which also makes flavoproteins one of the most studied enzyme families.

Compared to FMN, FAD has an extra adenine monophophate (AMP) group attached to FMN bridged via phosphate groups (**Figure 1.7**). They both function as prosthetic group of various oxidoreductases, During the catalytic cycle, a reversible interconversion of the (oxidized) quinone form (FMN, FAD), semiquinone (FMNH•, FADH•) and (reduced) hydroquinone ($FMNH_2$, $FADH_2$) forms occurs in the various oxidoreductases. FMN/FAD is an aromatic ring system, whereas $FMNH_2$ /$FADH_2$ is not. This means that $FADH_2$ is significantly higher in energy, without the stabilization through resonance that the aromatic structure provides, the change in the redox state of flavin also has great impact on the structure and function of these FMN/FAD binding proteins. Based on the oxidation state, flavins take specific colors in aqueous solution, take FAD as an example, FAD is yellow, FADH• is blue and $FADH_2$ is colorless. The specific spectroscopic properties of FMN/FAD and their variants allows the monitoring of the flavoprotein concentration and the catalyzed reactions using UV-Vis spectroscopy (two peaks at 380nm and 450nm) and fluorescence (Ex 450nm/Em 510-520nm).
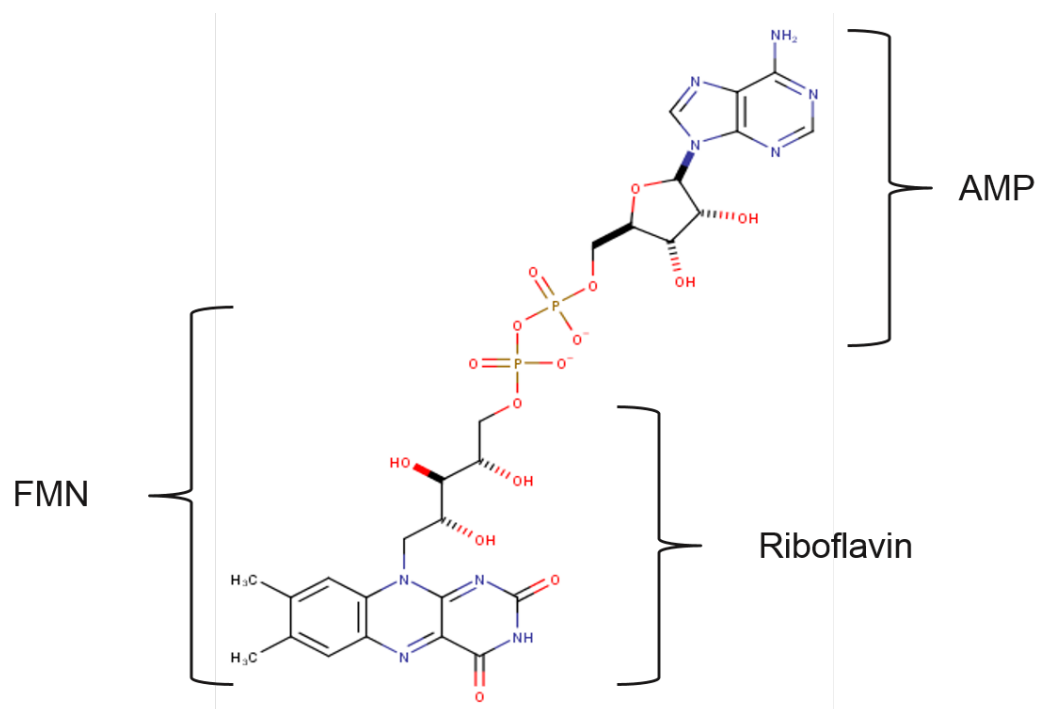
Figure 1.7. Chemical structure of FAD （by Marvin Sketch)

A lot of enzymes which involves in carbon metabolism and energy production utilize FMN/FAD as cofactors. One such well-characterized example is the pyruvate oxidase (POX) from *E.coli* (*Ec*POX), which catalyzes the decarboxylation of pyruvate to produce acetate and CO_2[87,88]. EcPOX noncovalently binds to FAD and thiamine pyrophosphate (TPP) and it has a homotetrameric structure consisting of 62 kDa subunits (572 residues), and when reduced, POX switches from a soluble cytosolic protein to a peripheral membrane-bound ubiquinone oxidoreductase[89–91]. Even though EcPOX is called a pyruvate ''oxidase'', it is well established that the physiological electron acceptor is membrane-bound ubiquinone-8[91–93]. Therefore, this enzyme has been more accurately referred to as a pyruvate:quinone oxidoreductase (PQO)[94]. In contrast, other prokaryotic POX enzymes readily use O_2 as the electron acceptor and are thus true oxidases generating H2O2 during every catalytic cycle[94]. One well-studied example is POX from Lactobacillus plantarum (*Lp*POX)[95], which is a comstitutively active pyruvate oxidase. *Lp*POX not only differs from *Ec*POX in oxygen reactivity, but also uses Pi to produce acetylphosphate[95].

To summarize the activation mechanism of *Ec*POX, the TPP cofactor of *Ec*POX is first reduced by pyruvate with subsequent electron transfer to the FAD cofactor. Reduction of the flavin cofactor then triggers the release of the C-terminal membrane binding domain, thereby opening up the active site which allows for Phe465 to swing into a position that facilities electron transfer from TPP to FAD in subsequent catalytic cycles. This activated conformation of Phe465 in EcPOX is thought to mimic Phe479 in *Lp*POX, explaining similar turnover numbers between the activated form of *Ec*POX and the constitutively active *Lp*POX[96].

CidC, as predicted by the in vivo studies, is a POX (or PQO). The sequence homology between CidC and EcPox is 31.72%. for LpPOX, the value is 33.28%. The

sequence alignment of the three homologous pyruvate oxidase is shown in **Figure 1.8.** Whether CidC is activated by binding to it's substrate and/or cofactors, or it's a constitutively active enzyme, is of great interest to our study.

```
CidC  -MAKIKANEALVKALQAWDIDHLYGIPGDSIDAVVDSLRTVRDQFKFYHVRHEEVASLAA 59
EcPOX --MKQTVAAYIAKTLESAGVKRIWGVTGDSLNGLSDSLNR-MGTIEWMSTRHEEVAAFAA 57
LpPOX MMTKMIAGQALVKVLEAWGVDHIYGIPGGSINHTVEGLYLEKADIDYIQVRHEEVGALAA 60
            *   .   :.*.*::  :.:::*: * *::   :.*      .:: .*****.::**

CidC  AGYTKLTGKIGVALSIGGPGLIHLLNGMYDAKMDNVPQLILSGQTNSTALGTKAFQETNL 119
EcPOX GAEAQLSGELAVCAGSCGPGNLHLINGLFDCHRNHVPVLAIAAHIPSSEIGSGYFQETHP 117
LpPOX SADAKFTGKIGVSFGSAGPGATHLFNGLYDAKMDHVPVLALVGQVPQATMNTNYFQEMDE 120
          .. ::::*::.*. .  ***  **:**::*.: :.** * : .:  .: : :  *** .

CidC  QKLCEDVAVYNHQIEKGDNVFEIVNEAIRTAYEQKGVAVVICPNDLLTEKIKDTTNKPVD 179
EcPOX QELFRECSHYCELVSSPEQIPQVLAIAMRKAVLNRGVSVVVLPGDVALKPAPEGATTHWY 177
LpPOX TPMFSDVAVYNRTVTTAGQLPYVINQAIREAYRQKGPAVVIIPENLSAEEIDYQPVSTPN 180
            :  : : *  . : .   ::   :: *:* *  ::* :**: * ::  :        .

CidC  T-SRPTVVSPKYKDIKKAVKLINKSKKPVMLIGVGAKHAKDELREFIEMAKIPVIHSLPA 238
EcPOX H-APQPVVTPEEEELRKLAQLLRYSSNIALMCGSGCAGAHKELVEFAGKIKAPIVHALRG 236
LpPOX TVSDTFEQRVDPQAITATLKMLKAAKHPLVYAGRGLLGAKADLVKFSEQFNIPVMNTVPA 240
            :       . : :    :::. :.. :  * *   *: :* :*    : *::.:: .

CidC  KTILPDDHPYSIGNLGKIGTKTSYQTMQEADLLIMVGTNYPYVDYLPKKNIKAIQIDTNP 298
EcPOX KEHVEYDNPYDVGMTGLIGFSSGFHTMMMNADTLVLLGTQFPYRAFYPT-DAKIIQIDINP 295
LpPOX TGVIPTSHPNAIGTFGRLGSKSGFEALQHADLILFLGSEFPFASFWPK-GIKIIQVNNNS 299
            .  :  ..* :*  * :*  .:.:.:: .** ::::*:::*:  : *.   * **:: *

CidC  KNIGHRFNINVGIVGDSKIALHQLTENIKHVAERPFLNKTLERKAVWDKWMEQDKNNNSK 358
EcPOX ASIGAHSKVDMALVGDIKSTLRALLPLVEEKADRKFLDKALEDYRDARKGLDDLAKPSEK 355
LpPOX FDIGKMVPIDYAVISDAQAYLQAMIATGETLPETAWLTTNRQNKRNWDKWLQQLAADDHD 359
            .**     :: .::.* : *:  :    : : :*  .  :       * :::    . .

CidC  PLRPERLMASINKFIKDDAVISADVGTATVWSTRYLNLGVNNKFIISSWLGTMGCGLPGA 418
EcPOX AIHPQYLAQQISHFAADDAIFTCDVGTPTVWAARYLKMNGKRRLLGSFNHGSMANAMPQA 415
LpPOX GLAPEAVMHKVASMVGPRDTYGVDTGNVSEWAVRGLPMDQEQRFALSGLFATMGFGLPAG 419
            : *: : .: :       *.*. : *:.* * : :.:: *   .:*. .:* .

CidC  IASKIAYPNRQAIAIAGDGAFQMVMQDFATAVQYDLPLTVFVLNNKQLAFIKYEQQAAGE 478
EcPOX LGAQATEPERQVVAMCGDGGFSMLMGDFLSVVQMKLPVKIVVFNNSVLGFVAMEMKAGGY 475
LpPOX MAGALSVPDSQAWSFSGDGGFAMVAPDIITEARYGLPVINVIFSNQRFGFIYREQVDTKQ 479
            :..  : *: *. ::.***.* *:  *: : .:  **: .:::.*. :.*:  *

CidC  LEYAVDFSDMDHAKFAEAAGGKGYTIKSASEVDAIVEEALAQD-----VPTIVDVYVDPN 533
EcPOX LTDGTELHDTNFARIAEACGITGIRVEKASEVDEALQRAFSID-----GPVLVDVVVAKE 530
LpPOX HLYGVDLTDADWAKVADGLGGIGFTVQNNQEVETVFDQIKALQAKGNKRPIVVNAVI-KN 538
             ..:: * : *:.*:. *  *  ::. .**: .:. : :      * :*:. : :

CidC  AAPLPGKIVNEEALGYGKWAFRSITEDKHLDLDQIPPISVAAKRFL--- 579
EcPOX ELAIPPQIKLEQAKGFSLYMLRAIISGRGDEVIELAKTNWLR------- 572
LpPOX DDPIGTAYMPLDPELYGQAEVDAYAKANHIDIKEQPSLGALLRAQGDQL 587
             :       :  :.   . :  .. ::  :
```

Figure 1.8 Sequence alignment of CidC, *Ec*POX and *Lp*POX. * indicate the identity (same amino acids)

1.3 Thrombin-binding aptamer G-quadruplex

G-quadruplexes constitute a unique class of highlyordered nucleic acids structures with various folding topologies and molecularities. They are present in naturally occurring nucleic acids, telomere and promoter region, and play important regulatory functions in many biological processes[97–100]. The occurrence of quadruplex structures in genomes of diverse organisms suggested the possibility to design potential drug components targeted towards G-quadruplexes or based on RNA or DNA G-quartets. The 15-mer DNA oligonucleotide 5'-GGTTGGTGTGGTTGG-3' is a thrombin binding aptamer (TBA), which was discovered in 1992 by in vitro selection and found to inhibit fibrin-clot formation by binding to the thrombin protein exocite I and II with high selectivity and affinity[101–103]. NMR and X-ray structural studies showed that TBA forms an intramolecular, antiparallel G-quadruplex with a chair-like conformation[102,104]. The core of the quadruplex consists of two G-quartets connected by three edge-wise loops: a central TGT loop and two TT loops (**Figure 1.9**). The aptamer interacts with two thrombin molecules but inactivates only one of them[102]. X-ray studies indicated that inhibition of fibrinogen-clotting is a consequence of specific blocking of the thrombin anion exosite I conducted by the central TGT loop. In the same studies it was also further reported that the two TT loops are involved in ionic interactions with the positive-charged heparin binding site of a second thrombin molecule to compensate the residual negative charge of the aptamer.

TBA G-quadruplex adopts a antiparallel conformation in the presence of cation including K^+, Rb^+, NH_4^+, Ba^{2+}, and Sr^{2+}, however, other cations like Li^+, Na^+, Cs^+, Mg^{2+}, and Ca^{2+} do not work as efficient in stabilizing the quadruplex. Since the cations are coordinated to guanine O6 carbonyl groups between the planes of neighboring guanine quartets, it has been observed that only metal ions with ionic radii in the range 1.3-1.5 Å fit well within the two G-quartets of the complex[105,106].

Although several efforts have been deployed to improve the binding properties of TBA to thrombin[107,108], there is still room for improvement to aim for a better therapeutic strategy. The awareness to fully understand the thermostability of the molecule, is essential for understanding its biological activity and useful in the future development of oligonucleotide-based therapeutics or drug design.

5'-GGTTGGTGTGGTTGG-3'
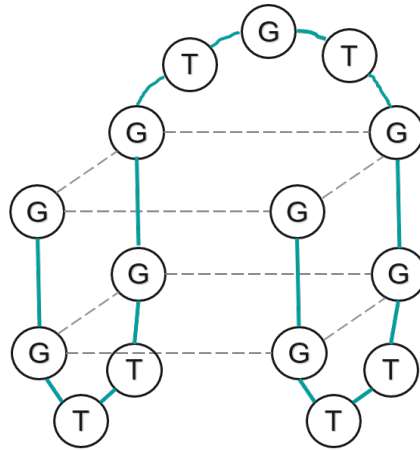
Figure 1.9 Schematic figure of G2 quadruplex

1.4 Objective of the study

The goal of the CidA/LrgA/CidC project to structurally and functionally characterize Cid/Lrg proteins with biochemical and biophysical methods in the context of purified proteins, with focus on CidA/LrgA and CidC. Regarding CidA/LrgA, it is hypothesized that CidA/LrgA form nanometer-size pores and thus leading to the membrane permeabilization of small molecules. To test this hypothesis, CidA/LrgA are successfully purified and reconstituted into the lipid membrane, then entrap several fluorescent dyes/proteins into the liposome to gauge the size of the pores that CidA/LrgA form. In terms of CidC, the hypothesis is that CidC converts pyruvate to acetic acid in vitro and it is a peripheral membrane enzyme, and it participate in a specific electron transport chain in *S.aureus*. To test the hypothesis, CidC was also purified and the purified enzyme was applied to subsequent biochemical and biophysical tests.

The goal of the thrombin binding aptamer G-quadruplex project is to study the conformation and thermostability changes under the condition when two single strands are attached to the 5' and 3' ends of the G-quadruplex, this could provide valuable indications on how the flanking sequence affects the stability of a G-quadruplex. The hypothesis is that one of the single strand has a deleterious effect on the formation of G-quadruplex, whereas its complementary strand will rescue the G-quadruplex when both of them are attached.

Chapter 2

Methods and Materials

2.1 Materials

2.1.1 Protein Expression

2.1.1.1 Plasmid

DNA genes optimized for the bacterial expression of the 131 amino acids long *S.aureus* CidA and 147 amino acids long LrgA were gifts kindly offered by Dr. Kenneth Bayles's Lab. These genes were cloned into pET24b vector (Novagen), generating C-terminal 6X His tag fusions. *cidA* and *lrgA* were amplified using forward primers containing an NdeI restriction site and reverse primers containing an XhoI site. For protein production, the resulting plasmids were transferred into *E. coli* strain C43, a mutant derivative of BL21(DE3) selected for optimal overproduction of membrane proteins[8,109].

2.1.1.2 Cell culture media

2 x TY medium was prepared as following: 12 g typtone, 7.5 g yeast extract, 3.75 g NaCl were dissolved in 750ml H_2O. The medium was then sterilized by autoclaving and cooled down to room temperature before use. All chemicals and isopropyl β-D-1-thiogalactopyranoside (IPTG) were purchased from Fisher Scientific.

2.1.2 Protein Purification

2.1.2.1 Detergents

SDS and Triton X-100 were purchased from Fisher Scientific. Empigen BB was purchased from Sigma Aldrich. B-octyl-glucoside (OG), DDM were purchased from Anatrace.

2.1.2.2 Chromatography Columns

HisPrepTM FF16/10, a ready-to-use column, prepacked with precharged Ni Sepharose 6 Fast Flow was purchased from GE Healthcare. Superdex 200 Increase 10/300 GL (prepacked gel filtration columns) was purchased from GE Healthcare.
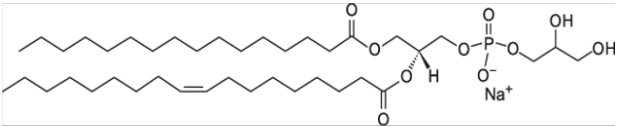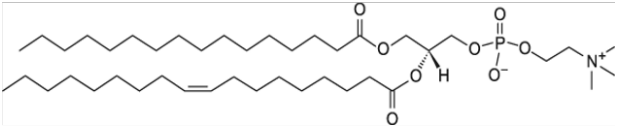
2.1.2.2 Chemicals

The Penta-His Antibody from Thermo Scientific (Waltham, MA) was used for western blot detection. Glucose oxidase from Aspergillus niger (160 kDa) and human serum albumin (66.5 kDa) were purchased from Sigma Aldrich. Tris(hydroxymethyl)aminomethane (Tris), urea, imidazole, ethylenediaminetetraacetic acid (EDTA), formic acid, acetonitrile and methanol and all other chemicals were all purchased from Fisher Scientific.

2.1.3 Membrane Reconstitution

2.1.3.1 Lipids

All the lipids were purchased from Avanti Polar Lipids. The name and molecular structures of the lipids were listed in **Table 2.1**. Lipids were dissolved in chloroform and kept in -20º C.

Name	Molecular Structure
1-palmitoyl-2-oleoyl-*sn*-glycero-3-phospho-(1'-*rac*-glycerol) POPG PG (16:0-18:1)	
1-palmitoyl-2-oleoyl-*sn*-glycero-3-phosphocholine POPC PC (16:0-18:1)	

Table 2.1 Lipids used in CidA/LrgA/CidC reconstitution

2.1.3.2 Other

Standard regenerated cellulose dialysis membrane tubing with cutoff of 10KD was purchased from Spectrum Labs. 5nm Ni-NTA-Nanogold for labeling of protein and NanoVan for negative staining were purchased from Nanoprobes.

2.2 Methods

2.2.1 Overexpression of Recombinant Protein

Proteins has essential roles in all kinds of forms of lives by playing roles like transporters, enzymes, transcriptional factors, receptors, etc[110,111]. The funtions and structures of a protein can be related by various techniques in vivo and in vitro. In vivo experiments provide information about the biological role of a protein in the context of a cell, tissue, organ or even whole organism and can be performed by manipulating the expression level or mutating protein[112,113]. To perform in vitro functional or structural studies, proteins need to be isolated away from other cellular components and prepared in relatively large quantities. Some proteins such as human growth hormone, monoclonal antibodies and insulin have very important therapeutic applications and are widely used for clinical treatment. Thus, overexpression of these proteins in vitro is of critical significance to both the biotechnology and medicine[114].

Recombinant DNA is a form of artificial DNA that is created by combining two or more DNA sequences via engineering methods. Generally, overexpression of the target protein is achieved by inserting genes encoding proteins of interest into special vectors to produce large amount of the desired protein. Overexpression can be achieved in several host expression system: bacterial, yeast, insects and mammalian cells[115–117]. An appropriate expression system is selected based on the features and intended applications of the recombinant protein. The cost and expression level of the expression system should also be taken into consideration.

Gram-negative bacterium *E.coli* remains to be one of the most efficient systems available for heterologous protein production due to several advantages: (a) the ability to grow rapidly and at high density on cheap substrates, (b) well-characterized genome

(proteome) and (c) increasingly large number of available cloning vectors and mutant host strains. pET system is a series of commercially available vector for the production of proteins fused with ketosteroid isomerase (KSI) and a 6x histidine tag in *E.coli*. After cloning of the gene of interest, they are transformed into a host bearing the T7 RNA polymerase gene such as BL21 (DE3) *E.coli* for expression. The expression of T7 polymerase in the host cell is controlled by lac promoter. Addition of IPTG releases the lac repressor, thereby allowing the transcription of T7 polymerase. T7 polymerase is selective and active that almost all of the cell's resources are converted to the overexpression of the target gene[118,119].

2.2.2 Protein Purification

Currently, a number of protein purification techniques are frequently used based on the properties of a protein such as solubility, size, charge, hydrophobicity and affinity towards specific ligands.

2.2.2.1 Affinity Chromatography (AC)

Recombinant protein is usually expressed with a fusion tag located either on the C- or N-terminus. The tags include glutathione s-transferase (GST), FLAG peptide, or a hexa-his peptide which each has high binding affinity for a specific ligand[112,120,121]. For example, GST binds strongly to glutathione and the hexa-his peptide strongly chelate with metal ions like nickel and cobalt. The protein purification is accomplished by loading the clarified cell lysate onto a column prepacked with resins conjugated with the corresponding ligand. Proteins with the correct fusion tag bind to the ligand and other proteins are washed away. At most times, the binding is dependent on the binding buffer. The target protein can be eluted by competing ligands such as salt or imidazole. If necessary, the tags can be removed by some proteases after expression if cleavage sites have been engineered along with the fusion proteins[122].

2.2.2.2 Gel Filtration Chromatography (GFC)

GF separates molecules according to their sizes. GF columns are usually packed with porous beads in the form of spherical particles that have been chosen due their chemical and physical stability, and inertness (low reactivity and absorption). When the sample is applied onto the column, molecules diffuse in and out of the pores of the beads matrix. Molecules that are larger than the pores are unable to diffuse inside of the pores and thus pass through the column fast, whereas smaller molecules move further inside the matrix and thus are delayed in their passage down the column. Thus, separation of molecules based on their size is accomplished. Compared with other purification techniques, GFC is less dependent on the

buffer conditions[123,124].

2.2.3 Protein characterization

Purity, mass, and amino acid N-terminal sequencing of the target protein are characterized using techniques listed below.

2.2.3.1 SDS-PAGE

SDS-PAGE is profoundly used to separate biological macromolecules like proteins and nucleic acids, based on their electrophoretic mobility which is a complex function of the size and conformation of the molecules. It can be used to test the composition of a protein sample by staining the gel with non-selective dyes such as Coomassie blue or silver. SDS-PAGE is also the first separation/purification step for other experiments such as western blot and mass spectrometry.

Generally, to make a SDS-PAGE sample, proteins are dissolved firstly in a loading buffer containing Tris-Hcl, glycerol, SDS and bromophenolblue. Sometimes, dithiothreitol or beta-mercaptoethanol is added to break the disulfide bonds. Boiling the sample also helps to break large oligomers. SDS linearizes proteins and imparts negative charges to the unfolded proteins. In most proteins, the stoichiometric binding of SDS molecules to the polypeptide chain imparts an even distribution of negative charges per unit mass, and leads to a fractionation of the proteins according to molecular weight. For some membrane proteins which are resistant to SDS denaturation, the results of SDS-PAGE should be treated carefully due to the variability in the ratio of bound SDS.

The gel typically is prepared by cross-linking acrylamide and bisacrylamide in a SDS buffer at certain pH. Free radicals and stabilizer, such as ammonium persulfate, TEMED is then added to initiate the polymerization. Bisacrylamide crosslinks linear polymers of

polyacrylamide concentration of the gel, generally in the range between 5% and 25%. Lower percentae gels with larger pores are better for resolving high molecules, while higher percentages gel with smaller pores is required to resolve smaller proteins.

An electric field voltage is applied and the negatively charged proteins migrate across the gel. The rate of migration is mainly dependent on their sizes. Small molecules move more quickly, whereas larger ones tend to be delayed. Biomolecules are therefore separated roughly according to size, which depends mainly on molecular weight under denaturing conditions, and conformation under native conditions.

2.2.3.2 Western blot

After the proteins are separated on the gel, western blot is another method besides staining which can also be used to "visualize" the proteins. Staining the protein gel with Commassie blue or other dyes is not selective and all the proteins in the mixture will be stained. However, by using a western blot, we are able to identify specific proteins from a complex mixture of proteins with specific antibodies. To achieve this, after SDS-PAGE, the proteins are firstly transferred to a nitrocellulose or polyvinylidene fluoride (PVDF) membrane via an electrical current. The membrane is then blocked with non-fat milk or BSA (Cohn fraction V) in order to prevent non-specific background binding. The membrane is subjected to staining with primary antibodies specific to the protein of interest under gentle agitation. Some of the antibodies will bind with specific proteins and unbound antibodies will be washed away. Secondary antibodies linked to biotin or to a reporter enzyme such as alkaline phosphatase or horseradish peroxidase (HRP) is applied to target the primary antibodies for further detection[125,126].

We used in our experiment anti-His antibodies directly conjugated to HRP to identify the proteins with 6x His tag. To detect the HRP, a mixture of 4-chloro-1-naphthol (CN) and

3,3'-diaminobenzidine (DAB) is used. HRP converts CN to a purple-colored precipitate on the blot that is readily visible to the eye. HRP also reacts with DAB to form a visible insoluble product. The combination of DAB and CN has a synergistic effect resulting in greater sensitivity than either reagent alone.

2.2.3.3 N-terminal protein sequencing

Edman degradation is performed to determine the exact sequence of amino acids at the N terminus of the protein and was developed by Pehr Edman. The principle is depicted below in **Figure 2.1**. Generally speaking, uncharged terminal amino group is reacted with phenylisothiocyanate under basic conditions, leading to the formation of a cyclical phenylthiocarbamoyl derivative. The amino acid is cleaved off in trifluoroacetic acid, as its nilinothialinone derivative which is selectively extracted into an organic solvent and converted to a more stable phenylthiohydantoin derivative (PTH-amino acid) when treated with 25% TFA/water. The PTH-amino acid is subjected to HPLC for analysis and quantification. A mixture of 19 PTH-amino acids is also injected onto the column and the resultant chromatogram provides standard retention time of each amino acid. The amino acid for the particular residue is determined by comparing each Edman degradation cycle chromatogram with the standard one. The procedure is repeated to provide the N-terminal sequence of the protein/peptide.
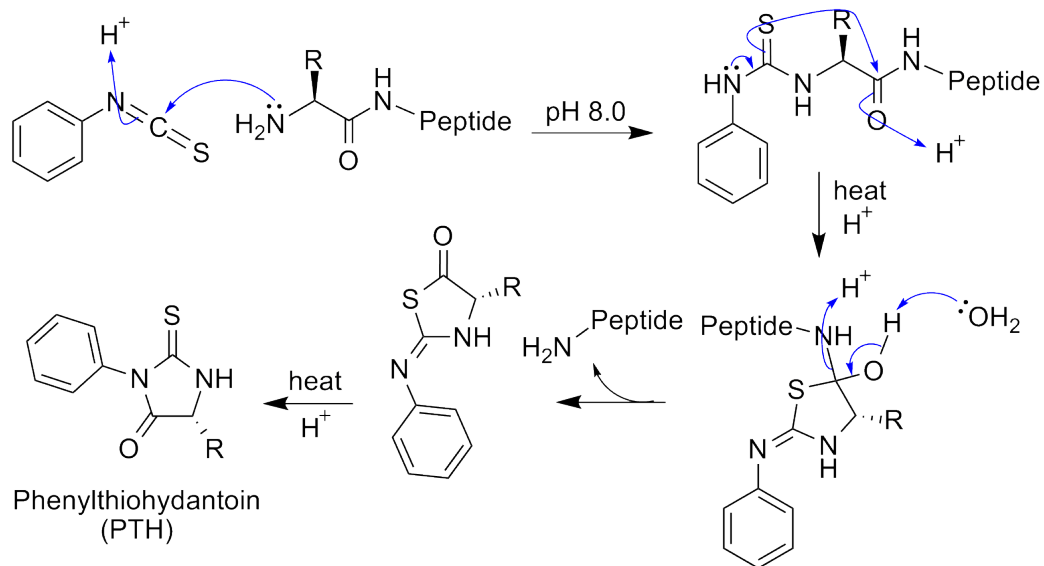
Figure 2.1 Edman degradation of a peptide. Phenylisothiocyanate first reacts with the amino acid residue at the N-terminaus at pH 8.0, forming a phenylthiocarbamyl derivative. Trifluoroacetic acid then cleaves off the first amino acid as its anilinothialinone derivative. The ATZ-amino acid is then converted to a phenylthiohydantoin derivative (PTH-amino acid) with 25% TFA/water.

2.2.4 Membrane Reconsititution

Purified membrane protein or synthesized hydrophobic peptides obtained from above procedures are functional only when they are inserted into biological lipid membranes. The reincorporation of membrane protein into an artificial membrane system facilitates the studies of both function and conformation of the proteins. The useof membrane with different phospholipid composition allow us to understand the significance of the specific lipids environment on protein function and structure. Several methods used for the reconstitution of full length membrane proteins and small peptides in this project are described below.

2.2.4.1 Detergent dialysis

As described in the introduction part, solubilization of cell membrane by detergents is accomplished via a three-stage model. It is generally accepted that detergent-mediated reconstitution of membrane protein into liposomes is the reversal process of the solubilization process. Initially, lipid and protein dissolved in detergents are fully mixed, allowing the formation of lipid protein-detergent micelles. Detergents are then removed via direct dilution, membrane dialysis or gel filtration. At a certain point (below the CMC of the detergents), the lipids self-assemble into liposomes with proteins incorporated into it. Residual detergents are further removed via dialysis, gel filtration chromatography, etc. Mild detergents such as nonionic detergents which do not denature the proteins are mostly used in this method.

2.2.4.2 Solvent injection

Solvent injection is a novel technique demonstrated to reintroduce membrane protein into liposomes. However, due to the denaturing effect of organic solvents to proteins, this method is mostly applied in the studies of small peptides representing the membrane part of membrane proteins. Several kinds of solvent such as acetone, ethanol, isopropanol and methanol can be used in the method and the choice is largely dependent on the solubility of

the peptides and lipids. The liposomes are prepared by rapidly injecting into water the mixture of lipids and peptides solubilized in water-miscible solvents. The size of the resultant liposomes can be controlled by adjusting the preparation conditions including: (I) injected amount of solvent; (ii) lipid concentration; (iii) emulsifier concentration in the aqueous phase.

2.2.5 Proteoliposomes characterization

The conformation of the protein, the phase behavior of lipid bilayer, and size as well as the morphology of the liposomes will be characterized using the technique listed below.

2.2.5.1 Circular dichroism (CD) spectroscopy

CD has been increasingly recognized as valuable technique for examining the structure of proteins in solution. The principle and basis of CD approach is summarized below.

Circularly polarized light occurs when the direction of the electric field vector rotates about its propagation direction while the vector retains constant magnitude, the electric field vector can either rotate counter-clockwise (left handed, L) or clockwise (right handed R). Chiral molecules such as proteins absorb the two components differently when the light goes through the molecules. Circular dichroism is defined as the difference in absorbance of left-handed and right-handed circularly polarized light, as follows:

$CD = A_L - A_R$; (**Equation 2.1**)

in which CD represents the circular dichroism signal or the delta absorbance; A_L and A_R are the absorbance of left-handed and right-handed circularly polarized light, respectively. The CD signal can be further converted to ellipticity (the arc-tangent of the ratio of the mninor eaxis to the major axis of the elliptical polarized light) which can be calculated from CD using the following equation:

$\theta = 2.303 * CD * 180/4\pi$ (**Equation 2.2**).

CD spectra is then obtained by measuring circular dichroism as a function of wavelength. These spectra allow us to determine the conformation of the peptides or protein. Typical far UV CD spectra associated with various types of structure are shown in **Figure 2.2**.
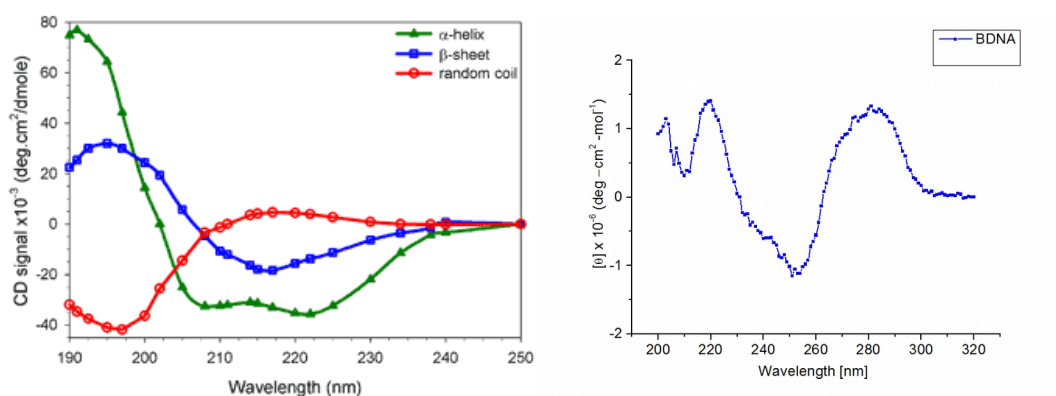
Figure 2.2 Typical CD spectra of protein and B-DNA secondary structures

2.2.5.2 Transmission Electron Microscopy (TEM)

TEM is an imaging technique which utilizes electrons as source rather than light. According to Rayleigh criterion, the resolution of a light microscope is limited by the wavelength of light source. The much lower wavelength electrons enables TEM resolutions which are a thousand times better than with a light microscope[127].

Generally, electrons emitted at the top of the microscope are focused into a very thin beam by electromagnetic lenses. The electron beam then hits a very thin specimen which has been deposited on a supporting grid. According to the density and nature of the material present in different region of the grid, the electrons which pass through the specimen hit a fluorescent screen, generating a "shadow image" of the specimen. The image can then be directly recorded with a camera equipped with a special sensor.

Two types of staining are commonly used to improve the contrast in TEM: positive and negative staining. Positive stains have affinity for the material itself while in negative stains, the biological object is surrounded or embed object in a suitable electrondense material which provides high contrast and appear brighter against the dark background. Commonly used stains include uranyl acetate (positive stain), sodium (potassium) phospotungstate (negative stain), NanoVan (negative stain), etc[127].

2.2.6 Enzymatic activity and binding assay

2.2.6.1 Enzymatic activity

Enzyme activity = moles of substrate converted per unit time = rate × reaction volume. Enzyme activity is a measure of the quantity of active enzyme present and is thus dependent on conditions, which should be specified. The SI unit is the katal, 1 katal = 1 mol

s^{-1}, but this is an excessively large unit. A more practical and commonly used value is enzyme unit (U) = 1 μmol min^{-1}. 1 U corresponds to 16.67 nanokatals.

The specific activity of an enzyme is another common unit. This is the activity of an enzyme per milligram of total protein (expressed in U/mg). Specific activity is a measure of enzyme activity as well as purity in the mixture. It is the moles of product produced by an enzyme in a given period of time (minutes) under given conditions per milligram of total proteins. Specific activity is a measure of enzyme processivity, at a specific (usually saturating) substrate concentration, and is usually constant for a pure enzyme.

An increased amount of substrate [S] will increase the rate of reaction with enzymes, however once past a certain point, the rate of reaction (v) will level out because the amount of active sites available has been saturated by the substrate, as shown in **Figure 2.3**.
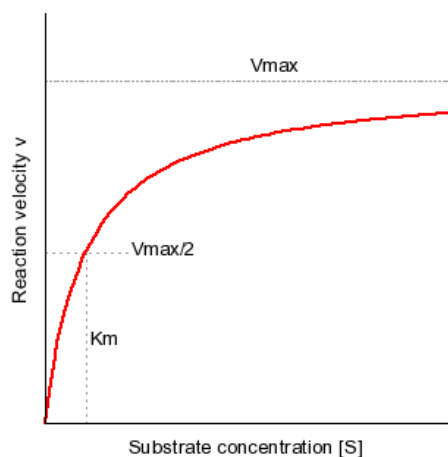
Figure 2.3 This is a plot of the Michaelis-Menten equation predicted reaction velocity as a function of substrate concentration, with the significance of the kinetic parameters V_{max} and K_M graphically depicted.

In biochemistry, the best known models of enzymatic kinetics which relates v to [S] is called Michaelis-Menten (MM) Equation[128]. Typically, in a first order enzymatic reaction (single substrate), the following situation is thought to occur:

$$E+S \leftrightarrow ES \rightarrow E+P$$ **Equation 2.1**

In **Equation 2.1,** E stands for the enzyme, S stands for the substrate, ES is the enzyme-sustrate complex and P is the product, for each reaction. This equation includes the assumption that during the early stages of the reaction, so little product is formed that the reverse reaction (product combining with enzyme and re-forming substrate) can be ignored (hence the unidirectional arrow to E+P). Another assumption is that the concentration of substrate is much greater than that of total enzyme ([S] >> [Et]), so [S] can essentially be treated as a constant.

Another important assumption of the MM equation is that the initial rate of the formation of [ES] is equals to that of the break down of [ES]. And [ES] is always equal to the total enzyme [E_t] substracted by the free enzyme [E]. Through a serial mathematical derivation, we have:

$$v = \frac{V_{max}[S]}{K_M + [S]}$$

Equation 2.2

Here, v stands for the rate of the reaction. V_{max} represents the maximum velocity achieved by the system, at maximum (saturating) substrate concentrations. K_M (the Michaelis constant; sometimes represented as K_S instead) is the substrate concentration at which the reaction velocity is 50% of the V_{max} (see **Figure 2.3**). [S] is the concentration of the substrate S.

Another two important parameters that can be derived from MM equation are K_{cat} and K_{cat}/K_m. Kcat is the "turnover number" and can be calculated as $V_{max}/[E_t]$ and its units are 1/seconds. It basically describes how much substrate is converted to product in one second.

K_{cat}/K_m is the specificity constant. It is a measure of "catalytic efficiency" which means how fast in M/seconds the enzyme reacts with the substrate once it encounters the substrate. Usually, the upper limit of K_{cat}/K_m is diffusion because the substrate has to diffuse and collide with the enzyme and fit into the active site before it can be converted into product.

2.2.6.2 Isothermal titration calorimetry (ITC)

A complete set of thermodynamic binding profiles (ΔG, ΔH, ΔS) as well as the stoichiometry (n) and binding affinity (K_b) that characterizes the interaction between a ligand and a macromolecular can be obtained using ITC[129]. An Omega isothermal titration calorimeter from Microcal (Northamptorn, MA), consisting of two cells (a sample and a reference cell) enclosed in an adiabatic compartment, and a titrating syringe that is inserted into the sample cell was used for all ITC experiments (**Figure 2.4**).

In a typical ITC experiment, the instrument is calibrated by means of a series of known standard electrical pulses that produce a given heat in microcalories for each pulse. After calibration of the instrument, 250 μl of substrate solution are placed in the reaction cell. This solution is titrated with a protein solution, placed in a 40 μl syringe, at a certain concentration. Typically, a computer-controlled stepper motor makes several injections of the syringe solution, at a temperature where the protein is stable. Complete mixing is accomplished by stirring the syringe at 750 rpm. The heat absorbed or released in each injection is measured by a thermoelectric device connected to a preamplifier. By observing the pattern of the injection generated heat, we can obtain a qualitative profile of the binding of the protein to its ligand. (As mentioned, ITC is mostly used as a quantitative technique which

we use to calculate the enthalpy and binding affinity, however, due to the stability issue of some protein/peptide, such complete binding profile can not be easily obtained).
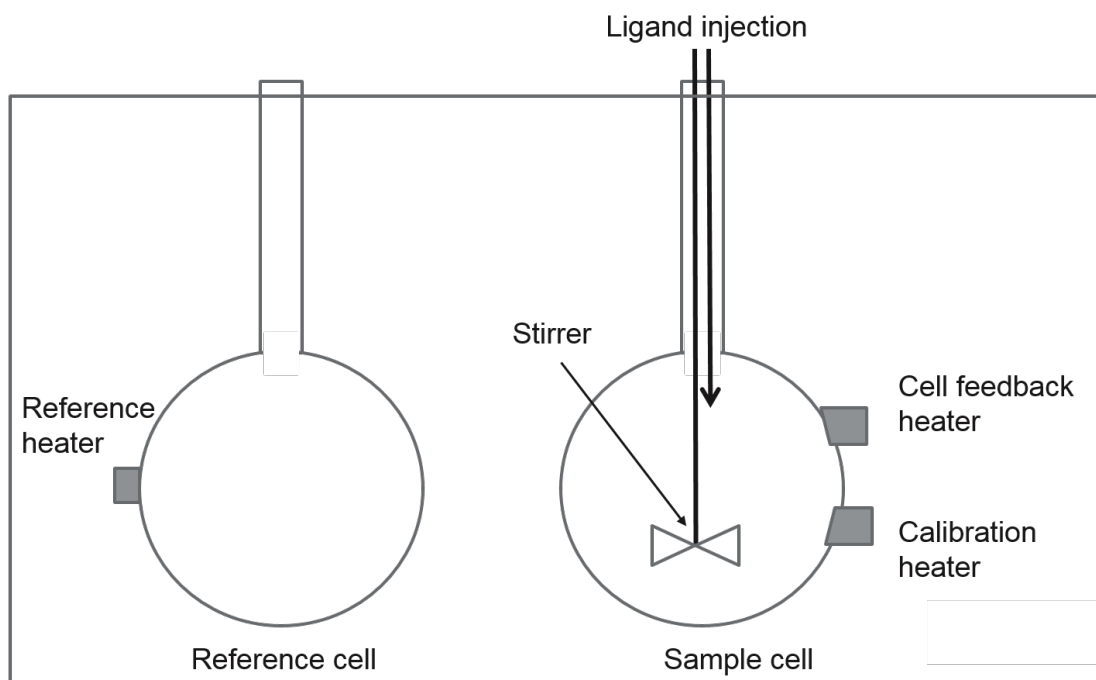
Figure 2.4 The typical set up of ITC experiment

2.2.7 DNA thermostability assays

2.2.7.1 Temperature-dependent UV spectroscopy

Absorbance versus temperature profiles (melting curves) for the helix to coil transition of DNA complexes were measured with a thermoelectrically controlled Aviv 14-DS spectrophotometer (Lakewood, NJ), or Lambda 10 Perkin-Elmer spectrophotometer, each interfaced to a PC computer for acquisition and analysis of experimental data. Water condensation on the exterior of the cuvette, at low temperatures, was removed by flushing the chamber with a constant stream of dry nitrogen gas. Nucleotide bases of DNA absorb light in the far UV region, and the absorbance was monitored at 260 nm and 295 nm, depending on the sequence of the oligonucleotide, while the temperature was increased at a constant rate of $0.5\ ^{\circ}C/min$. The structure of G-quadruplex, or the DNA double helical structure, is such that its aromatic bases are stacked while the sugar phsphate backbone is exposed to the solvent. Upon folding, the nucleotide bases are exposed to the solvent, yielding a hyperchromic effect, i.e., increase in absorbance at 260 nm, or a hyperchromic effect at 295nm for G-quadruplex. Therefore, these melting curves allow us to directly monitor the helix-coil transition of a given G-quadruplex or oligonucleotide.

The melting curve begins at low temperature, where the oligomer is in a helical state, i.e., the bases are away from the solvent and therefore the absorbance is low. As the temperature is increased, the nucleotide bases are exposed to the solvent resulting in a hyperchromic effect for a typical duplex DNA. As we reach higher temperatures, the oligomer transitions to the random coil state i.e., all nucleotide bases are exposed to the solvent and thus a plateau in absorbance is observed at 295 nm, so the UV melting curve begins at a higher absorbance and decreases until the random coil state is reached. Additionally, it is not

uncommon for a slight increase in the absorbance as temperature is increased beyond the coil state, due to a shift in the UV spectrum at high temperatures. From these experiments we can obtain standard thermodynamic parameters such as, the thermo stability or T_M, as well as model dependent parameters (van't Hoff enthalpy, free energy and entropy).

2.2.7.2 Differential Scanning Calorimetry

The total heat of the helix → coil transition of each G-quadruplex was measured directly with a Microcal VP-DSC (Northampton, MA) differential scanning calorimeter (DSC). In general, the DSC measures the aprent molar heat capacity of a given macromolecule as a function of temperature[130]. A typical DSC instrument consists of two cells: the sample cell, containing the matching buffer solution. Both cells are enclosed in an adiabatic compartment and heated at a constant rate (typically 60 ºC per hour), while the differential temperature between the reference and the sample cells is maintained at zero. When a temperature induced process takes place in the sample cell, the instrument compensates by adding or substracting electrical power (depending on whether the process is endothermic or exothermic) to the sample cell in order to maintain a differential temperature of zero. The instrument records this electric power difference, which is proportional to the difference in the apparent heat capacity between the sample and reference cells (ΔC_p^a), i.e. the changes in heat capacity that occur during a helix → coil transition. The resulting ΔC_p^a is plotted as a function of temperature and normalized for the heating rate. A buffer versus buffer scan is then substracted from the sample versus buffer scan, resulting in a typical bell shaped curve from which model-independent thermodynamics profiles are obtained. The T_M is obtained from the peak of the calorimetric curve and the enthalpy and entropy of unfolding are obtained from the area under the curve. ΔS is obtained from the area under the curve of plots of $\Delta C_p/T$ verus T. The resulting ΔH and ΔS are calculated at the TM according to the following equations:

$$\Delta H_{cal} = \int \Delta C_p^a \, dT \qquad\qquad \textbf{Equation 2.3}$$

$$\Delta S_{cal} = \int \frac{\Delta C_p^a}{T} \, dT \qquad\qquad \textbf{Equation 2.4}$$

We can extrapolate these parameters to the temperature of interest (T) using the following equations:

$$\Delta H_T = \Delta H_{TM} + \Delta C_p \, (T\text{-}T_M) \qquad\qquad \textbf{Equation 2.5}$$

$$\Delta S_T = \Delta S_{TM} + \Delta C_p \, \ln\left(\frac{T}{TM} \right) \qquad\qquad \textbf{Equation 2.6}$$

In these equations ΔC_p is the heat capacity change characterizing the unfolding process and can be calculated by substracting the heat capacity of the folded state, Cf, from that of the unfolded state, Cu:

$$\Delta C_p = C_u \text{-} \Delta C_f \qquad\qquad \textbf{Equation 2.7}$$

C_u and C_f can be obtained directly from the DSC plots, by measuring the ΔC_p values of the baseline at high and low temperature, respectively. Conversely, by measuring T_m and ΔH_{cal} under multiple buffer conditions a plot of ΔH_{cal} versus T_m can be constructed. The slope of this plot can indirectly determine ΔC_p, of the oligonucleotide in question.

The free energy, ΔG_T, is calculated using the Gibbs equation :

$$\Delta G_T = \Delta H_T - T\Delta S_T \qquad\qquad \textbf{Equation 2.8}$$

However, the unfolding of many nucleic acids is accomplished by small heat capacity changes and they can be ignored without compromising the overall results. Thus, Δhcal and

Δscal can be considered independent of temperature and can be calculated directly from equations 2. and 2., when no heat capacity effects are involved.

For monomolecular transitions, ΔG and ΔS can also be calculated according to the following derivation. For the following equilibrium:

Helix$\leftrightarrow$Coil
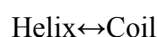
At T = T_M, the fraction of random cold (1-α) is equal the fraction of helical molecules (α). Thus:

$$K_{T=TM} = (1-\alpha)/ \alpha =1 \qquad\qquad \textbf{Equation 2.9}$$

$$\Delta G = -RT_M \ln K_{T=TM} = 0 \qquad\qquad \textbf{Equation 3.0}$$

$$\Delta G_T = \Delta H - T\Delta S = 0 \quad \text{and} \quad \Delta S = \Delta H/T_M \qquad\qquad \textbf{Equation 3.1}$$

In addition, shape analysis of the DSC curves allows for the calculation of the model dependent van't Hoff enthalpies, which can be obtained from the full width at half the maximum height according to the relationship:

$$\Delta H_{vH} = A/((1/T_1)- (1/T_2)) \qquad\qquad \textbf{Equation 3.2}$$

Where A is a constant that depends on the molecularity of the transition (A is equal to 7 and 10.14 for monomolecular and bimolecular transitions, respectively). T_1 and T_2 are the lower and upper temperatures that correspond to one half of the maximum height of Δcpa, respectively.

Comparison between the calorimetric and van't Hoff enthalpies is used to evaluate the nature of each transitions, or its cooperativity; whether the transition takes place in a two state manner ($\Delta H_{vH}/\Delta H_{cal} = 1$) or through the formation of intermediates ($\Delta H_{vH}/\Delta H_{cal} \neq 1$). A

ΔHvH/ΔHcal ratio smaller than one indicates an aggregation of the oligonucleotide. A special case is observed in the melting of polynucleotides, where the $\Delta H_{vH}/\Delta H_{cal}$ ratio is greater than one. In the case, the ΔH_{cal} is determined per mole of base-pairs, and the value of the $\Delta H_{vH}/\Delta H_{cal}$ ratio yields the size of the cooperative unit, or the number of base-pairs melting simultaneously.

2.2.7.3 Temperature-dependent CD spectroscopy

CD melting curves, ellipticity versus temperature profiles, for the helix to coil transition of DNA or G-quadruplex complexes can also be measured to obtain T_M and ΔH_{vH} values using standard procedures outlined above. Temperature dependent CD spectroscopy can also provide information about the unfolding temperature of a particular conformation in a solution that contains an oligonucleotide in multiple conformations.

Chapter 3

Recombinant CidA/LrgA Induces Leakage of Small Fluorescent Dyes, but not Proteins

3.1. Summary

Holins are a large family of membrane proteins that control the activity of bacteriophage-encoded murein hydrolases by regulating their access to the peptidoglycan substrate[55,131]. The two *S. aureus* membrane proteins CidA and LrgA exhibit holin and, respectively, anti-holin like properties[8]. They are believed to play an important role in the formation of biofilm by controling bacterial cell lysis during a novel mechanism of bacterial programmed cell death. This resembles the behavior of apoptotic (e.g. Bax/Bak) and antiapoptotic (e.g. Bcl-2/Bcl-xL) proteins in the outermembrane of mitochondria of eukaryotes[14]. Our hypothesis is that CidA can form nanoscale pores which allow the passage of small molecules. To test the hypothesized CidA function of pore formation, pure preparations of recombinant CidA were functionally reconstituted into synthetic lipid vesicles, as confirmed by circular dichroism spectroscopy and transmission electron microscopy. Fluorescent markers were entrapped into the protein reconstituted vesicles. A new method was developed to study the protein-induced leakage from vesicles since the conventional leakage assay could not be applied to CidA/LrgA. Our initial study has revealed that CidA induces leakage of small fluorescent dyes in a dose dependent manner, which is in agreement with our hypothesis.

3.2. Introduction

cid/lrg operon have been shown to regulate the autolysis/programmed cell death of

S.aureus. Two homologous small membrane proteins CidA and LrgA are of essential functions in this system[5,8,34,67,68]. CidA is the effector of cell lysis by regulating the murein hydrolase activity, as is indicated by the facts that *cidA* mutant *S.aureus* is more loosely compacted and is less adherent to the substrate and *cidA* mutant biofilm has much less lysis and eDNA compared to wild-type. However, *lrgAB* mutation resulted in increased murein hydrolase activity produced by the bacteria (LrgA function seems to rely on LrgB)[5]. Based on the above findings, it was hypothesized that CidA and LrgA encodes holin-like and anti-holin protein, respectively.

To dissect the in vitro function of CidA/LrgA, these proteins were expressed in *E.coli* using pET plasmid system with C-terminal 6 x histidine tag. Miligram level of pure protein was achieved through two-step chromatography purification, first step is the Ni-NTA column due to the affinity of the tag to Ni^{2+} ion, then the second step was using size exclusion chromatography. Purified proteins were then labeled with nanogold and reconstituted into artificial liposomes, their membrane localization were verified by TEM.

In order to confirm the hypothesis that CidA penetrate the membrane and LrgA inhibit it's function, a novel protocol was developed to entrap small fluorescent dyes (Carboxyfluorescein and Ethidium Bromide) into the liposome with CidA/LrgA inserted into the membrane, the liposomes are then separated from the free dyes and then the amount of the entrapped dye can thus be quantified, by comparing the control and protein group we understand the effect of those proteins. The result of experiment showed that CidA caused the maximum leakage (100% of the entrapped dye) at a relatively low concentration compared to LrgA, LrgA showed little inhibitory effect when present together with CidA.

We also gauze the size of pores by entrapping larger molecules like Green Fluorescent Protein (GFP) and Cytochrome c into the liposome. The result indicates that neither CidA nor LrgA allow the passage of proteins like GFP and cytochrome c at the

concentration at which small fluorescent dye.

In summary, under our experimental conditions, CidA and LrgA directly form small pores in the membrane and allow the passage of small molecules around 1 nm but not molecules bigger than 2nm. It is possible that CidA induces the leakage of small molecules and ions to gradually change the osmotic pressure, pH and/or membrane potential to cause the disruption of *S.aureus* membrane and thus the death of the bacteria.

3.3 Materials and Methods

Materials. For protein purification chromatographic columns and an AKTA Purifer 10 from GE Healthcare (Pittsburgh, PA), as well as rotors and an Allegra 25R centrifuge from Beckman Coulter (Indianapolis, IN) were employed. The noctyl-β-D-glucopyranoside (OG) and n-Dodecyl β-D-maltoside (DDM) detergent were from Anatrace (Maumee, OH). All other chemicals and reagents were from Fisher Scientific (Waltham, MA).

Plasmid. The CidA/LrgA containing pET 24b plasmids were provided as gift from our collaborator Dr. Bayles's lab. The plasmids were kept in DH5α *E.coli* strain and later transferred into C43 BL21 (DE3) cells for expression following standard manufacturer's procedure. The sequences and secondary structures of CidA/LrgA are shown in **Figure 3.1**.

CidA and LrgA sequence alignment (17.69% identity)

```
CidA -----MHKVQLIIKLLLQLGIIIVITYIGTEIQKIFHLPLAGSIVGLFLFYLLLQFKIVP 55
LrgA MVVKQQKDASKPAHFFHQVIVIALVLFVSKIIESFMPIPMPASVIGLVLLFVLLCTGAVK 60
          :...   ::: *: :* :: ::.. *:.:: :*: .*::**.*:::**     *


CidA LTWVEDGANFLLKTMVFFFIPSVVGIMDVASEITLNYILFFAVIIIGTCIVALSSGYIAE 115
LrgA LGEVEKVGTTLTNNIGLLFVPAGISVVNSLGVISQAPFLIIGLIIVSTILLLICTGYVTQ 120
     *  **. .. * :.: ::*:*: :.::  . *:   :*::.:**:.* :: :.:**:::


CidA KMSVKHKHRKGVDAYE----------- 131
LrgA IIMKVTSRSKGDKVTKKIKIEEAQAHD 147
     :     .: ** .. :
```
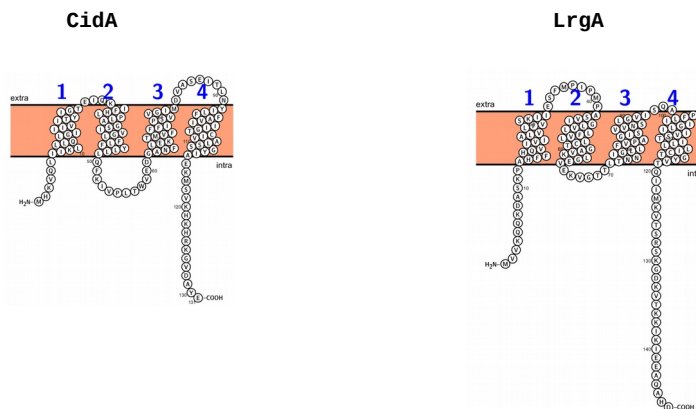

Figure 3.1 Sequence alignment (done via CLUSTAL, * indicate identity) and secondary structures of CidA and LrgA (picture credit to Protter)

Protein expression. The CidA/LrgA protein were expressed in *E.coli* BL21 (DE3). Fresh 2X TY medium was seeded with glycerol stock of the bacterial and incubated at 37ºC in the presence of Kanamycin (0.1mg/mL), shaking at 200RPM in a Excella E24 incubator shaker (Eppendorf). The growth of bacterial was monitored by measuring the UV absorbance at 600nm (OD600) with NanoDrop 2000c UV-Vis Spectrophotometer (Thermo Scientific). When OD600 reached 3.0, these cultures were cooled down to 27ºC for an hour in the incubator. 1mM isopropyl β-D-1-thiogalactopyranoside (IPTG) was then added to the culture to induce the expression. The expression was continued for another 4 hours and the OD600 reached between 5.0 to 6.0. The E. coli cells were centrifuged in a Backman S-5.1 rotor at 5000rpm for 10 minutes at 4ºC and stored at -20ºC. 2X TY medium was prepared as described. 16g tryptone, 10g yeast extract and 5g sodium chloride were codissolved in 1L of water and autoclaved.

Protein purification. Frozen cells were thawed and chemically lysed by adding 0.1% Triton X-100, 0.8M Urea, 0.25mg/ml lyzozyme and Pierce universal nuclease (Thermo Fisher Scientific) and incubating with stirring at room temperature for 1 hour. Total membrane solubilization was achieved by the addition of 1.75% empigen BB detergent (Sigma Aldrich) and further incubation at room temperature for 1 hour. Insoluble material was removed by centrifugation at 7500 g and 4ºC for 1 hour.

Protein purification was accomplished using an AKTA Purifer 10 (GE Healthcare) system via a two-step strategy. Firstly, the total cell solubilized material was loaded onto a 20ml HisPrep FF 16/10 column (GE Healthcare) pre-equilibrated with 20mM Tris, 0.7% Empigen, 3M Urea, 500mM NaCl and 60mM Imidazole buffer, pH 8.0. The column was then washed with 200ml of the same buffer and then 20mM Tris, 0.1% DDM and 60mM Imidazole, pH 8.0. Secondly, CidA/LrgA was eluted from the Ni resin using 20mM Tris, 0.1% DDM and 500mM

Imidazole, pH 8.0 and directly applied onto a 25ml 200 increase 10/300 Superdex column (GE healthcare) for a second-step purification in 20mM Tris, 0.1% DDM pH 8.0. Purified protein was stored at -20ºC in the presence of 20% glycerol.

Protein characterization. Purified CidA/LrgA were analyzed by SDS-PAGE using Coomassie blue staining and by western blotting using an anti-pentahistidine antibody conjugated with horseradish peroxidase. Samples were boiled at 95ºC for 10 minutes before loading.

Separation of monomeric, unfolded CidA/LrgA was accomplished first by precipitation of the OG-solubilized protein with methanol/chloroform and re-solubilization in neat formic acid. The sample was then diluted with FMA (20% each of formic acid, methanol and acetonitrile in water) and separated by size-exclusion chromtography on a Superdex 75 column (GE Healthcare) in FMA at the flow rate of 1ml/min. The fraction corresponding to monomeric CidA/LrgA were collected and used immediately. This sample was used to determine the CidA/LrgA molecular weight by direct injection into a eletro ionization quadrupole time-of flight (ESI-Q-TOF) mass spectrometer (Waters) and the CidA/LrgA N-terminal amino acid sequence by lyophillization and subsequent Edman degradation on a Procise 494 protein sequencer (Applied Biosystems) at the UNMC proteomics facility.

Membrane reconstitution (dialysis). In our project, CidA/LrgA purified in DDM was reconstituted into a membrane system of phospholipid composition POPG/POPC = 7:3 by detergent dialysis. Lipids were dissolved in chloroform and stored at -20ºC. Required aliguots were mixed and chloroform was then removed under low vacuum followed by overnight lyphillization. The dried lipid mixture were then dissolved in 20mM Tris, 60mM OG, pH 8.0 at a final concentration of 2.5mg/ml and vortexed until clear. OG-solubilized lipids and CidA/LrgA were then combined and incubated at room temperature for 30 minutes. After the incubation, the mixture was dialyzed using a 10 kDa cutoff membrane against 20mM Tris,

50mM NaCl, 2mM EDTA for 24 hours.

Carboxyfluorescein Liposome leakage assay. The newly-developed liposome leakage assay was based on the self-quenching property of carboxyfluorescein (CF, a negatively charged fluorescent dye). The POPG/POPC (7:3) lipids were dried and dissolved in 60mM OG as described above in the dialysis based membrane reconstitution method. The liposomes were combined with small amount of DDM dissolved CidA/LrgA protein in certain ratio and the mixture was directly injected into 50mM CF (self-quenches at this concentration), 20mM Tris, 50mM NaCl and 2mM EDTA solution, the proteo-liposomes with detergent molecules are formed upon dilution since the detergent concentration will be below critical micelle concentration (CMC, for CMC_{OG}= 15-17mM, CMC_{DDM}~0.2mM), meanwhile the newly-formed liposomes will each trap small amount of 50mM CF. Free dye and the proteoliposomes are separated by PD-10 columns and the collected liposomes are subjected to 10ul of 10% Triton X-100 and water, respectively. Upon lysis by Triton X-100, the 50mM CF entrapped inside the liposomes are immediately diluted and emits stronger fluorescent signal. Fluorescent signal is measured by spectrometer at endpoint excitation wavelength 492nm and emission wavelength 517nm. The signal is calculated as:

$$\Delta FL = FL_{Triton\ X-100} - FL_{water} \quad (\textbf{Equation 3.1})$$

ΔFL represents the difference in fluorescent signal, $FL_{Triton\ X-100}$ respresents the signal obtained from Triton X-100 added liposomes (lysed) and Fl_{water} stands for water added lipsomes (not lysed). A negative control was made by using plain DDM detergent without proteins. By comparing the ΔFL of CidA/LrgA proteo-liposome and the control liposome, the information on the effect of proteins (extent of leakage) can be obtained (see **Figure 3.2**).
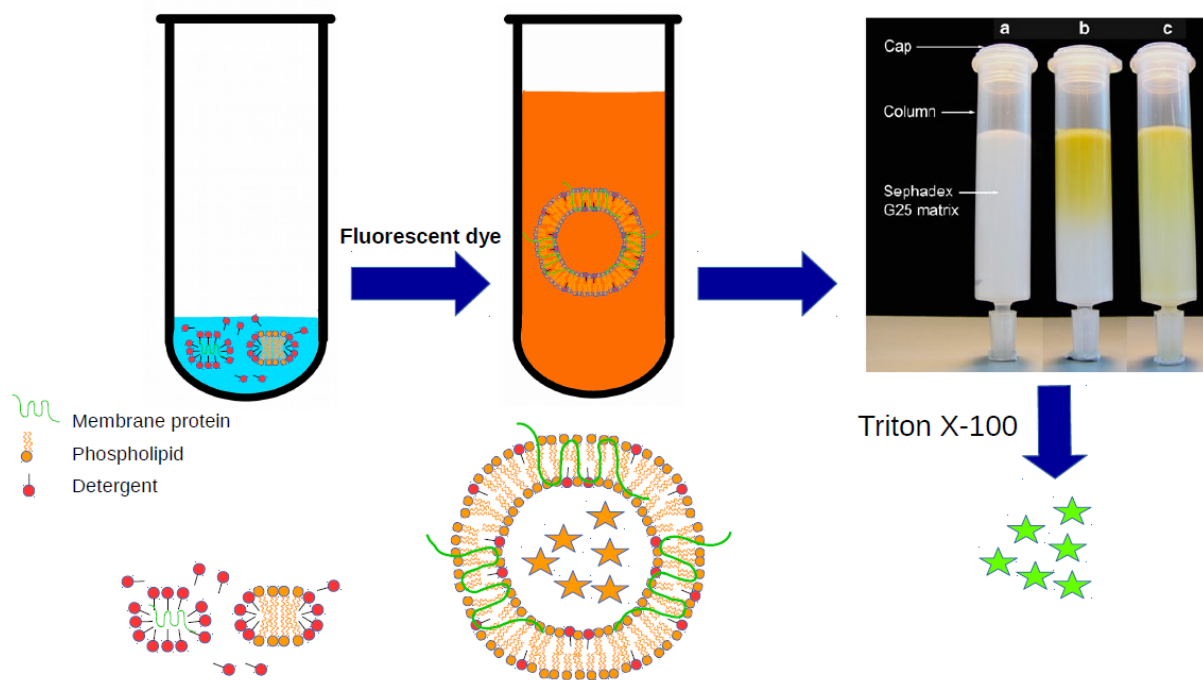
Figure 3.2 Schematic figure of the design of the liposome leakage assay

Transmission Electron Microscopy. Samples were incubated with 5 nm Ni-NTA-Nanogold (Nanoprobes, Yaphank, NY) to label CidA/LrgA for 30 minutes. 10 µL of the sample was then placed on thin carbon films on holey grids and allowed to absorb for 2 minutes, after which the grid was washed with 10 µL of deionized water twice and negatively stained with methylamine vanadate (Nanoprobes). Imaging was carried out with a Tecnai G2 transmission electron microscope (FEI) operated at 80 kV.

Circular Dichroism Spectroscopy. The secondary structure of CidA/LrgA in 60mM OG and in the lipid bilayer was obtained using a Model 202SF circular dichroism spectrometer (Aviv Biomedical). Spectra were obtained from 250 to 190nm in 1nm increments at 25ºC and the reported spectra correspond to the average of at least three wavelength scans. The data was analyzed using K2D3 software.

3.4 Results and discussion

Protein production. Large-scale preparations of recombinant Cid/Lrg proteins are routinely needed for the subsequent experiments. These requirements are non-trivial for membrane proteins. All aspects of *E. coli* expression have been optimized, as well as detergent solubilization and purification, as mentioned in the protocol. Typically, 2-3 mg of CidA/LrgA are currently purified per liter of culture. The proteins are purified in 0.1% DDM on size exclusion chromatography column, CidA peak mainly appears in 13ml and LrgA peak in 23ml, which suggest CidA under the experimental condition is in a oligomeric state whereas LrgA is more likely to be a monomer (see **Figure 3.3**). Monomeric Recombinant CidA (16 kDa) and LrgA (17 kDa) are also characterized by SDS-PAGE and Western-blot (see **Figure 3.3**). If samples are not treated with reducing agent, there will be oligomers and dimers (appear at 32kDa and 36kDa for CidA and LrgA, respectively), indicating that CidA and LrgA

are prone to dimerize or oligomerize. N-terminal sequencing and Mass spectrometry was employed to confirm that the N-termina of these proteins were intact (except for cleavage of the first Methionine).
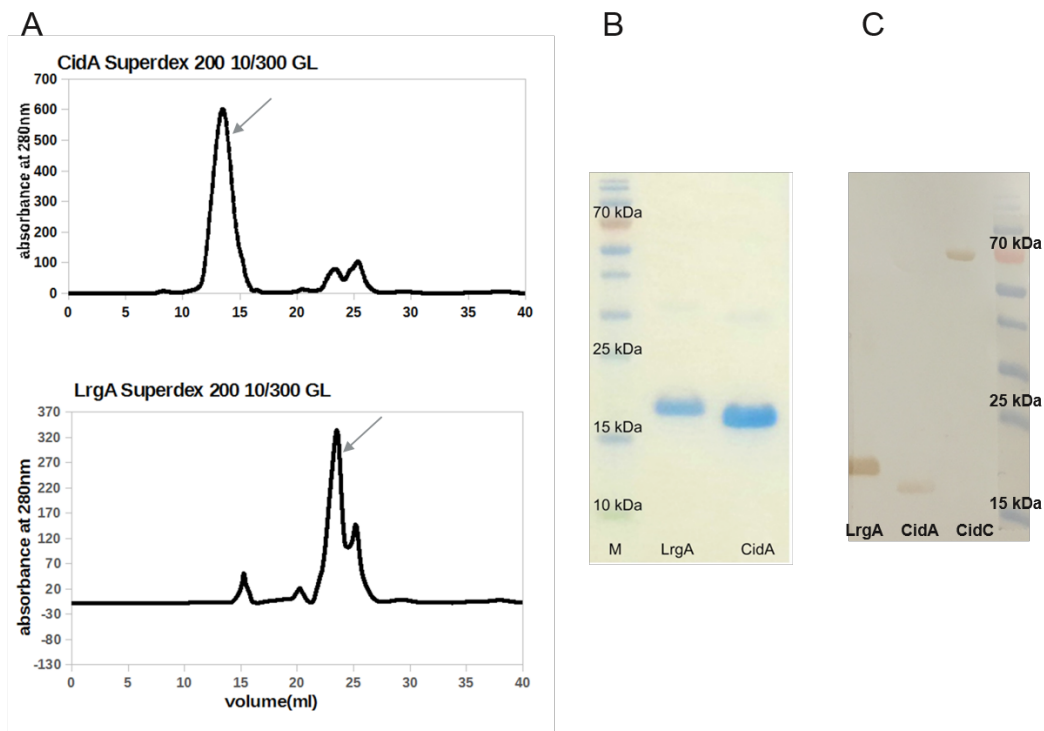
Figure 3.3 Purification of CidA/LrgA (A) CidA and LrgA chromatograpy, the arrows indicate the majority of the protein. (B) SDS-PAGE of purified CidA/LrgA (C) Western-blot of CidA/LrgA/CidC.

Membrane reconstitution. For dialysis based reconstitution, CidA/LrgA were reconstituted into a mixture of POPG/POPC (7:3), (all lipids from Avanti Polar Lipids) synthetic bilayers via detergent dialysis. 60mM OG-solubilized lipids were mixed with 0.1% DDM solubilized CidA/LrgA at room temperature at pH 8.0 for 30 min to allow the equilibration of the mixed micelles. Detergent was then extensively dialyzed out which resulted in the formation of CidA/LrgA-containing liposomes. To visualize the proteins, CidA/LrgA were labeled by 5nm nanogold, as the protein C-terminal histidine tag binds to the Ni^{2+} on the surface of nanogolds. By TEM, it was conclusively found that CidA/LrgA locate in the lipid membrane as transmembrane proteins, as indicated by the positions of the nanogold (see **Figure 3.4A**). Since there was no controlling the orientation of the proteins when they were inserted to the membrane, CidA/LrgA locate at both sides of the lipid membrane. When the protein concentration is low, they can be homogeneously distributed. Whereas in the high protein to lipid ratio group, those proteins can form clusters and cause some changes to the local membrane morphology. The secondary structures of CidA/LrgA are measured by CD, the results showed that CidA consists of 51.03% α-helix and 8.95% β-sheet and LrgA contains 67.4% α-helix and 2.2% β-sheet (by K2D2 software), which is in good agreement with the predicted secondary structure (**Figure 3.4B**).
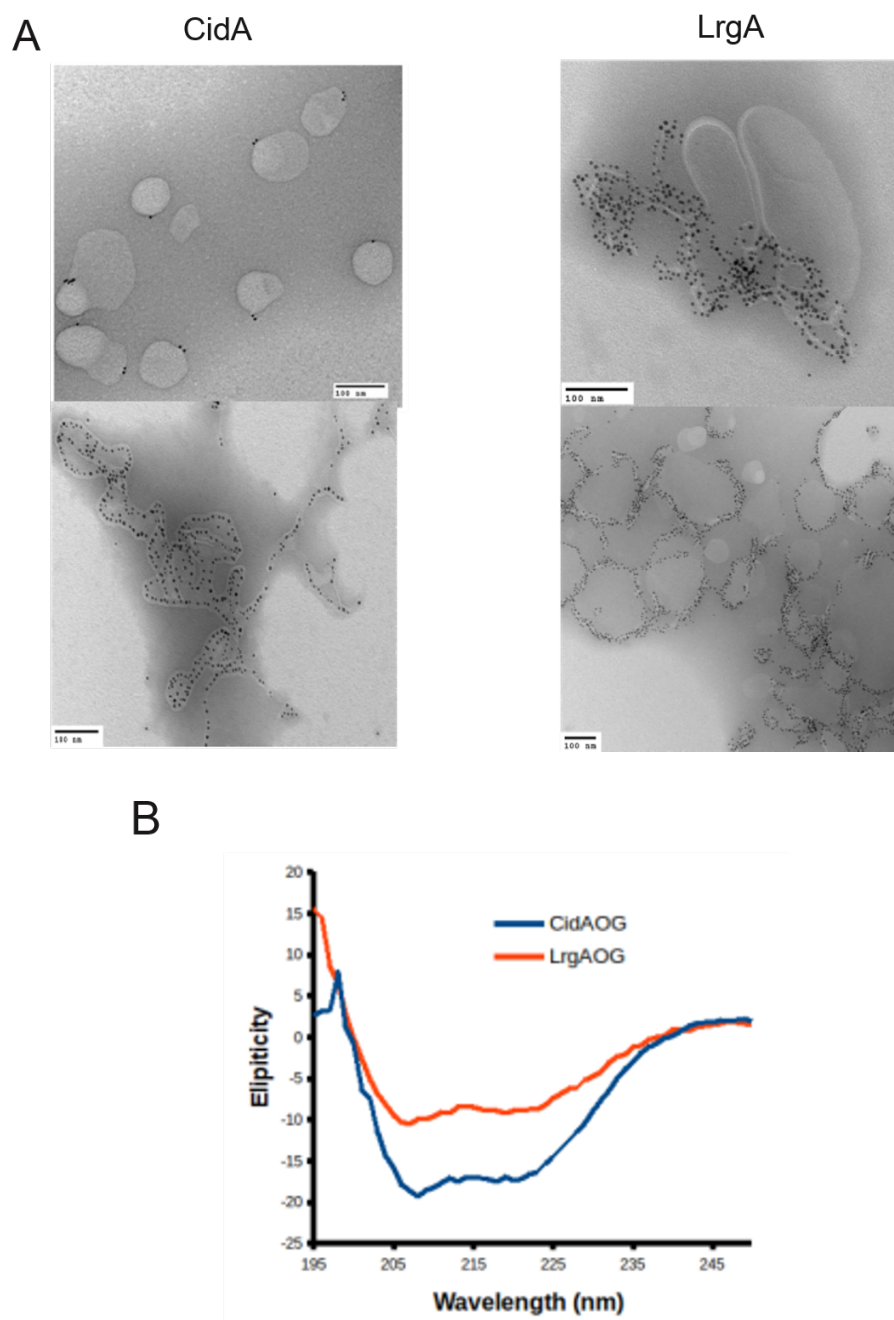
Figure 3.4 Membrane reconstitution of CidA/LrgA (A) TEM image of CidA and LrgA reconstituted on POPG/POPC (7:3) lipid membrane. (B) CD spectra of purified CidA/LrgA

Liposome Leakage assay. Liposome leakage assay is a common assay for studying the membrane disruption, penetration and pore-formation properties of membrane proteins and peptides, most assays are based on the entrapping of signal (Fluorescent/UV-Vis/chemiluminescent, etc) molecules into preformed liposome, then the protein/peptide is added to the liposomes and the signal change can then be recorded[132,133]. However, high concentration of membrane proteins must be first solubilized by detergent and the detergent concentration must be controlled so that the membranes are not disrupted due to the detergent. In our protocol, the major advantage is the simultaneous membrane incorporation of the membrane proteins CidA/LrgA and the entrapping of fluorescent dyes, and with the use of PD-10 column, liposomes and free dyes can be separated very fast, multiple groups of experiments with different membrane protein concentrations can be prepared in a 96-well plate within 1-2 hours.

To validate the protocol, we have first done experiments on Heme molecules and Influenza M2 ion channel transmembrane peptides. Heme has been shown to disrupt the biological membrane and thus can serve as a positive control, whereas Influenza M2 ion channel only allows the passage of protons (but not bigger chemicals like carboxyfluorecein) and is a negative control for the study. It's shown in **Figure 3.5** that heme causes extensive liposome leakage whereas Infuenza M2 does not induce leakage even at a relatively high concentration, as expected.
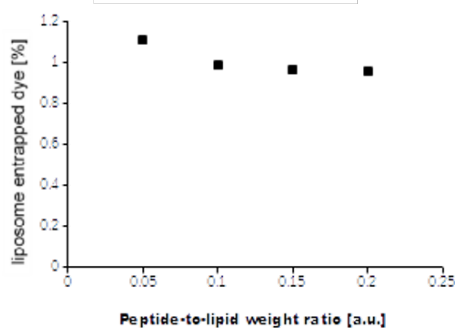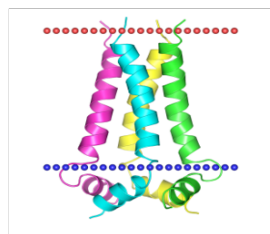
Influenza M2   Heme
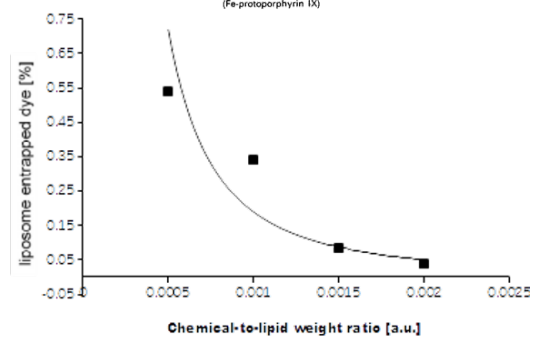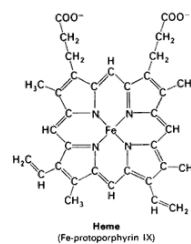
Figure 3.5 Liposome leakage assay of CF in the presence of Influenza M2 and Heme

In the case of CidA/LrgA, both CidA and LrgA can cause the leakage of CF, however, it was found that CidA induces the leakage at a relatively low concentration compared to LrgA, which is in agreement with the hypothesis that both holin and anti-holin can induce leakage and holin function is more effective and direct (**Figure 3.6**). When LrgA is mixed with CidA and both incorporated into the membrane, no apparent inhibitory effect of LrgA is seen (data not shown), indicating that either LrgA function is dependent on other proteins like LrgB or LrgA is likely to function under other experimental conditions (pH, buffer, chemicals, etc), which need to be further tested.
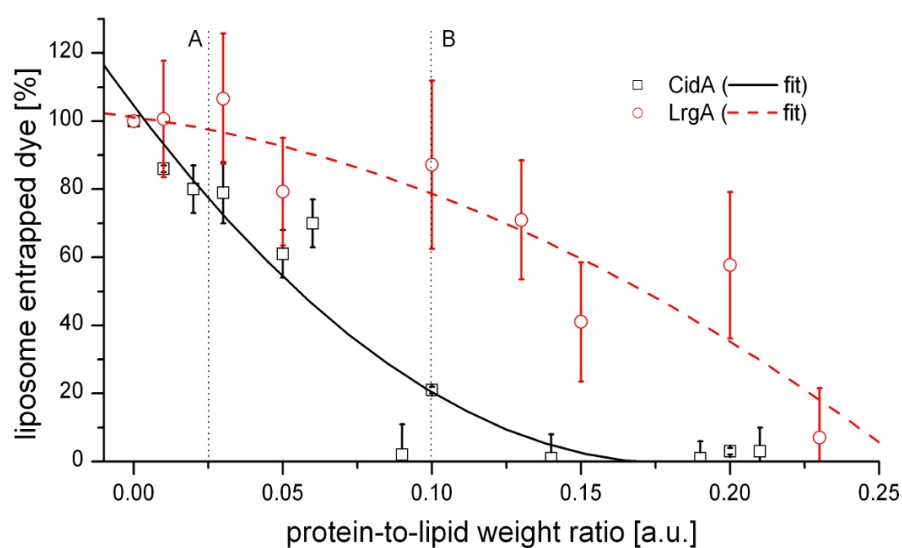
Figure 3.6 Liposome leakage assay of CF in the presence of CidA and LrgA

To further gauge whether CidA/LrgA cause leakage via membrane disruption or pore formation, larger cargoes like cytochrome c and GFP are used in the liposome leakage assay instead of CF and to better separate the liposomes and free cargoes, size-exclusion column is used instead of PD-10, liposomes were eluted in the void volume (before 10ml) and the free proteins appear in 14ml (GFP) and 17ml (cytochrome c), thus they are separated. The result showed that cytochrome c and GFP does not come out of liposome in the presence of CidA/LrgA at the concentration when CF is leaked (1:8 protein to lipid weight ratio, see **Figure 3.7**), though cytochrome c does leakage out a little more than GFP. It suggests that CidA/LrgA form pores in the membrane instead of causing massive membrane disruption, CidA/LrgA may mainly cause the leakage of small chemicals instead out larger proteins so the size of the pores that they form are 0.8 to 1.5nm.
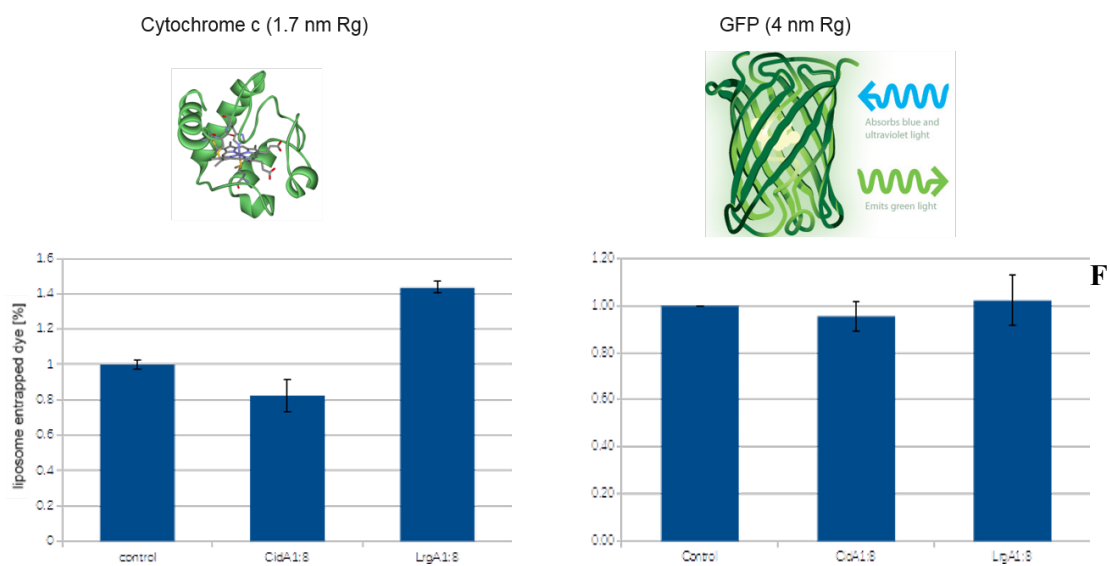
igure 3.7 Liposome leakage assay of cytochrome c and GFP in the presence of CidA and LrgA

3.5 Conclusions

Consistent with the model that the CidA and LrgA proteins are holin-like proteins, the data indicate that they regulate membrane permeability by forming pores. The goal here is to confirm this function at the protein level and to characterize the protein-induced membrane pores. Leakage assays, which monitor the release of fluorescent molecules and proteins from liposomes, is the method of choice to study such phenomena. We have therefore entrapped small fluorescent dyes (carboxyfluorescein, CF) and Cytochrome c/GFP into CidA- and LrgA-liposomes and quantified their release as a function of the CidA/LrgA concentration by separating liposomes from small molecules via gel filtration chromatography. The CF leakage from both CidA- and LrgA-liposomes is shown in **Figure 3.6** and demonstrates that CidA, but not LrgA, induces the formation of nanometer-size pores at biologically relevant protein concentrations (the hydrodynamic radius of CF is 0.8 nm). Similar results were obtained with EB (same hydrodynamic radius, but positively charged unlike the negatively-charged CF, data not shown), while the much larger cytochrome c and GFP protein (hydrodynamic radius of 3.6 nm) did not leak out of CidA-liposomes (in **Figure 3.7**). These results suggest that CidA induces nanometer-scale pores into the membranes, while LrgA does not. It is possible that LrgA induces the formation of much smaller angstrom-scale channels which will be further investigated. We note that a number of positive (using hemin as a membrane permeabilizing agent) and negative (using the M2 proton channel peptide) controls have been conducted to validate our liposome leakage approach.

Chapter 4

Characterization of the *Staphylococcus aureus* CidC pyruvate:menaquinone oxidoreductase

4.1. Summary

Recent studies have revealed an important role for the Staphylococcus aureus CidC enzyme in cell death during the stationary phase and in biofilm development, and have contributed to our understanding of the metabolic processes important in the induction of bacterial programmed cell death (PCD). To gain more insight into the characteristics of this enzyme we performed an in-depth biochemical analysis of its catalytic properties. In vitro experiments show that this flavoprotein catalyzes the oxidative decarboxylation of pyruvate to acetate and carbon dioxide. CidC can reduce cytochrome c via menaquinone, but not ubiquinone, suggesting participation in the bacterial aerobic respiratory chain. CidC functions as a monomer with no evidence for oligomerization, binds to artificial membranes which increases enzymatic activity, and does not appear to be activated by amphiphiles such as phospholipids and charged detergents. In addition, only reduced CidC is protected from proteolytic cleavage by chymotrypsin, and, unlike its homologues, protease treatment does not increase enzymatic activity. Finally, CidC activity is strongly pH-dependent with maximal activity observed at pH 5.5 to 6 and negligible activity at pH 7 to 8. The results of this study are consistent with a model in which the activity of the CidC pyruvate:menaquinone oxidoreductase is induced at the cellular membrane during cytoplasmic acidification, conditions that were previously shown to be important to the induction of bacterial PCD.

4.2. Introduction

Studies of the *cidABC* and *lrgAB* operons from *Staphylococcus aureus* have revealed a complex network of membrane-associated proteins and metabolic enzymes with a significant role in the regulation of bacterial viability. CidA and LrgA are functionally similar to members of the Bcl-2 family of proteins that control apoptosis in eukaryotic organisms[86] and *cidA* and *lrgA* mutations are associated with cell death phenotypes[5,66]. It has been therefore proposed that the widely conserved *cid* and *lrg* operons control bacterial PCD[10,69] which most dramatically manifests within the complex, multicellular environment of the biofilm[5,67].

The Cid and Lrg system has been shown to rely on the activities of two opposing membrane proteins that function in a manner that is analogous to bacteriophage-encoded holins, known to be required for the control of cell death and lysis during the lytic cycle of a bacteriophage infection[134]. Similar to holins, the CidA and LrgA proteins are small, membrane proteins that form high molecular weight oligomers[8]. In addition, CidA and LrgA appear to have opposing functions (analogous to holins and anti-holins, respectively) in the control of cell death and lysis, with CidA functioning as an effector of these processes[67] and LrgA functioning as an inhibitor[5,135]. These striking functional and biochemical properties of CidA and LrgA have laid the foundation for the model that these bacterial proteins represent the progenitors of the regulatory control of apoptosis in more complex eukaryotic organisms[136].

Our laboratory has recently demonstrated that the cidC gene, which encodes a pyruvate enzyme, also plays a major role in the control of bacterial PCD by potentiating cell death[70]. This process was shown to involve the CidC-mediated conversion of intracellular pyruvate to acetate, which leads to cytoplasmic acidification and respiratory inhibition and suggests that CidC is a pyruvate enzyme[9]. Pyruvate is an important intermediate in

carbohydrate metabolism that is directly metabolized by two types of flavoenzymes[137]. These enzymes are differentiated by the Enzyme Commission (EC) according to their immediate electron acceptor: pyruvate oxidases or pyruvate:oxygen 2-oxidoreductases (EC 1.2.3.3) pass the electron to oxygen, while pyruvate dehydrogenases or pyruvate:quinone oxidoreductases (EC 1.2.5.1) pass the electron to a quinone. The former enzyme requires phosphate and produces acetyl phosphate, while the latter requires water and generates acetate with the full reactions shown in Equation 1. These enzymes have been studied extensively and well-known examples include the pyruvate:oxygen 2-oxidoreductase SpxB from Streptococcus pneumoniae[138] and the pyruvate:ubiquinone oxidoreductase PoxB from Escherichia coli[139].

Equation 1

pyruvate + phosphate + $O_2 \rightarrow$ acetyl phosphate + CO_2 + H_2O_2

pyruvate + H_2O + quinone $\rightarrow$ acetate + CO_2 + quinol
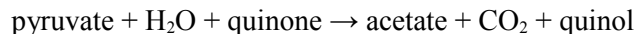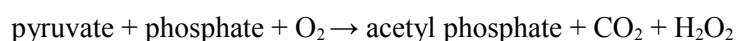
Pyruvate:oxygen 2-oxidoreductases consume oxygen and participate in cellular signaling via the generation of acetyl phosphate[140] and in cell death via the production of H_2O_2[141]. Pyruvate:quinone oxidoreductases directly feed electrons from the cytoplasm into the membrane respiratory chain. PoxB has been extensively characterized because it is an interesting membrane-activated enzyme: its enzymatic activity and kinetics are well known and its protein structure was determined[142,143]. The recently identified CidC shares about 33% identity in the amino acid sequence with either of SpxB and PoxB and previous in vivo studies suggest that it is an enzyme responsible for the conversion of pyruvate to acetate[9]. The current study focused on elucidating the basic biochemical properties of CidC and has conclusively demonstrated its activity as a pyruvate:quinone oxidoreductase which uses menaquinone as a direct electron acceptor. In addition, these studies demonstrate that the optimal pH range for CidC activity is between 5.5 and 6.0, consistent with a role for this

enzyme during cytoplasmic acidification and the potentiation of bacterial PCD.

4.3. Materials and Methods

Materials. For protein purification chromatographic columns and an AKTA Purifer 10 from GE Healthcare (Pittsburgh, PA), as well as rotors and an Allegra 25R centrifuge from Beckman Coulter (Indianapolis, IN) were employed. The Penta-His Antibody from Thermo Scientific (Waltham, MA) was used for western blot detection. Glucose oxidase from Aspergillus niger (160 kDa) and human serum albumin (66.5 kDa) were purchased from Sigma Aldrich (St. Louis, MO). The noctyl-β-D-glucopyranoside (OG) detergent was from Anatrace (Maumee, OH). All other chemicals and reagents were from Fisher Scientific (Waltham, MA).

Protein expression. The CidC protein was expressed in Escherichia coli BL21 (DE3). Fresh 2X TY medium was seeded with glycerol stock of the bacterial and incubated at 37ºC in the presence of Kanamycin (0.1mg/mL), shaking at 200RPM in a Excella E24 incubator shaker (Eppendorf) . The growth of bacterial was monitored by measuring the UV absorbance at 600nm (OD600) with NanoDrop 2000c UV-Vis Spectrophotometer (Thermo Scientific). When OD600 reached 3.0, 1mM isopropyl β-D-1-thiogalactopyranoside (IPTG) was added to the culture to induce the expression. The expression was continued for another 4 hours and the OD600 reached 6.0. The E. coli cells were centrifuged in a Backman S-5.1 rotor at 5000rpm for 10 minutes at 4ºC and stored at -20ºC. 2X TY medium was prepared as described. 16g tryptone, 10g yeast extract and 5g sodium chloride were codissolved in 1L of water and autoclaved.

Protein Purification. Frozen cells were resuspended in 20mM Tris, 500mM NaCl, pH 8.0 (Volume of buffer = 50ml/750ml cell culture). Lysozyme (0.25mg/mL), benzonase (5mg/ml), Triton X-100 (1%) and 1mM PMSF were added. The cell lysis was stirred and

incubated at room temperature for 30 minutes, followed by sonication with four 30-s burst on ice. Insoluble material was pelleted by centrifugation at 7500rpm at 4 °C for 30 minutes in Beckman A-14 rotor. The supernatant was recovered and stored at 4ºC. Protein purification was accomplished using AKTA purifier system via a two-step purification strategy. Firstly, recovered supernatant was loaded onto 25mL Ni-NTA affinity column (GE healthcare). The column was then washed with 10 bed volumes of washing-1 buffer (20mM Tris, 20mM Imidazole, 0.5M NaCl, pH 8.0). His-tagged protein was then eluted from the column with elution buffer (20mM Tris, 300mM Imidazole, 0.5M NaCl, pH 8.0). Secondly, eluted protein was applied onto a 25ml 200 increase 10/300 Superdex column (GE healthcare) for a second-step purification in 200mM sodium phosphate pH 7. Purified protein was stored at -20ºC in the presence of 20% glycerol.

Liposome preparation. Small phospholipid vesicles were formulated using a 7:3 w/w mixture of 1-palmitoyl-2-oleoylsn-glycero-3-[phospho-rac-(1-glycerol)] (POPG) and 1-palmitoyl-2-oleoyl-sn-glycero-3-phosphocholine (POPC) lipids (Avanti Polar Lipids, Alabaster, AL). The lipids were weighted and thoroughly dissolved in NaP7 buffer containing 60 mM OG detergent by incubating for 15 minutes at 37°C until the solution was clear. Liposomes were then formed via 10x dilution of the above lipid-detergent solution into NaP7 buffer while mixing vigorously, followed by detergent removal via overnight dialysis against NaP7 buffer using Spectra/Por 6 dialysis membranes with a 10 kDa cutoff (Spectrum Laboratories, Rancho Dominguez, CA). The liposomes were finally extruded 11 times through 400 nm Whatman nuclepore track-etched membranes (GE Healthcare, Pittsburgh, PA) using a Mini-Extruder (Avanti Polar Lipids, Alabaster, AL) and used immediately.

Ferricyanide assay for CidC activity. 2 μM CidC (with urea, Triton X-100, OG, citrate or liposomes added as indicated) was first incubated with 20 mM pyruvate, 10 μM TPP and 1 mM Mg2+ in NaP6.0 buffer for 20 min. 8 mM ferricyanide was then added and its

reduction was immediately visible as it lost its color. Consequently, the CidC activity was measured as a decrease in absorption at 450 nm over time. The pH-dependent CidC activity was similarly tested in 200 mM sodium acetate over pH 5.0 to 5.6 and 200 mM sodium phosphate buffer over pH 5.6 to 8.0. The enzyme activity was identical at pH 5.6 in both sodium acetate and sodium phosphate. One unit (1U) of pyruvate oxidase activity is defined as the amount of enzyme required to consume 1 μmole of pyruvate in one minute. The CidC specific activity was estimated accordingly within one minute of the ferricyanide addition, taking into account that (i) two equivalents of ferricyanide are reduced per equivalent of decarboxylated pyruvate and (ii) the extinction coefficient of ferricyanide at 450 nm is 0.218 mM-1 cm-1.

Acetate quantification. The "acetic acid test kit" (R-Biopharm AG, Darmstadt, Germany) was used with the provided instructions to measure acetate concentrations. Protein samples with 2 μM CidC (and optionally 0.05% Triton X-100 or 3M urea) were first incubated with 20 mM pyruvate, 10 μM TPP and 1 mM Mg2+ in NaPh6.0 buffer for 20 min. 8 mM sodium ferricyanide was then added and the acetate levels were measured in triplicate after 30 min when the reaction was completed. The urea-containing sample was used as a negative control, while a 5 mM acetate solution was used as a positive control.

H₂O₂ quantification. Peroxidase catalyzes the reaction of H2O2 with 4-aminoantipyrine and phenol to form 4-(pbenzoquinone-monoimino)-phenazone with a 510 nm absorbance proportional to the initial H2O2 concentration[8–10]. This reaction was calibrated for H2O2 quantification in the 1 to 10 mM range (R2=0.99). 20 mM pyruvate, 10 μM TPP, 1 mM Mg2+ were incubated with 2 μM CidC (and optionally 0.05% w/w Triton X-100) in NaP6.0 buffer for 20 min when 35 mM phenol, 10 mM 4-aminoantipyrine and 1 μM horseradish peroxidase were added. The activity of glucose oxidase was used as a positive control since it converts glucose to gluconolactone and H2O2.

CidC quinone electron transport assay. These experiments were conducted as the ferricyanide assay, except that the 8 mM ferricyanide was replaced by 250 μM quinone (the headgroup of either menaquinone or ubiquinone from a dimethylsulfoxide (DMSO) stock) and 80 μM cytochrome c. The cytochrome reduction was followed spectroscopically at 550 nm.

TEM imaging. Samples were incubated with 5 nm Ni-NTA-Nanogold (Nanoprobes, Yaphank, NY) to label CidC for 30 minutes. 10 μL of the sample was then placed on thin carbon films on holey grids and allowed to absorb for 2 minutes, after which the grid was washed with 10 μL of deionized water twice and negatively stained with methylamine vanadate. Imaging was carried out with a Tecnai G2 transmission electron microscope (FEI) operated at 80 kV.

Isothermal titration calorimetry (ITC). ITC was carried out on a MicroCal iTC200 (Malvern Instruments Ltd, Worcestershire, UK). 40 μl of 100 μM CidC in NaP7 buffer was injected into 250 μl NaPh6 buffer containing various ingredients as specified. A total of 20 injections (2 μL each, spaced by 5 minutes) were performed at room temperature. Data was analyzed using the Origin software (OriginLab Corporation, Northampton, MA).

Protease treatment. 2 μM CidC in NaP6 or NaP7 buffer containing either of 20 mM pyruvate, 10 μM TPP or 1 mM Mg^{2+} was incubated for 30 minutes. 1 μM trypsin or chymotrypsin was then added and proteolytic cleavage was conducted for 30 minutes. The solution was immediately tested for activity using the ferricyanide assay or was immediately precipitated using methanol:chloroform (4:1 v/v) and studied 201 by SDS-PAGE electrophoresis.

4.4 Results and Discussion

CidC preparation. To study the *S. aureus* CidC enzyme, a previously developed expression plasmid[9] was exploited to generate milligram amounts of purified protein. Initial screening using western blot analysis of the C-terminal histidine tag of CidC showed that the enzyme over-expresses very well in *E. coli* BL21(DE3) cells. A first-step affinity chromatography employing Ni-NTA resin resulted in pure and stable protein in pH 8 phosphate buffer containing 500 mM NaCl (**Figure 4.1A**). As expected for flavoproteins, CidC exhibited characteristic UV-VIS absorption at 380 and 450 nm and fluorescence at 530 nm (with 450 nm excitation) as shown in **Figure 4.1B**[144,145]. This finding suggests that the enzyme maintains its FAD-bound state throughout cell lysis and purification, and no attempts were made here to supplement FAD to the protein (although it is possible that a small enzyme population is not active because it lost its FAD cofactor). The intrinsic fluorescence of CidC was observed at 340 nm (with 280 nm excitation), also shown in **Figure 4.1B**[145]. The CidC molecular weight (calculated average of 64,806 Da) was qualitatively confirmed by SDS-PAGE (**Figure 4.1A**) and quantitatively by mass-spectroscopy to within a few Da (data not shown). The first six amino acids (Met, Ala, Lys, Ile, Lys and Ala) were verified by N-terminal sequencing (data not shown) strongly confirming the identity of the purified protein. The protein solution was made 15% glycerol and stored at -20°C until experiments were performed.

As shown below, the CidC protein is only active below pH 6.5, however it also precipitates quite rapidly under these conditions. The addition of high concentrations of NaCl delays this protein self-aggregation, but also inhibits its enzymatic activity. A NaCl-free and acidic solution is therefore required for an active CidC preparation and a second purification step was implemented to bring CidC from pH 8 to an intermediate pH 7 phosphate buffer without any NaCl by gel filtration chromatography. The sample was then immediately diluted

to or titrated into pH 6 phosphate buffer and activity assays were performed. This protein formulation provided consistent results among different protein batches while also minimizing the extent of self-aggregation.
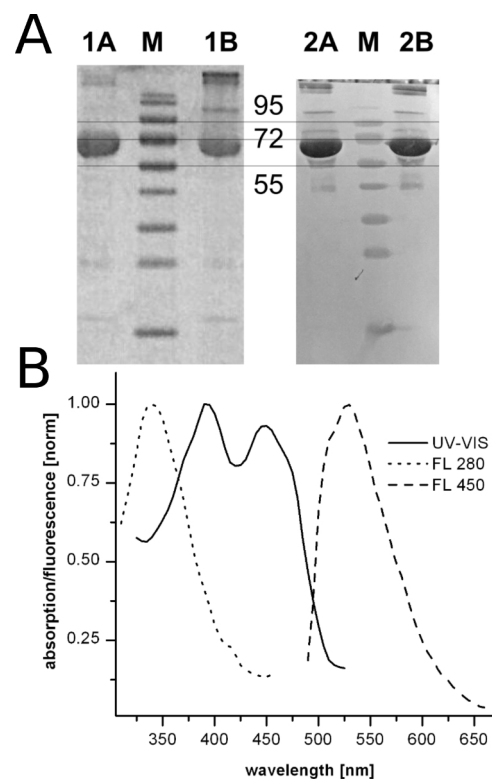
Figure 4.1. CidC purification and optical characterization. (A) SDS-PAGE gel (left) and western blot (right) of purified CidC in the presence (lanes 1A, 2A) or absence (lanes 1B, 2B) of β-mercaptoethanol. Relevant bands in the marker lanes (M) are identified by their MW in kDa. (B) UV-VIS and fluorescence with excitation at 280 (FL 280) and 450 nm (FL 450) spectra of CidC at pH7.

CidC oligomerization and aggregation. All previously studied bacterial pyruvate oxidoreductases were shown to be homo-tetramers in their functional form[142,143,145–148]. CidC oligomerization was studied here by gel filtration chromatography in pH 6 phosphate buffer (**Figure 4.2A**). Most CidC eluted under these conditions very closely to serum albumin (which has 98% of the molecular weight of the CidC monomer), strongly suggesting that CidC exists almost exclusively in a monomeric form. A remaining and very small amount of CidC eluted as a dimer, which was confirmed by (i) the disappearance of this peak under reducing conditions (when using 0.1% v/v 2-mercaptoethanol, data not shown) and (ii) its elution profile being very similar to that of glucose oxidase (which has 117% of the molecular weight of the CidC dimer). Any other CidC oligomers (trimers, tetramers or larger assemblies) would elute in the void volume between 8 and 10 mL when using the column employed here. Since very little A280 signal was detected in this region, only traces of such larger oligomers could exist, reinforcing the idea that CidC is predominantly monomeric at pH 6. No protein was trapped on the column during the purification as judged by comparison of the A280 signal between the injected and eluted protein.

Although CidC was rapidly eluted (within 15 minutes) as a monomer while the pH was exchanged from 7 to 6 (the sample was injected at pH 7 and purified in pH 6 buffer), the protein completely precipitates at pH 6 within approximately 30 minutes after purification (the protein concentration being 2-3 mg/mL). However, it was found that the addition of 500 mM NaCl to purified CidC in pH 6 delays its precipitation by several hours. CidC was also shown to be monomeric at pH 7 and 8 (both with and without 500 mM NaCl) using the same gel filtration assay (data not shown). These experiments show that CidC is monomeric and, although it appears stable at pH 7 to 8, it rapidly aggregates at high protein concentration and below pH 6.5. This CidC self-aggregation can be largely suppressed by the addition of high concentrations of NaCl.

Enzyme self-aggregation at pH 6 was also investigated by TEM. CidC was incubated for 1 hour in pH 6 phosphate buffer without (**Figure 4.3A-C**) and with 500 mM NaCl (**Figure 4.3D**) and then immediately imaged. Large protein aggregates were observed in the absence of NaCl, while only non-aggregated, randomly distributed protein was observed in the presence of NaCl, confirming that at high concentrations NaCl prevents CidC self-aggregation.
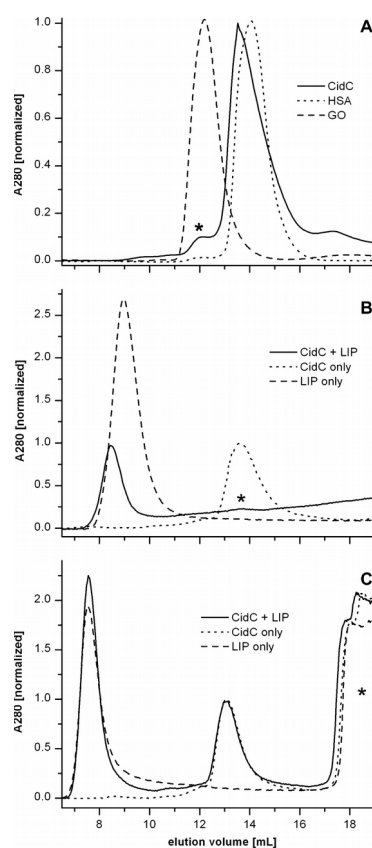
Figure 4.2. Purification of proteins and/or liposomes by gel filtration. (A) CidC, human serum albumin (HSA) and glucose oxidase (GO) were each separately purified. The asterisk denotes CidC dimers. (B) CidC, liposomes (LIP) and their mixture were purified. The asterisk denotes a minute amount of monomeric CidC eluting from the CidC-LIP mixture. (C) As in (B), except that 500 mM NaCl was used during purification. The asterisk denotes the elution of small molecules (e.g. salts, residual detergents, etc.). The inclusion of high salt slightly changes the physical properties of the column, e.g. the void volume and monomeric CidC elution are shifted when compared to (A-B). Data was scaled relative to the protein A280 in all cases.

CidC interaction with phospholipid membranes. The bacterial pyruvate oxidoreductases studied to date exist in a soluble, inactive form within the cytoplasm and localize at the cellular membrane to become active18,26–29. To study the interaction of CidC with membranes, liposomes prepared with a simple mixture of POPG:POPC (7:3 w/w) were used here to mimic the membrane lipid composition of S. aureus30–33. Three samples containing (i) CidC, (ii) liposomes and (iii) CidC-liposomes mixture were subjected to the same gel filtration procedure described above in pH6 phosphate buffer (**Figure 4.2B**). Due to their large dimensions, the liposomes elute in the void volume and also scatter light which translates into an apparent absorption at 280nm. The peak corresponding to the CidC monomer disappears completely when the CidC-liposomes mixture is analyzed, suggesting that CidC binds to the membranes and co-elutes with the liposomes. The sum of the A280 signals from the separately-injected liposomes and CidC samples is significantly larger than the signal obtained when their mixture is injected. This implies that some of the sample is lost during the purification and suggests that CidC not only binds to the membranes, but also induces aggregation of the liposomes into much larger assemblies that are trapped within the column and do not elute at all. To test this, the CidC membrane-binding experiment was repeated with 500 mM NaCl added to the running buffer as shown in Figure 4.2C. Under these conditions, CidC elutes independently from the liposomes when the CidC-liposome mixture is injected. Moreover, the chromatograph corresponding to the CidC-liposome mixture is quantitatively equal to the sum of the peaks obtained when CidC and liposomes are injected separately. These results support the notion that CidC induces liposome aggregation and that high concentrations of NaCl are able to completely suppress this interaction.

The CidC interaction with the membranes was further probed by TEM. In the absence of NaCl, co-localization of the nanogold-labeled CidC and the negatively-stained liposomes

was consistently observed (**Figure 4.3A1, A2**). Liposomes were in excess in these studies therefore many protein-free vesicles were observed. However, CidC was always found bound to clustered vesicles. Very large structures were observed most likely representing CidC-liposome aggregates in agreement with the gel filtration data above (data not shown). When the CidC cofactors TPP/Mg2+ where added to the sample, the same co-localization was thoroughly observed (**Figure 4.3B1, B2**). Combined, the data above demonstrates that CidC spontaneously binds to membranes and that this interaction is mostly electrostatic in nature.
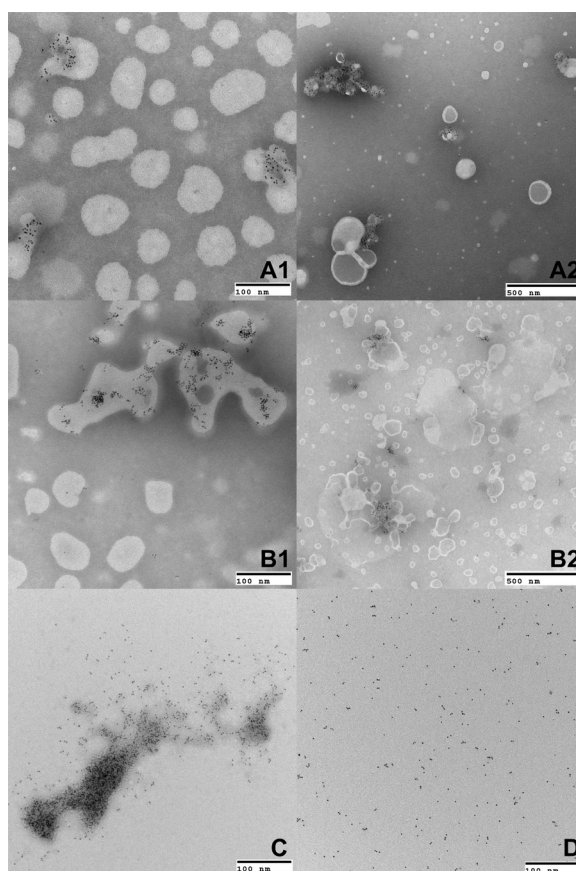
**Figure 4.3.** TEM characterization of CidC. TEM images showing CidC as labeled by 5 nm nanogold particles and liposomes by negative staining. Binding of CidC to membranes is demonstrated in mixtures of CidC and liposomes at pH 6 (A1, A2) without and (B1, B2) with the co-factors TPP/Mg2+. CidC self-aggregation is characterized by incubating the protein for 1 hour at pH 6 (C) without and (D) with 500 mM NaCl.

CidC converts pyruvate to acetate. Two possible enzymatic reactions are catalyzed by pyruvate oxidoreductases as detailed above: one converts pyruvate to acetate/carbon dioxide and the other to acetyl phosphate/hydrogen peroxide. The reactions can be easily identified by detecting acetate and, respectively, hydrogen peroxide in the end products. The production of both acetate (via a commercial kit) and hydrogen peroxide (via a well-established assay) was investigated here to determine which of these two reactions is facilitated by recombinant CidC *in vitro*. A note is made that the acetate pathway requires a quinone which was substituted with ferricyanide and that the acetyl phosphate pathway requires phosphate and oxygen which were present in the sodium phosphate buffer. Previous studies have shown that other pyruvate oxidoreductases are barely active in the absence of amphiphiles such as the Triton X-100 detergent or phospholipids[149–151]. Triton X-100 was incorporated in some assays to possibly activate CidC. Tests were initially performed at pH 6 which provides a good compromise between CidC activity and self-aggregation, however some pyruvate oxidoreductases exhibit a strong pH-dependent activity[147]. In order to ensure that CidC does not produce hydrogen peroxide at a different pH, a screening was conducted over a wide pH range.

CidC was incubated for 1 hour with the pyruvate substrate, the TPP/Mg^{2+} cofactor and the artificial electron acceptor ferricyanide in phosphate buffer pH 6 to allow complete enzymatic conversion of pyruvate by CidC. Initial tests showed that the reaction completes within several minutes under the employed conditions and that longer incubations do not change the enzymatic outcome. This solution was immediately tested for the presence of acetate and hydrogen peroxide. Acetate was quantitatively confirmed in the CidC enzymatic end products (**Figure 4.4A**). Two equivalents of ferricyanide are reduced per equivalent of decarboxylated pyruvate by pyruvate oxidases[149]. In this case, 20 mM pyruvate and 8 mM

ferricyanide were used, making ferricyanide the reaction-limiting ingredient. If all pyruvate is converted to acetate, the final acetate concentration is expected to be half that of ferricyanide (or about 4 mM). An average value of 4.4 mM acetate was indeed measured suggesting that CidC efficiently converted all pyruvate to acetate under these conditions. Inclusion of 1% w/w Triton X-100 did not significantly change the reaction outcome, while inclusion of 3 M urea severely limited the reaction most likely by denaturing the enzyme. Hydrogen peroxide was however absent from the end products of the CidC enzyme **(Figure 4.4B)**, even when 1% w/w Triton X-100 was added to the reaction. The above CidC catalytic reaction was also conducted at pH 5 to 8 in steps of 0.25, however hydrogen peroxide could not be detected in any of them.
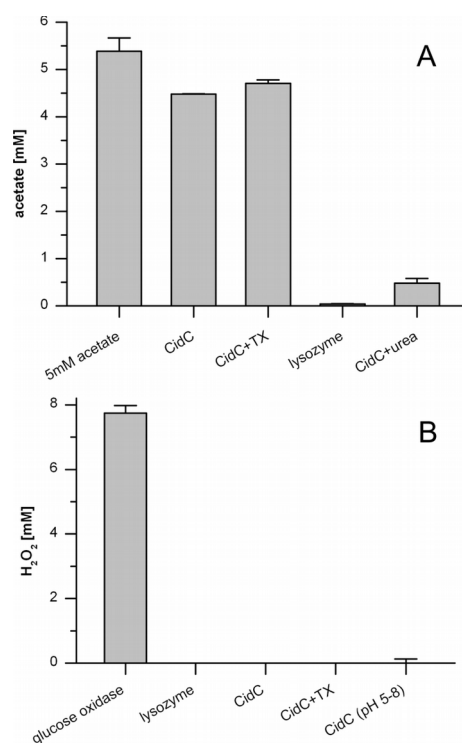
Figure 4.4. Products of the CidC enzyme. The production of either (A) acetate or (B) H_2O_2 by CidC was measured. (A) 5 mM acetate was used as a positive control. Acetate production was then measured as catalyzed by CidC, CidC with Triton X-100 (CidC+TX), lysozyme (negative control) and 3 M urea-denatured CidC (CidC+urea). (B) H_2O_2 production as catalyzed by glucose oxidase (positive control), lysozyme (negative control), CidC, CidC with Triton X-100 (CidC+TX). A range of pH values from 5 to 8 in steps of 0.25 was investigated for CidC, but no H_2O_2 levels were detected and the data is shown in aggregate as an average and labeled CidC (pH 5-8).

CidC couples to the respiratory chain via menaquinone. The other bacterial pyruvate:quinone oxidoreductases transfer electrons directly into the electron transport chain via a quinone such as ubiqionone (Q) in *E. coli*[92,152]. Similarly, CidC should utilize menaquinone (MK) which is produced by *S. aureus*. Although the electron transport chain occurs predominantly within membranes, it is preferable to conduct these experiments in solution, avoiding the problems associated with the membrane-induced CidC aggregation. For this reason, the reduction by CidC of the cytochrome c via the headgroups of ubiquinone (Q0) and menaquinone (MK0 or menadione) were investigated in aqueous solutions. This is possible because only the quinone headgroups participate in the redox reactions, while their hydrophobic chains mainly function as membrane anchors. Strikingly, very fast electron transfer was observed via MK0 (cytochrome c was completely reduced within 10 minutes of the start of the reaction), while very little transfer was observed via Q0 or in the absence of any quinone (*e.g.* directly to the cytochrome c) as indicated in **Figure 4.5**. It is important to note here that the time-scale for the cytochrome c reduction in the presence of MK0 (which is about 10 minutes) is identical to the reduction of the ferricyanide described below (**Figure 4.6A**). This implies that the electron transfer by CidC via MK0 to cytochrome c or directly to ferricyanide are equivalent, reinforcing that menaquinone is an efficient, biologically relevant electron carrier for CidC. This results demonstrate that CidC participates in the *S. aureus* respiratory chain via menaquinone.
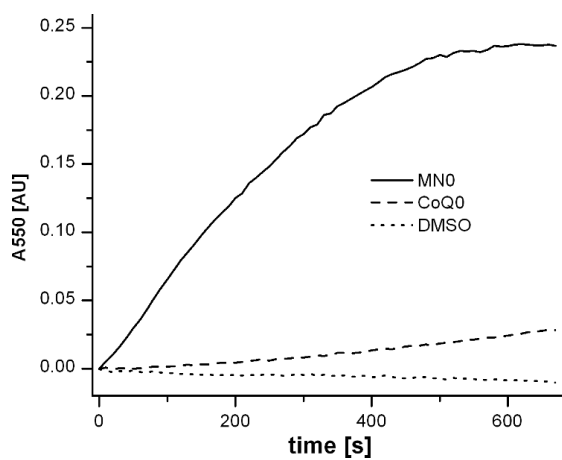
Figure 4.5. Quinone reduction by CidC. Electron transport by CidC to cytochrome c via MN0, CoQ0 or DMSO (control) was investigated. The oxidation state of cytochrome c was measured via A550 and is plotted as the change from its oxidized state.

Modulators of CidC enzymatic activity. Previously studied bacterial pyruvate oxidoreductases are activated by amphiphiles and barely active in their absence[149–151], however the experiments above demonstrate that this is not the case for CidC. More specifically, Triton X-100 has no effect on the end-point acetate or hydrogen peroxide production by CidC (Figure 4), e.g. the same total amount of acetate and no hydrogen peroxide are produced with or without Triton X-100. The CidC enzyme kinetics may however be different in the presence of Triton X-100 or other previously identified modulators of pyruvate oxidoreductase activity such as phospholipids. The effects of the Triton X-100 and OG detergents, POPG:POPC liposomes and NaCl on the CidC catalysis were therefore investigated.

CidC was incubated with pyruvate, TPP/Mg^{2+} and several activity modulators (as shown in **Figure 4.6A**). The enzymatic reaction was started by the addition of ferricyanide and monitored by the ferricyanide reduction via its change in color at 450 nm. No changes in enzyme kinetics could be detected when Triton X-100 was present at different concentrations, while OG induced only a minute decline in the kinetics. Interestingly, the presence of POPG:POPC liposomes which are instantaneously precipitated by CidC induces a significant increase in the enzyme kinetics. Under the employed conditions CidC alone completely reduces ferricyanide in about 10 minutes, however the addition of liposomes accelerates this reaction resulting in complete reduction in about 4 minutes. As expected, the presence of 3 M urea completely abolished the enzymatic activity of CidC and stoichiometric substitution of CidC with lysozyme in this experiment resulted in a complete loss of ferricyanide reduction.

Since NaCl was found above to influence CidC self-aggregation and interaction with membranes, its effect on CidC catalysis was also investigated and is shown in **Figure 4.6B**. Interestingly, even at small concentrations NaCl was able to inhibit CidC activity. For example, 50 mM NaCl extends the complete reduction of ferricyanide from about 10.0 to

11.7 minutes. At higher concentrations the effect is much bigger, e.g. at 100 mM NaCl the reduction is complete in about 20 minutes and at 500 mM only about 85% of the ferricyanide is reduced in 20 minutes. The effects of NaCl must be entirely due to the Cl^- ion, because Na^+ was present in the buffer at 200 mM.
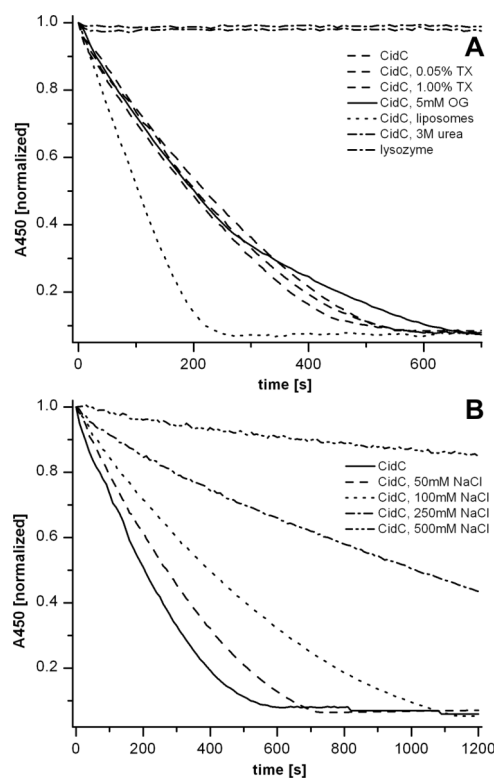
Figure 4.6. Modulators of CidC activity. The influence of several compounds on the CidC enzymatic activity was tested via the ferricyanide assay. (A) CidC alone and in the presence of 0.05% and 1.0% w/w Triton X-100 (TX), 5 mM OG, 0.5 mg/mL POPG:POPC liposomes and 3 M urea. A control was performed were CidC was stoichiometrically substituted with lysozyme. (B) CidC alone and in the presence of 50, 100, 250 and 500 mM NaCl.

CidC activity is strongly pH-dependent. The *Lactobacillus plantarum* (*L. plantarum*) pyruvate:oxygen 2-oxidoreductase displays maximal activity at acidic pH (5 to 6), while retaining about half of its maximal activity at neutral pH (7 to 8)[147]. To study the effect of pH on CidC activity, we varied the pH of the reaction buffer between 5 and 8 (**Figure 4.7**). The buffers used were 200 mM sodium phosphate between pH 5 and 7 and 200 mM Tris between pH 7 and 8. Both buffers were employed at pH 7 and identical results were obtained suggesting that sodium phosphate and Tris buffers do not affect CidC activity. **Figure 4.7A** shows selected enzymatic kinetic profiles for CidC which demonstrate a strong pH dependence. In particular, very little CidC activity is observed above pH 7, while the fastest kinetics was observed at pH 6. A more quantitative analysis was performed by measuring CidC specific activity at the beginning of these reactions as plotted in **Figure 4.7B**. It should be noted that CidC self-aggregates as the pH drops below pH 6, especially below pH 5.5, resulting in reduced experimental reproducibility (hence the more acidic the buffer, the larger the error bars in **Figure 4.7B**). CidC specific activity is observed to peak between pH 5.5 and 6.0 (similar to the pyruvate:oxygen 2-oxidoreductase from *L. plantarum*) with a specific activity of around 8 U/mg. However, the CidC activity is almost completely abolished above pH 7 with specific activity values below 0.5 U/mg. In stark contrast to the *L. plantarum* pyruvate:oxygen 2-oxidoreductase which maintains significant activity at neutral pH, CidC is barely active at pH 7 to 8.
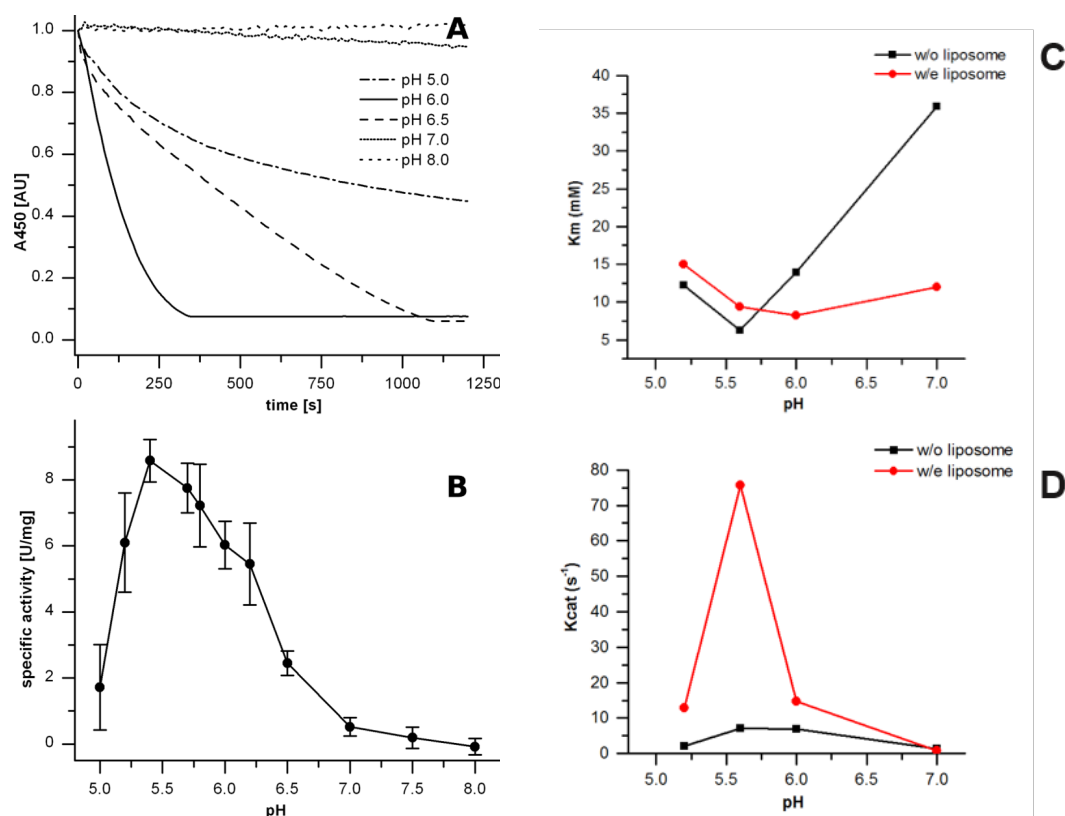
Figure 4.7. pH-dependence of CidC activity. The kinetic profile of CidC catalysis at different pHs as monitored by the ferricyanide assay. Note that twice the CidC concentration as in Fig. 6 was used to speed up the slow kinetics at neutral pH. (A) The kinetics at pH 5.0, 6.0, 6.5, 7.0 and 8.0 as indicated. (B) The calculated CidC specific activity as a function of pH 5 to 8. (C) CidC K_m for pyruvate under different pH with and without liposome (D) CidC k_{cat} for pyruvate under different pH with and without liposome.

The kinetics of CidC is pH dependent and changed dramatically upon binding to liposome. To better understand the mechanism of the pH dependent activity of CidC, we have also measured the two important enzymatic parameter K_m and kcat (turnover number) for substrate pyruvate of CidC under different pH, with and without the liposome (see in **Figure 4.7** right panel). Based on the results, the Km of CidC reached it's minimum at acidic pH around 5.6 (**Figure 4.7C**), which means CidC has the highest affinity for it's substrate under acidic pH. On the other hand, the k_{cat} value reaches the maximum under pH 5.6, indicating that CidC is most efficient under acidic pH as well.

When the liposomes are included in the substrate buffer, CidC activity is raised up by about 3 folds, as **Figure 4.7** shows. Based on the K_m and kcat value under different pH, it's obvious that K_m is not changed dramatically in the presence of liposome except for neutral pH. However, the kcat value was increased the most under acidic pH. Thus the kcat/km value also peaked at pH 5.6, suggesting that not only the enzyme itself reaches the maximum, but also the binding of liposomes greatly enhances the enzymatic kinetics under acidic pH.

CidC only binds its TPP/Mg^{2+} cofactor at acidic pH. ITC experiments (**Figure 4.8**) were performed in an attempt to investigate the CidC inactivity at pH 7 to 8. The interaction between CidC and TPP/Mg^{2+} was specifically measured at both pH 6 and 7. To minimize self-aggregation, CidC in pH 7 phosphate buffer was loaded into the ITC syringe and titrated into pH 6 or pH 7 phosphate buffer containing either of TPP, TPP/Mg^{2+} or pyruvate. A strong interaction between CidC and TPP/Mg^{2+} was observed in pH 6, but was very weak in pH 7 suggesting that CidC is inactive at neutral pH because it does not bind its TPP/Mg^{2+} cofactor. Unfortunately, the self-aggregation inherent to the current CidC formulation prohibits a full thermodynamic analysis of the binding between CidC and the TPP/Mg^{2+} cofactor.

Two controls were performed by injecting CidC in pH 6 phosphate buffer (**Figure. 4.8A**) and pH 7 phosphate buffer (**Figure. 4.8E**). In pH 6 control CidC undergoes a pH-jump with an exothermic structural change corresponding to about -50 kCal/mole of CidC. In pH 7 control CidC is simply diluted in the same buffer and, correspondingly, no significant energies are measured. When CidC is titrated into TPP alone, an endothermic binding is observed with about 100 kCal/mole of CidC in the first injections (**Figure. 4.8B**). Titration into TPP/Mg^{2+} reveals an even stronger interaction with between 200 to 250 kCal/mole of CidC in the first injections (Figure 4.8C). These data demonstrate that CidC binds in pH 6 its TPP cofactor and that Mg^{2+} greatly enhances the CidC/TPP interaction. Interestingly, the CidC titration into pyruvate in pH 6 phosphate buffer (**Figure. 4.8D**) was identical to the protein dilution into the same buffer (**Figure. 4.8A**), suggesting that either CidC does not bind pyruvate in the absence of the TPP/Mg^{2+} cofactor or that negligible energies are associated with this binding. Titration of CidC into TPP (data not shown) or TPP/Mg^{2+} (**Figure 4.8F**) at pH 7 was, however, very different as no endothermic binding was observed. This finding strongly suggests that CidC may not be able to bind its TPP/Mg^{2+} cofactor at neutral pH, resulting in enzyme inactivity.
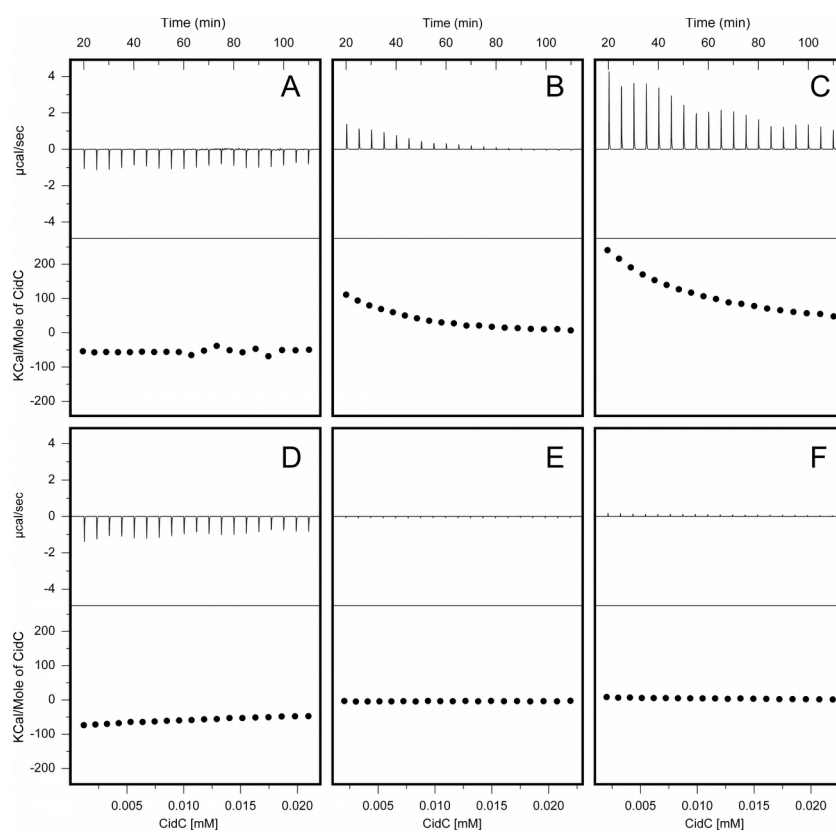
Figure 4.8. ITC studies of the TPP/Mg^{2+} binding to CidC. CidC in (A-D) NaPh6 or (E-F) NaPh7 buffer was injected into NaPh7 buffer containing (A, E) nothing else, (B) TPP, (C) TPP/Mg^{2+}, (D) pyruvate and (F) TPP/Mg^{2+}. Each panel contains (top) the raw ITC data and (bottom) the integrated ITC data. The x-axis is labeled as both the timing of the injection and the CidC concentration in the ITC cell.

Citrate inhibits CidC activity. When testing the pH dependence of CidC activity, citrate-based buffers were initially found to have a concentration-dependent effect on CidC activity. Further analysis using the ferricyanide assay (**Figure 4.9A**) demonstrated that citrate actually inhibits the CidC enzyme with an IC50 of about 10 mM and complete inhibition at 100 mM. ITC experiments similar to those presented above indicate that citrate directly binds to CidC at pH 6 (in the absence of pyruvate and TPP/Mg^{2+}). When CidC is titrated into pH 6 phosphate buffer an exothermic protein structural change of about -50 kCal/mole of CidC is observed (**Figure 4.9B**), as shown in Figure 4.8A. However titration into pH 6 phosphate buffer supplemented with 10 mM citrate reveals a reaction with approximately -200 kCal/mole of CidC (in the first injections, **Figure 4.9C**), most likely due to binding of citrate to CidC in addition to the pH-induced CidC conformational change.
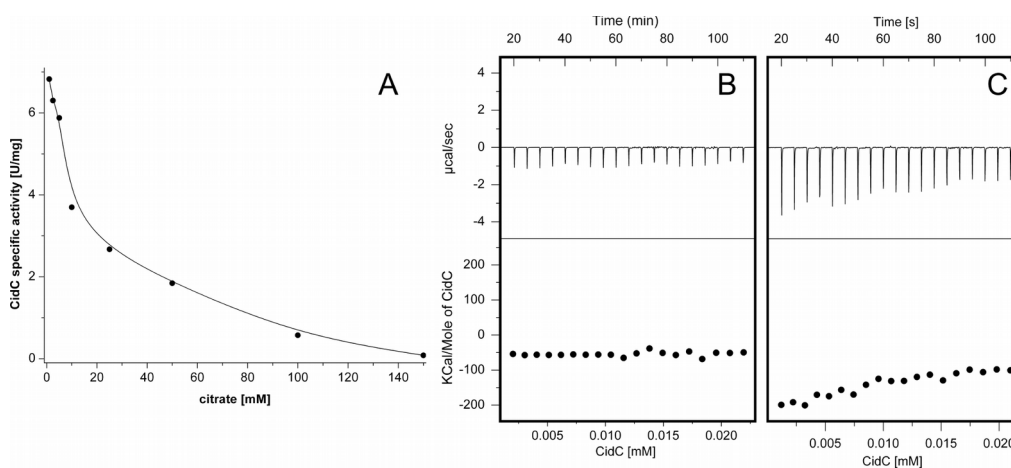
Figure 4.9. Citrate inhibition of CidC. (A) The CidC specific activity in the presence of citrate in NaPh6 buffer was measured by the ferricyanide assay. (B-C) ITC experiments as in Figure 4.8, except that CidC was titrated into (B) NaPh6 buffer and (C) 10 mM citrate, NaPh6 buffer.

CidC proteolysis maintains enzymatic activity. Other bacterial pyruvate oxidoreductases were shown to be activated by proteolytic treatment with chymotrypsin[87,142]. The effects of both trypsin and chymotrypsin were therefore investigated here at both pH 6 when CidC is active and at pH 7 when CidC is mostly inactive. The results for trypsin are shown in Figure 4.10 noting that identical results were obtained for chymotrypsin (data not shown). Similar to previous results for other pyruvate oxidoreductases, CidC was protected from proteolytic cleavage only if pyruvate and TPP/Mg^{2+} were all available to the enzyme, *e.g.* the enzyme was fully reduced. However, the protection is very efficient only at pH 6 and is completely absent at pH 7 in the case of CidC. During 30 minutes of cleavage at pH 6, only a minute fraction of CidC cleaved to a product labeled as CidC^a, while at pH 7 most of the enzyme is converted to CidC^a and CidC^b. CidC^a and CidC^b are only a few kDa and, respectively, about 20 kDa smaller than CidC and resemble the 58 and 51 kDa species obtained by proteolysis of the *E. coli* PoxB previously reported[153]. No further attempts were made to characterize these truncated proteins at the amino acid sequence level.

When either of (i) pyruvate, (ii) TPP/Mg^{2+}, or (iii) Mg^{2+} were provided to CidC, trypsin was very effective in cleaving CidC at both pH 6 and 7 (**Figure 4.10**). This data suggests that CidC is protected from trypsin only when it is active (at pH 6) and when both the pyruvate substrate and the TPP/Mg^{2+} cofactor are present. The activity of the CidC^a and CidC^b proteins was also investigated by the ferricyanide assay and were found to be as active as their CidC parent at pH 6, however no measurable activity could be detected at pH 7 (data not shown).
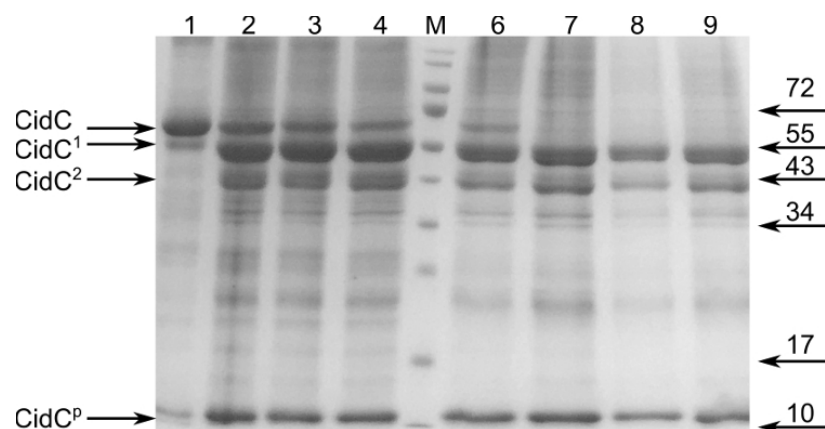
Figure 4.10. Proteolysis of CidC. SDS-PAGE showing the CidC cleavage products after 30 minutes incubation with trypsin at pH 6 (lanes 1-4) and pH 7 (lanes 6-9). Before proteolysis, CidC was incubated with (lanes 1, 6) pyruvate, TPP and Mg^{2+}, (lanes 2, 7) TPP and Mg^{2+}, (lanes 3, 8) pyruvate, (lanes 4, 9) Mg^{2+}. CidC products are shown on the left with $CidC^1$ and $CidC^2$ being several kDa and, respectively, about 20 kDa smaller than CidC, while $CidC^p$ indicates small peptides. Several bands from the marker (lane M) are labeled on the right.

4.5 Conclusions

The extensively studied PoxB pyruvate:ubiquinone oxidoreductase from *E. coli* directly shuffles electrons from the cytoplasm to the membrane-bound mobile carrier ubiquinone of the electron transport chain when it converts pyruvate to acetate. PoxB is inactive within the cytoplasm where the C-terminus sterically hinders the active site from both the pyruvate substrate and the ubiquinone electron acceptor[93,154,155]. PoxB becomes active *in vivo* by binding to the membrane via this C-terminus which undergoes a structural rearrangement exposing the active binding site to the solvent and activating the enzyme by two orders of magnitude (affecting both turnover and pyruvate affinity). This behavior can be reproduced *in vitro* by binding to artificial phospholipid membranes and detergent micelles, or by proteolytic cleavage of the C-terminus[142]. This current *in vitro* study reveals novel insights into the CidC pyruvate:menaquinone oxidoreductase from *S. aureus* which turns out to be quite different from PoxB. CidC is also a membrane-bound protein, however it is only modestly activated by binding to artificial membranes or by proteolytic cleavage when the activity increases by only a factor of about two. This behavior may be explained by a slightly different CidC structure where the C-terminus may not inhibit solvent access to the active site in the membrane-free form of the protein. Another important conformational difference of CidC resides in its inability to oligomerize, unlike the tetrameric PoxB found in several organisms[142,143,146,148]. CidC is able to efficiently pass electrons to menaquinone, the quinone found within the *S. aureus* membranes which are lacking ubiquinone, and thus appears to actively participate in the electron transport chain. CidC is active under conditions slightly more acidic than pH 6.5 and is largely inactive at pH 7 to 8 most likely due to its inability to bind the TPP cofactor at neutral pH. This contrasts to PoxB which retains about 50% and 20% of its activity at pH 7 and, respectively, pH 8[147]. CidC therefore appears to be intrinsically "activated" only when the cytoplasm becomes sufficiently acidic, at which point it further

contributes to intracellular acidification by generating acetate.

Our laboratory has recently demonstrated the role of *cidC* and cytoplasmic acidification in bacterial cell death: stationary phase death was found to be dependent on CidC-generated acetate and, respectively, extracellular acetic acid which, in the protonated and uncharged form, freely passes across the cytoplasmic membrane where it then disassociates and acidifies the cytoplasm[70]. As in eukaryotic cells undergoing apoptosis[156,157], death in *S. aureus* under these conditions was shown to be associated with the accumulation of reactive oxygen species (ROS) and diminished when the production of these reactive molecules was limited[70]. It was also demonstrated that the physiological features that accompany the metabolic activation of cell death are strikingly similar to the hallmarks of eukaryotic apoptosis, including ROS generation and DNA fragmentation. Although the *cidC* gene is co-expressed with *cidA*, previously shown to be involved in the control of PCD in *S. aureus*, there is currently limited information about the potential interactions between these proteins. Recent experiments conducted in our laboratory indicate that the association of CidC protein with the membrane, as well as CidC-induced acetate generation, can be modulated by the CidA and CidB proteins (manuscript in preparation). The functions of these proteins in PCD may therefore be interdependent and current investigations in our laboratory are investigating this possibility.

Another important finding of this study was that CidC converts pyruvate exclusively to acetate transferring electrons directly to menaquinone during this process. These results are consistent with previous studies in our laboratory[9] and indicate that CidC should be described as a pyruvate:menaquinone oxidoreductase, rather than a pyruvate oxidase as was previously presumed based on the close sequence alignment of these two classes of enzymes[9]. Interestingly, pyruvate:oxygen 2-oxidoreductases have also been shown to be involved in cell death in the organisms that produce them. For example, the well-described death of

Streptococcus pneumoniae in stationary phase has been shown to be dependent on the expression of the *spxA* gene encoding a pyruvate:oxygen 2-oxidoreductase which generates hydrogen peroxide and induces cell death[141]. Thus, despite catalyzing distinct enzymatic reactions with different metabolic end-products, both enzymes appear to play major roles in the induction of bacterial cell death. In summary, the results of the current study provide critical new details of the activity of the CidC enzyme previously shown to be important for the generation of acetate and the potentiation of PCD. This will be particularly important as we explore the possible interactions of CidC with CidA and/or CidB and will be critical as we dissect the molecular mechanisms underlying bacterial cell death.

Chapter 5

Attachment of GC-rich single strand/duplex to thrombin binding aptamer G-quadruplex

5.1. Summary

The thrombin binding aptamer (TBA, 5'-GGTTGGTGTGGTTGG-3') is a well characterized chair-like, antiparallel quadruplex structure that binds specifically to thrombin at nanomolar concentrations and therefore it has interesting anticoagulant properties. In this article we attached either of the two complementary GC-rich single strands separately or duplex (formed by the single strands) to the 5' and/or 3' end of TBA, we observed different effects of the single strands/duplex on the stability of the G-quadruplex by using UV/CD/DSC techniques. Based on the results, 5' attached single strand A (5'-GCACCACT-3') has a deleterious effect on quadruplex formation by base pairing with 5 nucleotides of the TBA, thus destabilizing the G-quadruplex. Whereas 3' attached single strand B (5'-AGTGGTGC-3') has no significant effect on G-quadruplex stability. When both single strands A and B are attached to the 5' and 3' of TBA, they form a duplex that destabilize the G-quadruplex, but the duplex was greatly stabilized.

5.2. Introduction

Aptamers are oligonucleotides that were generated by an *in vitro* selection and polymerase chain reaction process known as SELEX (systematic evolution of ligands by exponential enrichment)[101,158,159] which selects them based on their specific and tight binding affinity to a target from a protein library. Through this approach, a large amount of aptamers with moderate or high affinity have been chosen for diagnostics, therapeutics and other

technical applications[159].

α-Thrombin is a serine protease which has multiple functions in homeostasis, and it is the only protein that catalyzes the cleavage of fibrinogen to produce fibrin clot[160]. The multiple functions of α-thrombin in hemostasis involve the procoagulant, anticoagulant, and fibrinolytic pathways with large amount of substrates[161].

Excessive coagulation results in dissemination of the clot in undamaged tissues, which will cause thrombosis. Achieving the ability to specifically inhibit thrombin *in vivo* with synthetic compounds to prevent thrombosis is an important goal in the pharmaceutical field. In 1992, a potent inhibitor of thrombin was selected by Bock et al. from a pool of synthetic oligonucleotides based on a single-stranded 15-mer DNA with the sequence 5'GGTTGGTGTGGTTGG3' (thrombin binding aptamer, TBA)[103]. TBA forms a unimolecular G-quadruplex in solution, arranged in a chair-like structure, consisting of two G-quartets connected by two TT loops and one TGT loop. The crystal structure revealed that TBA may interact with both exosites I and II of thrombin. The three dimensional structures of thrombin and TBA are preserved in the complex, and specific interactions are found involving the exosites and the loops of the aptamer[102,104].

Although several efforts have been deployed to improve the binding properties of TBA to thrombin[100,107,159], there is still room for improvement to aim for a better therapeutic strategy. Full understanding of the thermostability of the molecule is essential for understanding its biological activity and useful for the future development of oligonucleotide-based therapeutics or drug design.

In this work, we report by CD/UV/DSC methods the study on the stability of TBA in the presence of 5' and/or 3' GC-rich single strands, which helps us better understanding the important effects of different junction sequences on the thermostability of TBA. Also, since

G-quadruplex structures are found throughout genomic DNA sequence, especially in the telomere and promoter regions, the current study will have great implication on how flanking sequences affects the folding and unfolding of G-quadruplex.

5.3. Materials and Methods

Materials. The 5'-3' sequences of oligonucleotides (ODNs) and designations (**Figure 5.1.**): d(GGTTGGTGTGGTTGG), G_2; d(GCACCACT), A; d(AGTGGTGC), B; d(GCACCACTGGTTGGTGTGGTTGG), AG_2; d(GGTTGGTGTGGTTGGAGTGGTGC), G2B; d(GCACCACTGGTTGGTGTGGTTGGAGTGGTGC), AG_2B were purchased from Eurofins MWG Operon LLC (Huntsville, AL). The ODN were dissolved in water and desalted on G-50 Sephadex column, and lyophilized to dryness. The experiments were conducted in a 10 mM HEPES-K 100 mM KCl buffer at pH 7.5. The concentrations of the ODN solutions were determined at 260 nm and 90 °C using a Perkin-Elmer Lambda-10 spectrophotometer. and the following molar extinction coefficients for the single strands (mM^{-1}cm^{-1}): 116 (G_2), 52 (A), 60 (B), 213 (AG_2), 203 (G_2B), 292 (AG_2B). These values were obtained by extrapolation of the tabulated values for dimers and monomeric bases at 25°C[162–164] to higher temperatures using procedures reported previously[165]. Inorganic salts from Sigma were reagent grade, and used without further purification. Different concentration of ODNs were used for different experiments, as mentioned in the following parts.

Temperature-Dependent UV (UV melting). Absorbances versus temperature profiles (UV melting curves) were obtained at 295 nm and 260 nm for all molecules, using a thermoelectrically controlled Aviv 14DS spectrophotometer (Lakewood, NJ). The temperature was scanned from 5 °C to 100 °C at a heating rate of ~0.5°C/min. Shape analysis of the melting curves yielded T_M and ΔH_{vH}'s using standard procedures[165,166]. The transition molecularity for the unfolding of a particular complex was obtained by monitoring the T_M as a function of the strand concentration. Intramolecular complexes show a T_M-independence on

strand concentration while the T_M of intermolecular complexes does depend on strand concentration. The concentration of each ODN is adjusted to an absorbance of ~0.6 at 260nm (90°C). The data was normalized and smoothed using Originlab software.

Circular Dichroism (CD) Spectroscopy. The CD spectra of each ODN, from 200 nm to 320 nm, were obtained at 25 °C and 90 °C using an Aviv Model-202SF spectrometer (Lakewood, NJ), equipped with a peltier system for temperature control. This allowed us to determine the conformation of each ODN. From simple inspection of their CD spectra at low temperatures, and to select appropriate wavelengths for their temperature-induced unfolding. Ellipticity versus temperature profiles (CD melting curves) were obtained at 260nm and 295 nm for all molecules. The temperature was scanned from 5 °C to 90 °C at a heating rate of ~1 °C/min, and the cell compartment was flushed with nitrogen to prevent water condensation. The concentration was adjusted to 50μM for single ODN and 50 + 50μM for the ODN mixture (e.g. AmixG$_2$B means that A and G$_2$B are in 50μM:50μM mixture). The data was normalized and smoothed using Originlab software.

Differential Scanning Calorimetry (DSC). The total heat required for the unfolding of each ODN was measured with a VP-DSC differential scanning calorimeter from Microcal (Northampton, MA). Standard thermodynamic profiles and T_{MS} are obtained from a DSC experiment using the following relationships: $\Delta H_{cal} = \int \Delta Cp(T)\, dT$; $\Delta S_{cal} = \int \Delta Cp(T)/T\, dT$, and the Gibbs equation, $\Delta G^\circ{}_5 = \Delta H_{cal} - T\Delta S_{cal}$; where ΔCp is the anomalous heat capacity of the ODN solution during the unfolding process, ΔH_{cal} is the unfolding enthalpy, ΔS_{cal} is the entropy of unfolding; both latter terms are temperature-dependent i.e., the heat capacity difference between the initial and final states is non-zero. Alternatively, $\Delta G^\circ{}_T$ can be calculated using the equation $\Delta G^\circ(T) = \Delta H_{cal} (1 - T/T_M)$ which is implicitly correct for intramolecular transitions such as these G-quadruplexes. The ΔH_{vH} terms are also obtained from the DSC profiles using the temperatures at the half-width height of the experimental

curve. The $\Delta H_{vH}/\Delta H_{cal}$ ratio can tell us about the nature of the transition. For a two-state transition $\Delta H_{vH} = \Delta H_{cal}$, while for a non-two-state $\Delta H_{vH} \neq \Delta H_{cal}$. The concentration is adjusted to 50µM for single ODN and 50 + 50 µM for the ODN mixture (e.g. AmixG$_2$B means that A and G$_2$B are in 50 µM:50 µM mixture). The data was normalized and smoothed using Originlab software.
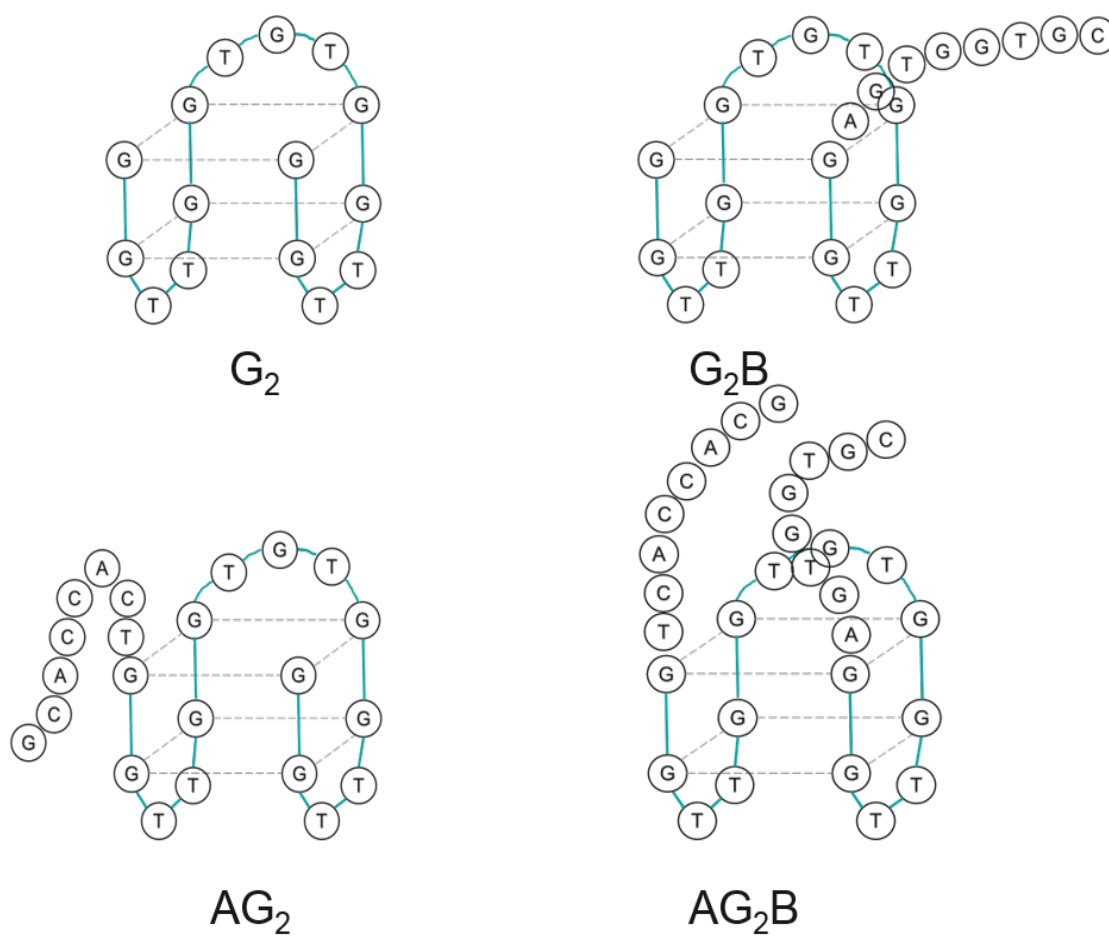
Figure 5.1 Schematic figures of the ODNs containing G-quadruplex sequence in the study (from 5' to 3')

G_2: GGTTGGTGTGGTTGG;

G_2B: GGTTGGTGTGGTTGGAGTGGTGC;

AG_2: GCACCACTGGTTGGTGTGGTTGG;

AG_2B: GCACCACTGGTTGGTGTGGTTGGAGTGGTGC.

5.4. Results and Discussion

CD spectroscopy. The conformation of ODNs can be obtained using CD spectroscopy. CD spectra are taken at different temperature to determine the preferential conformation of the cation-aptamer helical complex at lower temperature (25 °C) and of the random coil state at higher temperatures (90 °C). 100 mM K^+ serves to stabilize the DNA ODNs containing runs of guanine.

Representative spectra of each ODN in 10 mM K-HEPES, pH = 7.5, at 100 mM K^+ and 25 °C, are shown in **Figure 5.2.** The spectrum of the TBA, also designated as G_2, has a large positive band centered at 292 nm, a smaller negative band at 264 nm, and a smaller positive band at 246 nm[105,167]. The GC rich (62.5% G+C) duplex AB, has a broad peak centered at 280nm, indicating the adoption of a B-DNA conformation (see **Figure 5.2A top**). When the duplex AB is attached to G_2 (AG_2B), the G-quadruplex structure is preserved since the peak at ~292nm is maintained and shifted to lower wavelength as a consequence of the attachment. However, the intensity of the peak is larger than the sum of original the G-quadruplex and duplex (see **Figure 5.2A bottom**), indicating a possible slight twisting, leading to a more open conformation in the guanine quartet plane due to the formation of the duplex, which has an apparent effect on the junction part.

When only the single strand B is attached to the 3' end of G_2, the G-quadruplex conformation remains stable, as indicated by **Figure 5.2B top** (G_2B red line). When the complementary strand A is mixed with G_2B, A prefers to form a duplex with B but has little interaction with the quadruplex, as the sum of A and G_2B spectra is equal to that of the mixture of A and G_2B (see **Figure 5.2B bottom**). Interestingly, upon the attachment of A single strand to the 5' of G_2, the G-quadruplex formation is almost abolished (see **Figure 5.2C top**). The addition of B is not able to rescue the quadruplex, indicating that the interaction
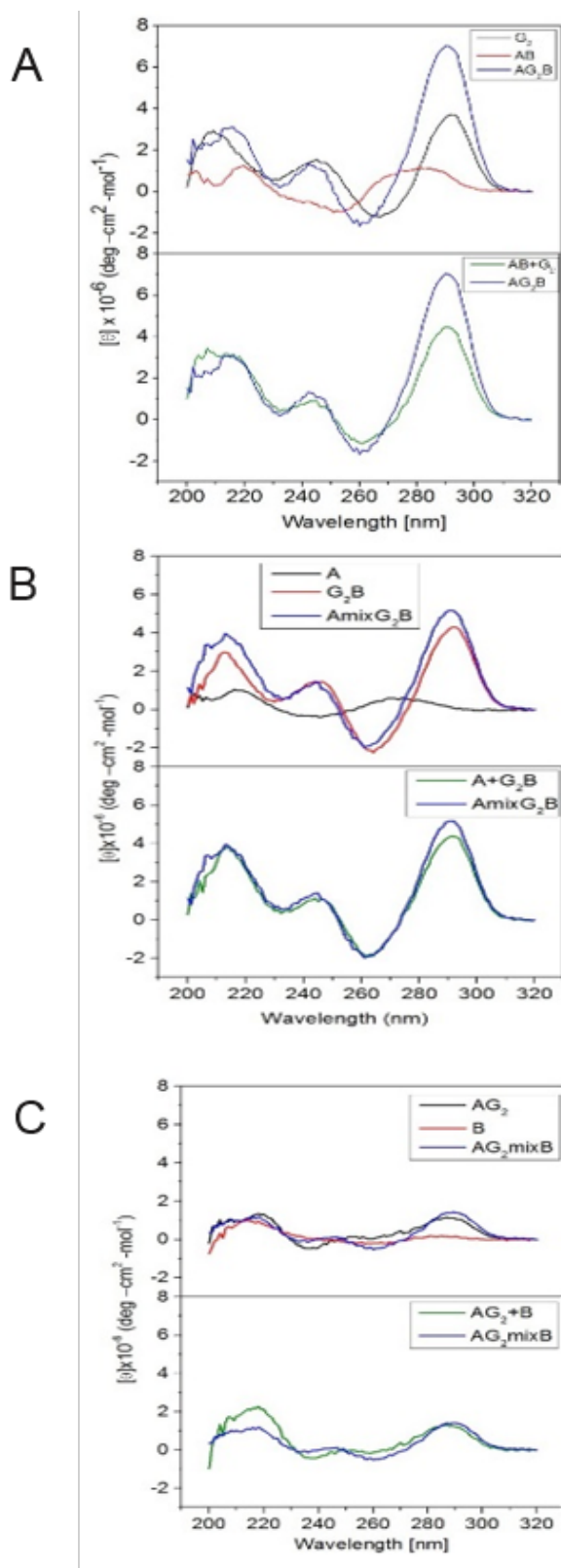
Figure 5.2 CD spectra of three groups of junctions (A) upper: AG_2B, G_2 and AB, lower: sum of the spectra of AB and G_2 (AB+G_2), AG_2B; (B) upper: A, G_2B and $AmixG_2B$, lower: sum of the spectra of A and G2B (A+G_2B), $AmixG_2B$; (C) upper: B, AG_2 and AG_2mixB, lower: sum of the spectra of B and AG_2 (AG_2+B), AG_2mixB.

between A and the G_2 is dominant since it's an intramolecular interaction, which is more favorable than the intermolecular interaction between the complementary strands A and B.

In addition, the random coil state of G_2 at high temperatures ($\geq$ 90 °C) has no distinctive positive or negative peaks, while the random coil states of all other junctions show similar CD spectra (data not shown). To summarize this part, the formation of the G-quadruplex structure is evident by CD spectroscopy when G_2 is attached to the AB duplex or single strand B. However, the single strand A has a deleterious effect on G-quadruplex formation, possibly by interaction and base pairing with part of the G_2 sequence.

UV and CD melting. Typical UV melting curves and CD melting curves at 295 nm are shown in **Figure 5.3**, which mainly monitors the unfolding of the G-quadruplex in each junction. The curves are sigmoidal and show a hypochromic effect at the wavelengths. The UV melts yielded hypochromicities (only for those which form a G-quadruplex) of 25% (G_2), 23% (G_2B) A+G_2B mixture (19%) and 45% (AG_2B), while the CD melts yielded changes of 31% (G_2), 49% (G_2B) A+G_2B mixture (51%) and 25% (AG_2B).
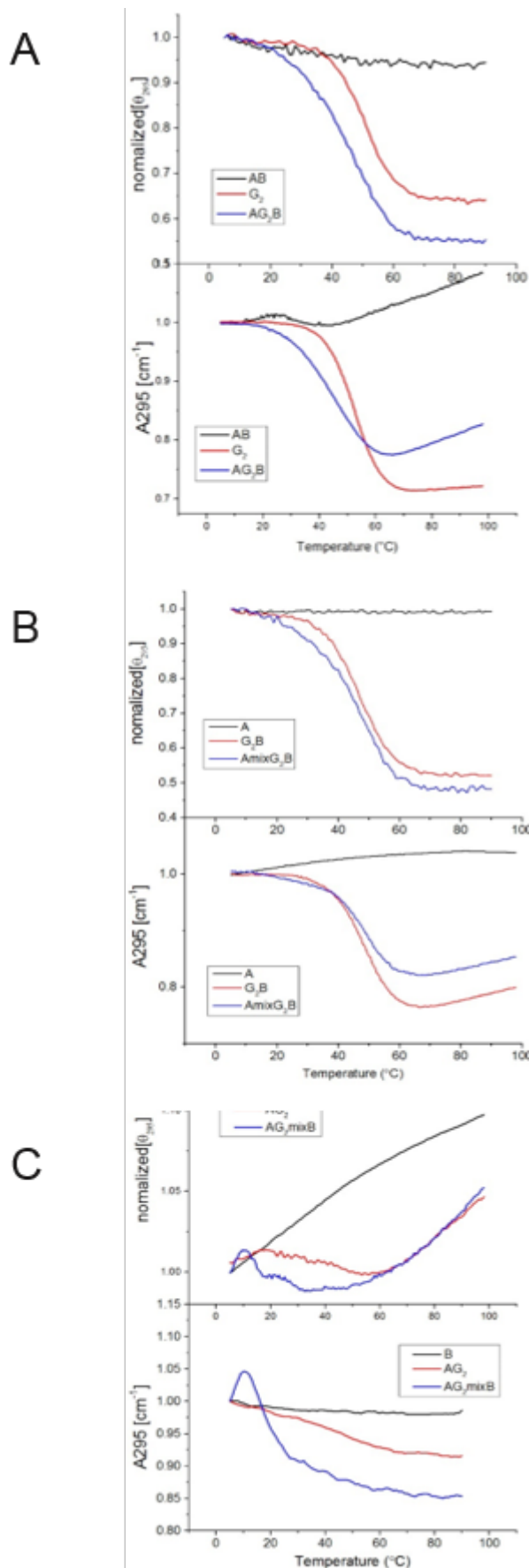
Figure 5.3 CD and UV melting at 295nm. (A) upper: CD melting of AG$_2$B, G$_2$ and AB, lower: UV melting of AG$_2$B, G$_2$ and AB; (B) upper: CD melting of A, G$_2$B and AmixG$_2$B, lower: UV melting of A, G$_2$B and AmixG$_2$B; (B) upper: CD melting of B, AG$_2$ and AG2mixB, lower: UV melting of B, AG$_2$ and AG$_2$mixB.

Shape analysis of these melting curves[165] yielded transition temperatures, T_M, and van't Hoff enthalpies, H_{vH}, see **Table 5.1.** The T_ms in the UV melts at 295nm have the following order: AG_2B (47.1°C) ~ G_2B (49.0°C)< $A+G_2B$ (50.1°C, A and G_2B 1:1 mixture) G_2 (52.2°C), while the T_M for the unfolding of the unattached AB duplex is 46 °C. The order of the T_Ms in the CD melts is as follows: G_2B (46.4°C) ~ AG_2B (47.9°C) < $A+G_2B$ (48.9°C)< G_2 (51.6°C), which are in fair agreement with those obtained from UV-melts. For AG_2+B and AG_2, since they have no clear transition at 295nm, their T_M can not be determined.

The UV and CD melting data strongly confirms the CD spectra and provide even more information on the stability of ODNs. G_2, G_2B, AG_2B and $A+G_2B$ all form a G-quadruplex, whereas AG_2 and AG_2+B don't. However, the attachment of the B strand appear to destabilize the G-quadruplex, but not much, as indicated by a slightly lower T_M (2-4 °C). Moreover, the addition of A to G_2B seems to bring the T_M higher and closer to that of the original G_2, suggesting that A interacts with B and may form a duplex which hangs out of the G-quadruplex. On the other hand, when both A and B are attached to the ends of G_2 (AG_2B), the stability of G_2 is decreased, which is probably due to the formation of the intramolecular duplex and its effect on the junction.

Figure 5.4 shows the UV melting curves for the ODNs at 260nm, monitoring the unfolding of the duplex portion (if there is any). The G_2 itself displayed hypochromicity, however, AG_2B produced a totally different unfolding profile, which is similar to that of duplex AB. Furthermore, the T_M for AG_2B at 260nm (60 °C) is 7.3 °C larger than that of G_2, strongly indicating that new base pairs or specific DNA local structure form during the unfolding of the G-quadruplex. Together with the melting curve at 295nm (**Figure 5.3**), we conclude that the unfolding of AG_2B is of two stages, first the unfolding of G-quadruplex and then the unfolding of the rest of sequence.

Meanwhile, as is the case of unfolding at 295nm, the T_M at 260nm of A+G_2B (48 °C) is also similar to that of G_2B (48 °C) (**Figure 5.4B**). Considering the T_M of A+G_2B is the average of the T_M of duplex AB (46.1 °C) and G_2 (52.7 °C), the profile of A+G_2B is the equivalent of the sum of duplex AB and G_2. Single strand A forms a duplex hanging on the side of the G-quadruplex in the folded state and the unfolding of the duplex part and G-quadruplex almost proceed simultaneously.

AG_2 does not form a G-quadruplex as previously discussed, however, it seems to form a partial duplex and the addition of single strand B has little effect on the stability of the duplex, as indicated by similar T_M (both ~60 °C) shown in **Figure 5.4C**. Interestingly, AG_2 and AG_2+B also have a similar T_M to that of AG_2B. This may suggest that the latter stage of unfolding of AG_2B is also the equivalent of the unfolding of AG_2. Single strand B, whether it's attached to the G-quadruplex or mixed with it, can't interact with A since the temperature is too high for them to base pair.

DNA	CD melt		UV melt	
	T_M (°C)	ΔH_{vH} (kcal/mol)	T_M (°C)	ΔH_{vH} (kcal/mol)
G_2	51.6	44	52.2	45
AG_2	NA	NA	NA	NA
AG_2B	47.9	25	47.1	28
AG_2+B	NA	NA	NA	NA
G_2B	46.4	42	49.0	38.2
A+G_2B	48.9	43.6	50.1	44.3

Table 5.1 Transition temperatures and van't Hoff Enthalpies from Shape Analysis of UV and CD melting curves at 295nm.
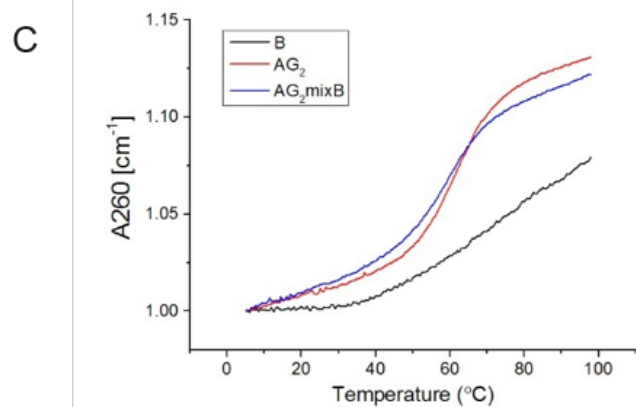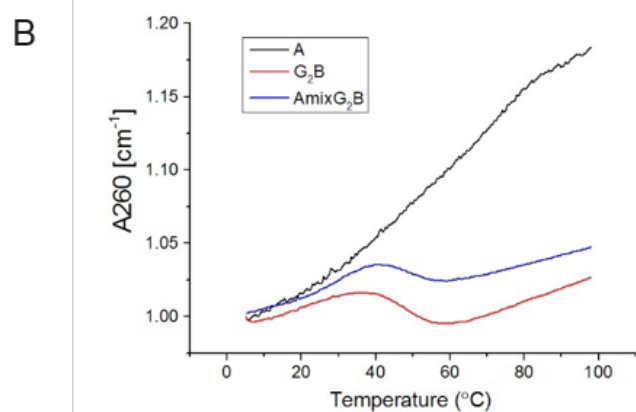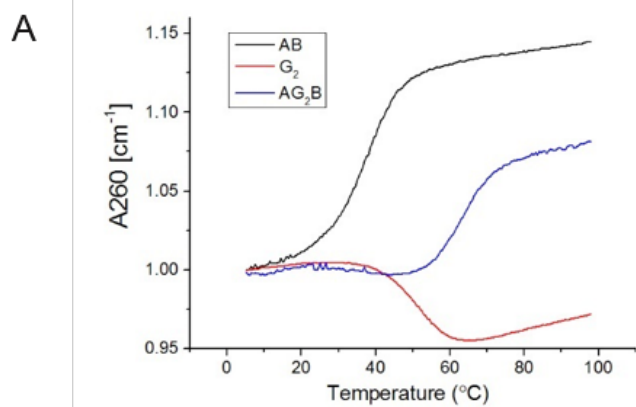
Figure 5.4 UV melting at 260nm. (A) UV melting of AG_2B, G_2 and AB; (B) UV melting of A, G_2B and $AmixG_2B$; (B) UV melting of B, AG_2 and AG_2mixB.

DSC Unfolding. Typical DSC melting curves for each oligonucleotide and G-quadruplex are shown in **Figure 5.5**. All DSC thermograms were reproducible and the transitions of all the ODNs were monophasic. Furthermore, the initial and final states of all transitions have similar heat capacity values, indicating negligible heat capacity effects accompany each transition.

The DSC curves show that G_2 has a single transition with a T_M of 52.7 °C, with a negligible difference between the UV and CD melt. G_2B has a single transition of 48.7 °C with a similar unfolding enthalpy (ΔH_{cal}) value (-30.2 kcal/mol). This indicates that the attachment of single strand B results in a less thermally stable G-quadruplex possibly as a result of minor interactions, but B does not change the unfolding profile of the G-quadruplex, as shown in **Figure 5.5, Table 5.2 and Table 5.3**. The AG_2B junction unfolds into a large asymmetric transition with T_M of 59.9 °C, which can be explained by the unfolding of both duplex and G-quadruplex portions. The explanation is also supported by the fact that the unfolding enthalpy (-65.3 kcal/mol) is almost equal to that of the sum of duplex AB (-44.3 kcal/mol) and G_2 (-24.9 kcal/mol). Furthermore, the unfolding of the equamolar mixture of single strand A and G_2B showed a similar T_M (48.7 °C) to G_2B, but a much bigger unfolding enthalpy (-65.1 kcal/mol), and is similar to that of AG_2B, strongly supporting the formation of both duplex and G-quadruplex in the equamolar mixture of A and G_2B.

However, in the case of AG_2 and AG_2+B, both the T_M (59.63 °C and 60.53 °C) and ΔH_{cal} (-28.1 and -30.9 kcal/mol) are close, proving that B has no effect on AG_2. Their T_MS are simlar to that of AG_2B but the unfolding enthalpy is much lower, in agreement with the fact that there is no G-quadruplex formation but A strongly favors the intramolecular base pairing with part of the G-quadruplex sequence.
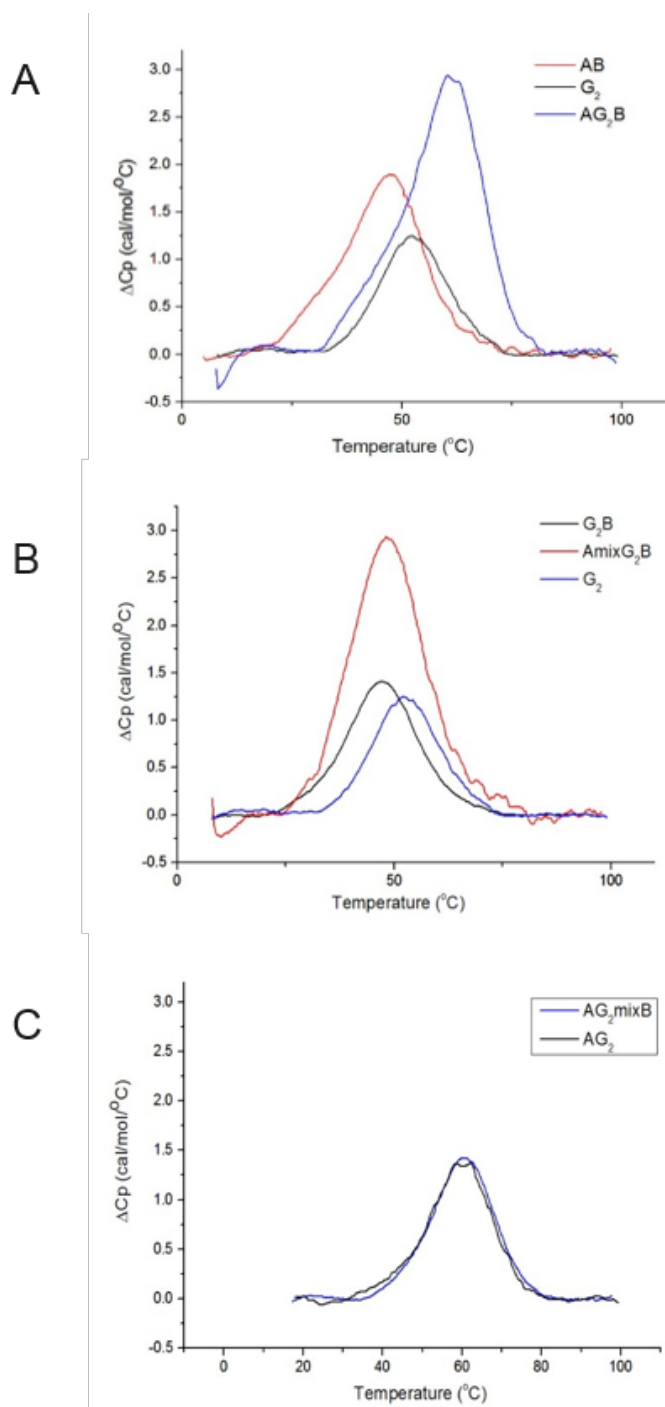
Figure 5.5 Unfolding profile of the ODNs by DSC. (A) DSC curves of AB, G_2, AG_2B; (B) DSC curves of G_2B, G_2, and $AmixG_2B$; (C) DSC curves of AG_2 and AG_2mixB.

DNA	DSC				
	T_M (°C)	ΔH_{cal} (kcal/mol)	$\Delta G°_5$ (kcal/mol)	$T\Delta S_{cal}$ (kcal/mol)	ΔH_{vH} (kcal/mol)
G_2	52.7	-24.9	-3.6	-21.3	-42.5
AG_2	59.63	-28.1	-4.6	-23.5	-43.3
AG_2B	59.93	-65.3	-10.8	-54.5	-38.3
AG_2+B	60.53	-30.9	-5.1	-25.8	-41.4
G_2B	48.74	-30.2	-4.1	-26.1	-38.2
$A+G_2B$	48.65	-65.1	-8.8	-56.3	-37
AB	46.1	-44.3	-5.7	-38.6	-33.5

Table 5.2 Folding Thermodynamic profiles for all molecules at 5 °C

| DNA	DSC			
	Tm (°C)	ΔH_{cal} (kcal/mol)	ΔG^o_5 (kcal/mol)	$T\Delta S_{cal}$ (kcal/mol)
	AG_2B			
G_2	52.7	-24.9	-3.6	-21.3
AG_2	59.63	-28.1	-4.6	-23.5
G_2B	48.74	-30.2	-4.1	-26.1
AG_2B	59.93	-65.3	-10.8	-54.5
AB	46.1	-44.3	-5.7	-38.6
	$A+G_2B$			
G_2B	48.74	-30.2	-4.1	-26.1
$A+G_2B$	48.65	-65.1	-8.8	-56.3
	AG_2+B			
AG_2	59.63	-28.1	-4.6	-23.5
AG_2+B	60.53	-30.9	-5.1	-25.8

Table 5.3 Folding Thermodynamic profiles for all molecules at 5 °C according to different origins of ODNs

5.5 Conclusions

Attachment and mixing of GC-rich single strand A and B have quite different and interesting effects on the thermostability of the TBA G-quadruplex, as indicated in the CD spectroscopy, UV/CD melting and DSC unfolding studies. Six scenarios were analysed in the studies and they are shown in schematic representation in **Figure 5.6.** When single strand A is attached to the 5' end of G_2, G-quadruplex formation is abolished because A probably base pairs with the 5 ' end of the G-quadruplex. This leads to the destruction of the quartets and the formation of an intramolecular duplex, and the unfolding process of AG_2 is accompanied by substantial communication between the melting domains. Meanwhile, the addition of B strand does not rescue the quadruplex since the intramolecular base pairing is more thermodynamically favorable than intermolecular base pairing. In another senario, when B strand is attached to the 3' end of G-quadruplex, the entropy of the system is reduced and A and B strands are within one molecule, and A favors base pairing with B instead of the quadruplex because the AB duplex has three more base pairs than A-G_2. The thermostability of the AB duplex is increased by the attachment to G_2 as shown by increased T_M in UV-melting at 260nm. As an energetic compensation, the thermostability of G_2 is decreased. The unfolding for AG_2B starts at the G_2 portion and then the duplex as indicated by the unsymmetrical DSC unfolding profile. The reason for the destabilization of the G-quadruplex by the duplex is because the first GC-base pair of the duplex is stacked into the nearby G quartet, thus causing the instability between the stacking of the two quartet planes. However, the stacking between the duplex (first base pair) and the G-quadruplex in turn greatly stabilize the duplex, and upon unfolding, the unfolded quadruplex probably forms a hairpin-like structure together with the duplex, stabilizing the duplex even more.

In conclusion, we have comprehensively studied the intramolecular and intermolecular interaction between two GC-rich complementary single strands with the G_2

quadruplex, gaining valuable information about how the flanking sequence affects the quadruplex thermostability. This gives great indication on the design of TBA aptamer quadruplex drugs as well as the *in vivo* folding-unfolding mechanism of telomeric or promoter region G-quadruplex.
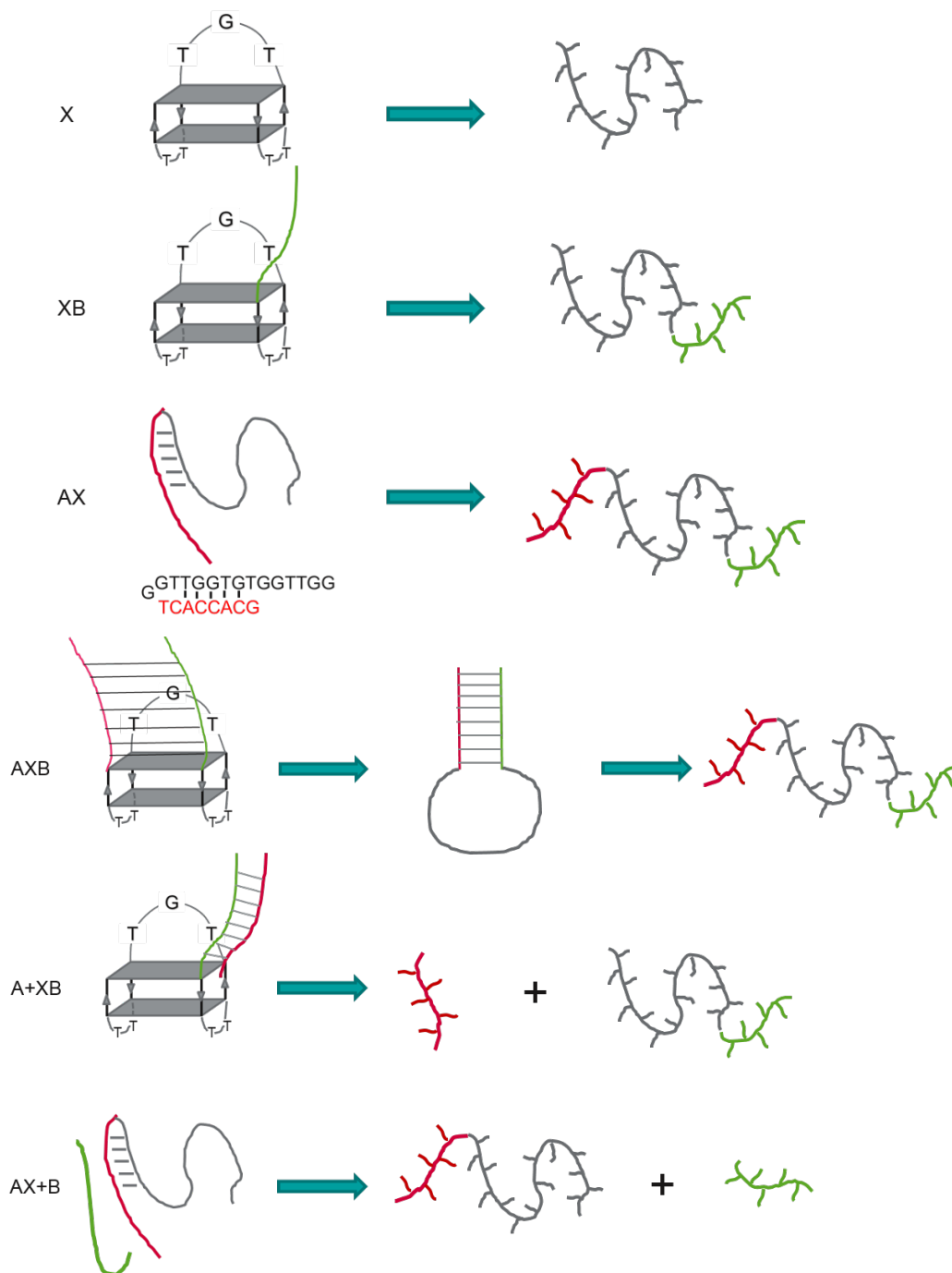
Figure 5.6 Unfolding profile of each ODN/ODN mixture in the study.

Chapter 6

Conclusions and Future Studies

6.1 Summary

Recombinant CidA and Lrg were purified through two step-purification via Ni-NTA and gel-filtration chromatography, the purified protein was applied to various biochemical and biophysical studies. The localization of CidA/LrgA in the membrane was confirmed by TEM and the secondary structure of the proteins is mainly composed of α-helices, as indicated by CD spectra. A newly developed liposome leakage assay has proved that CidA induced the formation of nanometer-size pores and lead to the passage of small fluorescent dyes other than bigger cargoes like GFP and cytochrome c. LrgA is less capable of inducing the leakage of fluorescent dyes. Our experiments are in good agreement of previous proposed model that CidA is a holin-like protein, whereas LrgA might act as an anti-holin under some other conditions or with the help of other protein partners like LrgB.

The third gene product of *cid operon* CidC, was also purified and the detailed function mechanism was studied. The assay has conclusively proved that CidC is a pyruvate oxidoreductase and binds to the biological membrane only in acidic pH, CidC passes the electron to menaquinone in vivo and converts pyruvate to acetate instead of hydrogen peroxide. The activity of CidC is only functional in pH 5.6 to 5.8 and replies on the cofactor thiamine pyrophsophate and Mg^{2+} ion. The protein showed a dramatic conformational change upon binding to pyruvate, TPP and Mg^{2+} (reduced state), as proved by the trypsination assay.

The goal of the third project was to study the unfolding profile and thermodynamics of G2-quadruplex upon the attachment of two complementary GC-rich single strands. The result has undoubtedly indicated that single strand A has a deleterious effect on the formation

of quadruplex whereas single strand B is able to rescue it, but only through intramolecular interaction.

6.2 Future study

Given that CidA/B/C are adjacent gene product on the same operon, it makes intuitive sense to test the interactions between them. In fact, recent in vivo work done in Dr. Bayles's Lab showed that CidA and CidB are related to the activity and membrane localization of CidC , which might have indicated the interactions between CidA/B/C. To test the interaction between these proteins, isothermal calorimetry titration (ITC) will be applied. DDM solubilized CidA and CidB will be dialyzed against the same buffer (with 0.05% DDM), whereas CidC will be dialyzed against the same buffer except for the absence of the detergent. The binding affinity of each pair of proteins will be measured by ITC under different pH (6 and 8) and with or without pyruvate and TPP. Similar experiments will also be done in the conditions when CidA/B/C are reconstituted into/onto the POPG/POPC membrane.

It will be also very interesting to study if CidA induced leakage under different pH and whether it's dependent on the lipid components of the membrane. Also, the regulatory mechanism of the transcriptional factor CidR on *cid operon* remains to be thoroughly studied via biophysical and biochemical methods like is mentioned in the thesis.

References

1. Nübel, U. *et al.* A timescale for evolution, population expansion, and spatial spread of an emerging clone of methicillin-resistant Staphylococcus aureus. *PLoS Pathog.* **6,** e1000855 (2010).

2. Pozzi, C. *et al.* Methicillin resistance alters the biofilm phenotype and attenuates virulence in staphylococcus aureus device-associated infections. *PLoS Pathog.* **8,** (2012).

3. Rezaei, M., Moniri, R., Mousavi, S. G. A. & Shiade, M. J. Prevalence of biofilm formation among methicillin resistance staphylococcus aureus isolated from nasal carriers. *Jundishapur J. Microbiol.* **6,** 0–4 (2013).

4. Bayles, K. W. The biological role of death and lysis in biofilm development. *Nat. Rev. Microbiol.* **5,** 721–6 (2007).

5. Mann, E. E. *et al.* Modulation of eDNA release and degradation affects Staphylococcus aureus biofilm maturation. *PLoS One* **4,** e5822 (2009).

6. Xu, Y. & Kreth, J. Role of LytF and AtlS in eDNA Release by Streptococcus gordonii. *PLoS One* **8,** (2013).

7. Patton, T. G., Yang, S. J. & Bayles, K. W. The role of proton motive force in expression of the Staphylococcus aureus cid and lrg operons. *Mol. Microbiol.* **59,** 1395–1404 (2006).

8. Ranjit, D. K., Endres, J. L. & Bayles, K. W. Staphylococcus aureus CidA and LrgA proteins exhibit holin-like properties. *J. Bacteriol.* **193,** 2468–76 (2011).

9. Patton, T. G., Rice, K. C., Foster, M. K. & Bayles, K. W. The Staphylococcus aureus cidC gene encodes a pyruvate oxidase that affects acetate metabolism and cell death in stationary phase. *Mol. Microbiol.* **56,** 1664–74 (2005).

10. Rice, K. C. & Bayles, K. W. Molecular control of bacterial death and lysis. *Microbiol. Mol. Biol. Rev.* **72,** 85–109, table of contents (2008).

11. Probst-Cousin, S., Rickert, C. H., Schmid, K. W. & Gullotta, F. Cell death mechanisms in multiple system atrophy. *J. Neuropathol. Exp. Neurol.* **57,** 814–21 (1998).

12. Elmore, S. Apoptosis: A Review of Programmed Cell Death. *Toxicol. Pathol.* **35,** 495–516 (2007).

13. Saelens, X. *et al.* Toxic proteins released from mitochondria in cell death. *Oncogene* **23,** 2861–2874 (2004).

14. Youle, R. & Strasser, A. The BCL-2 protein family: opposing activities that mediate

cell death. *Nat. Rev. Mol. Cell Biol.* **9,** 47–59 (2008).

15. Tait, S. W. G. & Green, D. R. Mitochondria and cell death: outer membrane permeabilization and beyond. *Nat. Rev. Mol. Cell Biol.* **11,** 621–632 (2010).

16. Gogvadze, V., Orrenius, S. & Zhivotovsky, B. Multiple pathways of cytochrome c release from mitochondria in apoptosis. *Biochim. Biophys. Acta - Bioenerg.* **1757,** 639–647 (2006).

17. Schuler, M. & Green, D. R. Mechanisms of p53-dependent apoptosis. *Biochem. Soc. Trans.* **29,** 684–688 (2001).

18. Locksley, R. M., Killeen, N. & Lenardo, M. J. The TNF and TNF receptor superfamilies: Integrating mammalian biology. *Cell* **104,** 487–501 (2001).

19. Ashkenazi, A. Death Receptors: Signaling and Modulation. *Science (80-.).* **281,** 1305–1308 (1998).

20. Hsu, H., Xiong, J. & Goeddel, D. V. The TNF receptor 1-associated protein TRADD signals cell death and NF-kappa B activation. *Cell* **81,** 495–504 (1995).

21. Kelliher, M. A. *et al.* The death domain kinase RIP mediates the TNF-induced NF-kappaB signal. *Immunity* **8,** 297–303 (1998).

22. Wajant, H. The Fas signaling pathway: more than a paradigm. *Science (80-.).* **296,** 1635–1636 (2002).

23. Kischkel, F. C. *et al.* Cytotoxicity-dependent APO-1 (Fas/CD95)-associated proteins form a death-inducing signaling complex (DISC) with the receptor. *EMBO J.* **14,** 5579–88 (1995).

24. Kataoka, T. *et al.* FLIP prevents apoptosis induced by death receptors but not by perforin/granzyme B, chemotherapeutic drugs, and gamma irradiation. *J. Immunol.* **161,** 3936–42 (1998).

25. Scaffidi, C., Schmitz, I., Krammer, P. H. & Peter, M. E. The role of c-FLIP in modulation of CD95-induced apoptosis. *J. Biol. Chem.* **274,** 1541–1548 (1999).

26. Hitoshi, Y. *et al.* Toso, a cell surface, specific regulator of Fas-induced apoptosis in T cells. *Immunity* **8,** 461–471 (1998).

27. Stockman, J. a. Invasive Methicillin-Resistant Staphylococcus aureus Infections in the United States. *Yearb. Pediatr.* **2009,** 260–263 (2009).

28. Filice, G. a *et al.* Excess costs and utilization associated with methicillin resistance for patients with Staphylococcus aureus infection. *Infect. Control Hosp. Epidemiol.* **31,** 365–373 (2010).

29. Kostakioti, M., Hadjifrangiskou, M. & Hultgren, S. J. Bacterial biofilms: development, dispersal, and therapeutic strategies in the dawn of the postantibiotic era. *Cold Spring Harb. Perspect. Med.* **3,** 1–23 (2013).

30. Bao, Y., Zhang, X., Jiang, Q., Xue, T. & Sun, B. Pfs promotes autolysis-dependent release of eDNA and biofilm formation in Staphylococcus aureus. *Med. Microbiol. Immunol.* **204,** 215–226 (2015).

31. Mai-prochnow, A. Autolysis in the development and dispersal of biofilms formed by the marine bacterium Pseudoalteromonas tunicata A thesis in fulfilment of the requirements for the degree of. (2006).

32. Archer, N. K. *et al. Staphylococcus aureus* biofilms: properties, regulation, and roles in human disease. *Virulence* **2,** 445–459 (2011).

33. Allocati, N., Masulli, M., Di Ilio, C. & De Laurenzi, V. Die for the community: an overview of programmed cell death in bacteria. *Cell Death Dis.* **6,** e1609 (2015).

34. Yang, S. J. *et al.* A LysR-type regulator, CidR, is required for induction of the Staphylococcus aureus cidABC operon. *J. Bacteriol.* **187,** 5893–5900 (2005).

35. Yang, S.-J. *et al.* Role of the LytSR two-component regulatory system in adaptation to cationic antimicrobial peptides in Staphylococcus aureus. *Antimicrob. Agents Chemother.* **57,** 3875–82 (2013).

36. Sauer, K. The genomics and proteomics of biofilm formation. *Genome Biol.* **4,** 219 (2003).

37. Pratt, L. A. & Kolter, R. Genetic analysis of Escherichia coli biofilm formation: roles of flagella, motility, chemotaxis and type I pili. *Mol. Microbiol.* **30,** 285–93 (1998).

38. Beveridge, T. J., Makin, S. A., Kadurugamuwa, J. L. & Li, Z. Interactions between biofilms and the environment. *FEMS Microbiol. Rev.* **20,** 291–303 (1997).

39. Lewis, K. Persister cells. *Annu. Rev. Microbiol.* **64,** 357–72 (2010).

40. Spoering, A. L. & Lewis, K. Biofilms and Planktonic Cells of Pseudomonas aeruginosa Have Similar Resistance to Killing by Antimicrobials. *J. Bacteriol.* **183,** 6746–6751 (2001).

41. Lewis, K. Persister cells and the riddle of biofilm survival. *Biochem. Biokhimiiã˜***70,** 267–74 (2005).

42. Saunders, J. Biofilm resistance to antimicrobial agents. 547–549 (2000).

43. Singh, R., Ray, P., Das, A. & Sharma, M. Penetration of antibiotics through Staphylococcus aureus and Staphylococcus epidermidis biofilms. *J. Antimicrob. Chemother.* **65,** 1955–1958 (2010).

44. Boyd, A. & Chakrabarty, A. M. Role of alginate lyase in cell detachment of Pseudomonas aeruginosa. *Appl. Environ. Microbiol.* **60,** 2355–9 (1994).

45. Miller, M. B. & Bassler, B. L. Quorum sensing in bacteria. *Annu. Rev. Microbiol.* **55,** 165–99 (2001).

46. Rutherford, S. T. *et al.* Bacterial Quorum Sensing : Its Role in Virulence and

Possibilities for Its Control. 1–26 (2014). doi:10.1101/cshperspect.a012427

47. Pandey, D. P. & Gerdes, K. Toxin-antitoxin loci are highly abundant in free-living but lost from host-associated prokaryotes. *Nucleic Acids Res.* **33,** 966–76 (2005).

48. Yamaguchi, Y. & Inouye, M. Regulation of growth and death in Escherichia coli by toxin-antitoxin systems. *Nat. Rev. Microbiol.* **9,** 779–90 (2011).

49. Aizenman, E., Engelberg-Kulka, H. & Glaser, G. An Escherichia coli chromosomal 'addiction module' regulated by guanosine [corrected] 3',5'-bispyrophosphate: a model for programmed bacterial cell death. *Proc. Natl. Acad. Sci. U. S. A.* **93,** 6059–63 (1996).

50. Hazan, R., Sat, B. & Engelberg-Kulka, H. Escherichia coli mazEF-Mediated Cell Death Is Triggered by Various Stressful Conditions. *J. Bacteriol.* **186,** 3663–3669 (2004).

51. Engelberg-Kulka, H., Amitai, S., Kolodkin-Gal, I. & Hazan, R. Bacterial programmed cell death and multicellular behavior in bacteria. *PLoS Genet.* **2,** 1518–1526 (2006).

52. Amitai, S., Kolodkin-Gal, I., Hananya-Meltabashi, M., Sacher, A. & Engelberg-Kulka, H. Escherichia coli MazF leads to the simultaneous selective synthesis of both 'death proteins' and 'survival proteins'. *PLoS Genet.* **5,** e1000390 (2009).

53. Kolodkin-Gal, I., Hazan, R., Gaathon, A., Carmeli, S. & Engelberg-Kulka, H. A linear pentapeptide is a quorum-sensing factor required for mazEF-mediated cell death in Escherichia coli. *Science* **318,** 652–5 (2007).

54. Wang, I., Smith, D. L. & Young, R. H OLINS : The Protein Clocks of Bacteriophage Infections. 799–825 (2000).

55. Gründling, A., Bläsi, U., Young, R. & Bla, U. D. O. Genetic and Biochemical Analysis of Dimer and Oligomer Interactions of the λ S Holin Genetic and Biochemical Analysis of Dimer and Oligomer Interactions of the S Holin. **182,** 6082–6090 (2000).

56. Wang, I.-N., Deaton, J. & Young, R. Sizing the Holin Lesion with an Endolysin- -Galactosidase Fusion. *J. Bacteriol.* **185,** 779–787 (2003).

57. Xu, M., Struck, D. K., Deaton, J., Wang, I.-N. & Young, R. A signal-arrest-release sequence mediates export and control of the phage P1 endolysin. *Proc. Natl. Acad. Sci. U. S. A.* **101,** 6415–20 (2004).

58. Xu, M. *et al.* Disulfide isomerization after membrane release of its SAR domain activates P1 lysozyme. *Science* **307,** 113–7 (2005).

59. Park, T., Struck, D. K., Deaton, J. F. & Young, R. Topological dynamics of holins in programmed bacterial lysis. *Proc. Natl. Acad. Sci. U. S. A.* **103,** 19713–19718 (2006).

60. Raab, R., Neal, G., Sohaskey, C., Smith, J. & Young, R. Dominance in lambda S mutations and evidence for translational control. *J. Mol. Biol.* **199,** 95–105 (1988).

61. Bläsi, U. & Young, R. Two beginnings for a single purpose: the dual-start holins in the

regulation of phage lysis. *Mol. Microbiol.* **21,** 675–82 (1996).

62. Brunskill, E. W. & Bayles, K. W. Identification of LytSR-regulated genes from Staphylococcus aureus. *J. Bacteriol.* **178,** 5810–2 (1996).

63. Patel, K. & Golemi-Kotra, D. Signaling mechanism by the Staphylococcus aureus two-component system LytSR: role of acetyl phosphate in bypassing the cell membrane electrical potential sensor LytS. *F1000Research* **4,** 79 (2015).

64. Behr, S. M. The LytS / LytTR-like histidine kinase / response regulator systems in Escherichia coli and their function in carbon source selectivity. (2014).

65. Groicher, K. H., Firek, B. A., Fujimoto, D. F. & Bayles, K. W. The Staphylococcus aureus lrgAB operon modulates murein hydrolase activity and penicillin tolerance. *J. Bacteriol.* **182,** 1794–1801 (2000).

66. Rice, K. C. *et al.* The Staphylococcus aureus cidAB Operon : Evaluation of Its Role in Regulation of Murein Hydrolase Activity and Penicillin Tolerance. **185,** 2635–2643 (2003).

67. Rice, K. C. *et al.* The cidA murein hydrolase regulator contributes to DNA release and biofilm development in Staphylococcus aureus. *Proc. Natl. Acad. Sci. U. S. A.* **104,** 8113–8 (2007).

68. Rice, K. C., Nelson, J. B., Patton, T. G., Yang, S. & Bayles, K. W. Acetic acid induces expression of the Staphylococcus aureus cidABC and lrgAB murein hydrolase regulator operons. *J. Bacteriol.* **187,** 813–21 (2005).

69. Bayles, K. W. Bacterial programmed cell death: making sense of a paradox. *Nat. Rev. Microbiol.* **12,** 63–9 (2014).

70. Thomas, V. C. *et al.* A central role for carbon-overflow pathways in the modulation of bacterial cell death. *PLoS Pathog.* **10,** e1004205 (2014).

71. Yang, S. J., Dunman, P. M., Projan, S. J. & Bayles, K. W. Characterization of the Staphylococcus aureus CidR regulon: Elucidation of a novel role for acetoin metabolism in cell death and lysis. *Mol. Microbiol.* **60,** 458–468 (2006).

72. Chaudhari, S. S. *et al.* The LysR-type transcriptional regulator, CidR, regulates stationary phase cell death in Staphylococcus aureus. *Mol. Microbiol.* **0,** 1–12 (2016).

73. Maddocks, S. E. & Oyston, P. C. F. Structure and function of the LysR-type transcriptional regulator (LTTR) family proteins. *Microbiology* **154,** 3609–3623 (2008).

74. Diamond, M. & McCabe, P. F. in *Plant Mitochondria* (ed. Kempken, F.) 439–465 (Springer New York, 2011). doi:10.1007/978-0-387-89781-3_17

75. Lam, E., Kato, N. & Lawton, M. Programmed cell death, mitochondria and the plant hypersensitive response. *Nature* **411,** 848–853 (2001).

76. De Pinto, M. C., Locato, V. & De Gara, L. Redox regulation in plant programmed cell

death. *Plant. Cell Environ.* **35,** 234–44 (2012).

77. Doyle, S. M., Diamond, M. & McCabe, P. F. Chloroplast and reactive oxygen species involvement in apoptotic-like programmed cell death in Arabidopsis suspension cultures. *J. Exp. Bot.* **61,** 473–482 (2010).

78. Mitsuhara, I., Malik, K. A., Miura, M. & Ohashi, Y. Animal cell-death suppressors Bcl-x(L) and Ced-9 inhibit cell death in tobacco plants. *Curr. Biol.* **9,** 775–8 (1999).

79. Lacomme, C. & Santa Cruz, S. Bax-induced cell death in tobacco is similar to the hypersensitive response. *Proc. Natl. Acad. Sci. U. S. A.* **96,** 7956–61 (1999).

80. Chen, S. & Dickman, M. B. Bcl-2 family members localize to tobacco chloroplasts and inhibit programmed cell death induced by chloroplast-targeted herbicides. *J. Exp. Bot.* **55,** 2617–23 (2004).

81. Kleffmann, T. *et al.* The Arabidopsis thaliana chloroplast proteome reveals pathway abundance and novel protein functions. *Curr. Biol.* **14,** 354–62 (2004).

82. Ferro, M. *et al.* Integral membrane proteins of the chloroplast envelope: identification and subcellular localization of new transporters. *Proc. Natl. Acad. Sci. U. S. A.* **99,** 11487–92 (2002).

83. Yang, Y. *et al.* A chloroplast envelope membrane protein containing a putative LrgB domain related to the control of bacterial death and lysis is required for chloroplast development in Arabidopsis thaliana. *New Phytol.* **193,** 81–95 (2012).

84. Yamaguchi, M. *et al.* Loss of the plastid envelope protein AtLrgB causes spontaneous chlorotic cell death in arabidopsis thaliana. *Plant Cell Physiol.* **53,** 125–134 (2012).

85. Bayles, K. W. Are the molecular strategies that control apoptosis conserved in bacteria? *Trends Microbiol.* **11,** 306–11 (2003).

86. Pang, X. *et al.* Active Bax and Bak are functional holins. *Genes Dev.* **25,** 2278–90 (2011).

87. Russell, P., Hager, L. P. & Gennis, R. B. Characterization of the proteolytic activation of pyruvate oxidase. Control by specific ligands and by the flavin oxidation-reduction state. *J. Biol. Chem.* **252,** 7877–82 (1977).

88. Russell, P., Schrock, H. L. & Gennis, R. B. Lipid activation and protease activation of pyruvate oxidase. Evidence suggesting a common site of interaction on the protein. *J. Biol. Chem.* **252,** 7883–7 (1977).

89. Grabau, C. & Cronan, J. E. Molecular cloning of the gene (poxB) encoding the pyruvate oxidase of Escherichia coli, a lipid-activated enzyme. *J. Bacteriol.* **160,** 1088–92 (1984).

90. Schrock, H. L. & Gennis, R. B. High affinity lipid binding sites on the peripheral membrane enzyme pyruvate oxidase: Specific ligand effects on detergent binding. *J. Biol. Chem.* **252,** 5990–5995 (1977).

91. Marchal, D., Pantigny, J., Laval, J. M., Moiroux, J. & Bourdillon, C. Rate Constants in Two Dimensions of Electron Transfer between Pyruvate Oxidase, a Membrane Enzyme, and Ubiquinone (Coenzyme Q 8), Its Water-Insoluble Electron Carrier. *Biochemistry* **40,** 1248–1256 (2001).

92. Koland, J. G., Miller, M. J. & Gennis, R. B. Reconstitution of the membrane-bound, ubiquinone-dependent pyruvate oxidase respiratory chain of Escherichia coli with the cytochrome d terminal oxidase. *Biochemistry* **23,** 445–453 (1984).

93. Cunningham, C. C. & Hager, L. P. Reactivation of the lipid-depleted pyruvate oxidase system from Escherichia coli with cell envelope neutral lipids. *J. Biol. Chem.* **250,** 7139–46 (1975).

94. Schreiner, M. E., Riedel, C., Holátko, J., Pátek, M. & Eikmanns, B. J. Pyruvate:quinone oxidoreductase in Corynebacterium glutamicum: molecular analysis of the pqo gene, significance of the enzyme, and phylogenetic aspects. *J. Bacteriol.* **188,** 1341–50 (2006).

95. Muller, Y. A. & Schulz, G. E. Structure of the thiamine- and flavin-dependent enzyme pyruvate oxidase. *Science* **259,** 965–7 (1993).

96. Becker, D. F., Zhu, W. & Moxley, M. A. Flavin redox switching of protein functions. *Antioxid. Redox Signal.* **14,** 1079–91 (2011).

97. Zahler, A. M., Williamson, J. R., Cech, T. R. & Prescott, D. M. Inhibition of telomerase by G-quartet DNA structures. *Nature* **350,** 718–720 (1991).

98. Bambara, R. A., Murante, R. S. & Henricksen, L. A. Eukaryotic DNA Replication Fork *. 3–6

99. Pasternak, A., Hernandez, F. J., Rasmussen, L. M., Vester, B. & Wengel, J. Improved thrombin binding aptamer by incorporation of a single unlocked nucleic acid monomer. *Nucleic Acids Res.* **39,** 1155–1164 (2011).

100. Avino, A., Fabrega, C., Tintore, M. & Eritja, R. Thrombin Binding Aptamer, More than a Simple Aptamer: Chemically Modified Derivatives and Biomedical Applications. *Curr. Pharm. Des.* **18,** 2036–2047 (2012).

101. Deng, B. *et al.* Aptamer binding assays for proteins: The thrombin example-A review. *Anal. Chim. Acta* **837,** 1–15 (2014).

102. Wang, K. Y., Krawczyk, S. H., Bischofberger, N., Swaminathan, S. & Bolton, P. H. The tertiary structure of a DNA aptamer which binds to and inhibits thrombin determines activity. *Biochemistry* **32,** 11285–92 (1993).

103. Bock, L. C., Griffin, L. C., Latham, J. a, Vermaas, E. H. & Toole, J. J. Selection of single-stranded DNA molecules that bind and inhibit human thrombin. *Nature* **355,** 564–566 (1992).

104. Kelly, J. a, Feigon, J. & Yeates, T. O. Reconciliation of the X-ray and NMR structures of the thrombin-binding aptamer d(GGTTGGTGTGGTTGG). *J. Mol. Biol.* **256,** 417–

422 (1996).

105. Kankia, B. I. & Marky, L. A. Folding of the thrombin aptamer into a G-quadruplex with Sr(2+): stability, heat, and hydration. *J. Am. Chem. Soc.* **123,** 10799–804 (2001).

106. Olsen, C. M., Gmeiner, W. H. & Marky, L. A. Unfolding of G-quadruplexes: energetic, and ion and water contributions of G-quartet stacking. *J. Phys. Chem. B* **110,** 6962–9 (2006).

107. Pagano, B., Martino, L., Randazzo, A. & Giancola, C. Stability and binding properties of a modified thrombin binding aptamer. *Biophys. J.* **94,** 562–569 (2008).

108. Avino, A., Fabrega, C., Tintore, M. & Eritja, R. Thrombin binding aptamer, more than a simple aptamer: chemically modified derivatives and biomedical applications. *Curr. Pharm. Des.* **18,** 2036–47 (2012).

109. Miroux, B. & Walker, J. E. Over-production of proteins in Escherichia coli: mutant hosts that allow synthesis of some membrane proteins and globular proteins at high levels. *J. Mol. Biol.* **260,** 289–298 (1996).

110. Gutteridge, A. & Thornton, J. M. Understanding nature's catalytic toolkit. *Trends Biochem. Sci.* **30,** 622–629 (2005).

111. Huls, M. *et al.* The breast cancer resistance protein transporter ABCG2 is expressed in the human kidney proximal tubule apical membrane. *Kidney Int.* **73,** 220–225 (2008).

112. Terpe, K. Overview of bacterial expression systems for heterologous protein production: From molecular and biochemical fundamentals to commercial systems. *Appl. Microbiol. Biotechnol.* **72,** 211–222 (2006).

113. Yuan, Q., Liao, Y., Torres, J., Tam, J. P. & Liu, D. X. Biochemical evidence for the presence of mixed membrane topologies of the severe acute respiratory syndrome coronavirus envelope protein expressed in mammalian cells. *FEBS Lett.* **580,** 3192–200 (2006).

114. Yonesaka, K. *et al.* Anti-HER3 monoclonal antibody patritumab sensitizes refractory non-small cell lung cancer to the epidermal growth factor receptor inhibitor erlotinib. *Oncogene* 1–9 (2015). doi:10.1038/onc.2015.142

115. Edwards, A. M. *et al.* Protein production : feeding the crystallographers and NMR spectroscopists Cloning : Expression constructs. 970–972 (2000).

116. Tate, C. G. *et al.* Comparison of seven different heterologous protein expression systems for the production of the serotonin transporter. *Biochim. Biophys. Acta - Biomembr.* **1610,** 141–153 (2003).

117. Sm, M., Irani, S., Davoudi, N. & Bolhassani, A. Different protein expression systems can influence the direction of the immune responses against HCV core protein in animal model. **2,** 54–58 (2015).

118. Downing, A. K. *Protein NMR Techniques*. *Methods in molecular biology (Clifton,*

N.J.) **278,** (2004).

119. Rosano, G. L. & Ceccarelli, E. A. Recombinant protein expression in Escherichia coli: Advances and challenges. *Front. Microbiol.* **5,** 1–17 (2014).

120. Hage, D. S. Affinity chromatography: a review of clinical applications. *Clin. Chem.* **45,** 593–615 (1999).

121. Rosetta, P. E. GST-Tagged Protein Expression and Purification. 15–17 (2010).

122. Agarose, P. N. & Columns, P. N. Purification of His-tag proteins User manual. (2012).

123. Ó'Fágáin, C., Cummins, P. M. & O'Connor, B. F. in *Methods in molecular biology (Clifton, N.J.)* **694,** 25–33 (2011).

124. Hong, P., Koza, S. & Bouvier, E. S. P. Size-Exclusion Chromatography for the Analysis of Protein Biotherapeutics and their Aggregates. *J. Liq. Chromatogr. Relat. Technol.* **35,** 2923–2950 (2012).

125. Yang, P.-C. & Mahmood, T. Western blot: Technique, theory, and trouble shooting. *N. Am. J. Med. Sci.* **4,** 429 (2012).

126. Gibbons, J. Western blot: Protein transfer overview. *N. Am. J. Med. Sci.* **6,** 158 (2014).

127. Pennycook, S. J. *et al.* Transmission Electron Microscopy: Overview and Challenges. *AIP Conf. Proc.* **683,** 627–633 (2003).

128. Johnson, K. A. & Goody, R. S. The Original Michaelis Constant: Translation of the 1913 Michaelis–Menten Paper. *Biochemistry* **50,** 8264–8269 (2011).

129. Freyer, M. W. & Lewis, E. A. Isothermal Titration Calorimetry: Experimental Design, Data Analysis, and Probing Macromolecule/Ligand Binding and Kinetic Interactions. *Methods Cell Biol.* **84,** 79–113 (2008).

130. Prenner, E. & Chiu, M. Differential scanning calorimetry: An invaluable tool for a detailed thermodynamic characterization of macromolecules and their interactions. *J. Pharm. Bioallied Sci.* **3,** 39 (2011).

131. Young, R. Phage lysis: Do we have the hole story yet? *Curr. Opin. Microbiol.* **16,** 790–797 (2013).

132. Barbet, J., Machy, P., Truneh, A. & Leserman, L. Weak acid-induced release of liposome-encapsulated carboxyfluorescein. *Biochim. Biophys. Acta ...* **772,** 347–356 (1984).

133. Faudry, E., Perdu, C. & Attrée, I. Pore formation by T3SS translocators: liposome leakage assay. *Methods Mol. Biol.* **966,** 173–85 (2013).

134. Wang, I. N., Smith, D. L. & Young, R. Holins: the protein clocks of bacteriophage infections. *Annu. Rev. Microbiol.* **54,** 799–825 (2000).

135. Beltrame, C. O. *et al.* Inactivation of the Autolysis-Related Genes lrgB and yycI in Staphylococcus aureus Increases Cell Lysis-Dependent eDNA Release and Enhances

Biofilm Development In Vitro and In Vivo. *PLoS One* **10,** e0138924 (2015).

136. Wang, J. & Bayles, K. W. Programmed cell death in plants: Lessons from bacteria? *Trends Plant Sci.* **18,** 133–139 (2013).

137. Kanehisa, M. *et al.* Data, information, knowledge and principle: Back to metabolism in KEGG. *Nucleic Acids Res.* **42,** 199–205 (2014).

138. Spellerberg, B. *et al.* Pyruvate oxidase, as a determinant of virulence in Streptococcus pneumoniae. *Mol. Microbiol.* **19,** 803–813 (1996).

139. Ying Ying Chang & Cronan, J. E. Genetic and biochemical analyses of Escherichia coli strains having a mutation in the structural gene (poxB) for pyruvate oxidase. *J. Bacteriol.* **154,** 756–762 (1983).

140. Wolfe, A. J. The acetate switch. *Microbiol. Mol. Biol. Rev.* **69,** 12–50 (2005).

141. Regev-Yochay, G., Trzcinski, K., Thompson, C. M., Lipsitch, M. & Malley, R. SpxB is a suicide gene of Streptococcus pneumoniae and confers a selective advantage in an in vivo competitive colonization model. *J. Bacteriol.* **189,** 6532–6539 (2007).

142. Neumann, P., Weidner, A., Pech, A., Stubbs, M. T. & Tittmann, K. Structural basis for membrane binding and catalytic activation of the peripheral membrane enzyme pyruvate oxidase from Escherichia coli. *Proc. Natl. Acad. Sci. U. S. A.* **105,** 17390–17395 (2008).

143. Muller, Y. a, Schumacher, G., Rudolph, R. & Schulz, G. E. The refined structures of a stabilized mutant and of wild-type pyruvate oxidase from Lactobacillus plantarum. *Journal of molecular biology* **237,** 315–35 (1994).

144. Tittmann, K., Golbik, R., Ghisla, S. & Hubner, G. Mechanism of elementary catalytic steps of pyruvate oxidase from Lactobacillus plantarum. *Biochemistry* **39,** 10747–10754 (2000).

145. Risse, B., Stempfer, G., Rudolph, R., Möllering, H. & Jaenicke, R. Stability and reconstitution of pyruvate oxidase from Lactobacillus plantarum: Dissection of the stabilizing effects of coenzyme binding and subunit interaction. *Protein Sci.* **1,** 1699–1709 (1992).

146. Carlsson, J., Edlund, M. B. & Lundmark, S. K. Characteristics of a hydrogen peroxide-forming pyruvate oxidase from Streptococcus sanguis. *Oral Microbiol. Immunol.* **2,** 15–20 (1987).

147. Sedewitz, B., Schleifer, K. H. & Gotz, F. Purification and biochemical characterization of pyruvate oxidase from Lactobacillus plantarum. *J. Bacteriol.* **160,** 273–278 (1984).

148. Schreiner, M. E. & Eikmanns, B. J. Pyruvate:quinone oxidoreductase from Corynebacterium glutamicum: purification and biochemical characterization. *J. Bacteriol.* **187,** 862–71 (2005).

149. Blake, R. & Hager, L. P. Activation of pyruvate oxidase by monomeric and micellar

amphiphiles. *J. Biol. Chem.* **253,** 1963–71 (1978).

150. Grabau, C. & Cronan, J. E. Molecular cloning of the gene (poxB) encoding the pyruvate oxidase of Escherichia coli, a lipid-activated enzyme. *J. Bacteriol.* **160,** 1088–92 (1984).

151. Grabau, C. & Cronan, J. E. In vivo function of Escherichia coli pyruvate oxidase specifically requires a functional lipid binding site. *Biochemistry* **25,** 3748–3751 (1986).

152. Carter, K. & Gennis, R. B. Reconstitution of the ubiquinone-dependent pyruvate oxidase system of Escherichia coli with the cytochrome o terminal oxidase complex. *J. Biol. Chem.* **260,** 10986–10990 (1985).

153. Chang, Y. Y. & Cronan, J. E. An Escherichia coli mutant deficient in pyruvate oxidase activity due to altered phospholipid activation of the enzyme. *Proc. Natl. Acad. Sci. U. S. A.* **81,** 4348–52 (1984).

154. Mather, M. W. & Gennis, R. B. Spectroscopic studies of pyruvate oxidase flavoprotein from Escherichia coli trapped in the lipid-activated form by cross-linking. *J. Biol. Chem.* **260,** 10395–7 (1985).

155. Recny, M. A. & Hager, L. P. Isolation and characterization of the protease-activated form of pyruvate oxidase. Evidence for a conformational change in the environment of the flavin prosthetic group. *J. Biol. Chem.* **258,** 5189–95 (1983).

156. Simon, H. U., Haj-Yehia, A. & Levi-Schaffer, F. Role of reactive oxygen species (ROS) in apoptosis induction. *Apoptosis* **5,** 415–418 (2000).

157. Granot, D., Levine, A. & Dor-Hefetz, E. Sugar-induced apoptosis in yeast cells. *FEMS Yeast Res.* **4,** 7–13 (2003).

158. Parashar, A. Aptamers in Therapeutics. *J. Clin. Diagnostic Res.* **10,** 1–6 (2016).

159. Kusser, W. Chemically modified nucleic acid aptamers for in vitro selections: evolving evolution. *J. Biotechnol.* **74,** 27–38 (2000).

160. Cascade, C. The Coagulation Cascade: Initiation, Maintenance, and Regulation? **30,** (1991).

161. Huntington, J. A. Molecular recognition mechanisms of thrombin. *J. Thromb. Haemost.* **3,** 1861–1872 (2005).

162. Self, B. D. & Moore, D. S. Nucleic Acid Vibrational Circular Dichroism , Absorption , and Linear Dichroism Spectra . 1 . A DeVoe Theory Approach. **73,** 339–347 (1997).

163. Cantor, C. R., Warshaw, M. M. & Shapiro, H. Oligonucleotide interactions. 3. Circular dichroism studies of the conformation of deoxyoligonucleotides. *Biopolymers* **9,** 1059–77 (1970).

164. Marky, L. A., Blumenfeld, K. S., Kozlowski, S. & Breslauer, K. J. Salt-dependent conformational transitions in the self-complementary deoxydodecanucleotide

d(CGCAATTCGCG): evidence for hairpin formation. *Biopolymers* **22,** 1247–57 (1983).

165. Marky, L. A. & Breslauer, K. J. Calculating thermodynamic data for transitions of any molecularity from equilibrium melting curves. *Biopolymers* **26,** 1601–20 (1987).

166. Privalov, P. L. & Potekhin, S. A. Scanning Microcalorimetry in Studying Temperature-Induced Changes in Proteins. *Methods Enzymol.* **131,** 4–51 (1986).

167. Lu, M., Guo, Q. & Kallenbach, N. R. Thermodynamics of G-tetraplex formation by telomeric DNAs. *Biochemistry* **32,** 598–601 (1993).